COPPE
UFRJ

Instituto Alberto Luiz Coimbra de
Pós-Graduação e Pesquisa de Engenharia

DESIGN AND CHARACTERIZATION OF STRAIN HARDENING CURAUÁ FIBER CEMENT-BASED COMPOSITES

Bartosz Żukowski

Tese de Doutorado apresentada ao Programa de Pós-graduação em Engenharia Civil, COPPE, da Universidade Federal do Rio de Janeiro, como parte dos requisitos necessários à obtenção do título de Doutor em Engenharia Civil.

Orientadores: Romildo Dias Toledo Filho
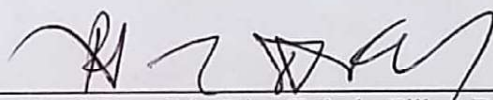   Flávio de Andrade Silva

Rio de Janeiro
Dezembro de 2017

DESIGN AND CHARACTERIZATION OF STRAIN HARDENING CURAUÁ FIBER CEMENT-BASED COMPOSITES
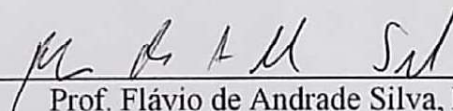
Bartosz Żukowski

TESE SUBMETIDA AO CORPO DOCENTE DO INSTITUTO ALBERTO LUIZ COIMBRA DE PÓS-GRADUAÇÃO E PESQUISA DE ENGENHARIA (COPPE) DA UNIVERSIDADE FEDERAL DO RIO DE JANEIRO COMO PARTE DOS REQUISITOS NECESSÁRIOS PARA A OBTENÇÃO DO GRAU DE DOUTOR EM CIÊNCIAS EM ENGENHARIA CIVIL.
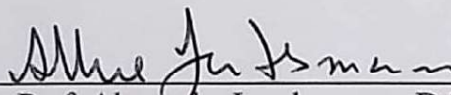
Examinada por:

_____
Prof. Romildo Dias Toledo Filho, D.Sc.
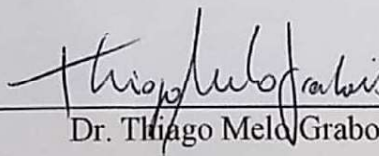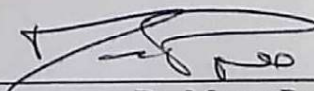
_____
Prof. Flávio de Andrade Silva, D.Sc.

_____
Prof. Conrado de Souza Rodrigues, D.Sc.

_____
Prof. Alexandre Landesmann, D.Sc.

_____
Dr. Thiago Melo Grabois, D.Sc.

_____
Dr. Marco Pepe, D.Sc.

RIO DE JANEIRO, RJ - BRASIL
DEZEMBRO DE 2017

AGRADECIMENTOS

Gostaria de agradecer ao Professor Conrado de Souza Rodrigues, graças a quem a minha aventura com fibras naturais começou anos atrás no CEFET-MG, pelo todo o apoio durante meus primeiros passos no laboratório e no Brasil também, e o incentivo para continuar a pesquisa.

Ao Professor Flávio de Andrade Silva pelo apoio durante o doutorado e toda a orientação que me motivou fazer esse trabalho melhor.

Ao Professor Romildo Dias Toledo Filho que formulou esse desafio para mim sempre motivando e colocando metas na minha frente mostrando o caminho para alcançar objetivo dessa tese. Obrigado pela a orientação, pelas todas as discussões, pelo todo.

Gostaria de agradecer a minha companheira e amada Larissa Helena da Silveira, que colocou um lar para mim no Brasil, sempre acreditando e apoiando meu trabalho mesmo nos momentos duros.

Gostaria de agradecer toda a equipe da NUMATS pela toda ajuda e apoio, especialmente Yasmim Gabriela dos Santos Mendonça, sem ela esse trabalho nunca seria apresentado. Gostaria de agradecer também Edson Rodrigo Fernandes dos Santos pela ajuda, apoio e troca das ideias durante essa pesquisa.

DESENVOLVIMENTO E CARATERIZÇÃO DOS COMPOSITOS CIMENTÍCIOS REFORÇADOS COM FIBRA NATURAL DE CURAUÁ COM ENDURECIMENTO NA DEFORMAÇÃO

Bartosz Żukowski

Dezembro/2017

Este trabalho apresenta a aplicação do modelo teórico para desenvolver os compósitos cimentícios reforçados com fibra natural de curauá com endurecimento na deformação. O trabalho investiga as propriedades das fibras curauá e a influência dos ciclos de lavagem e secagem e do tratamento alcalino na resistência da fibra. A aderência entre fibra e matriz foi verificado pelos ensaios de arrancamento. Os dados dos ensaios foram implementados no modelo teórico para verificar o mínimo teor da fibra necessário para endurecimento do compósito acontecer. A influência do cumprimento da fibra no comportamento mecânico do compósito foi verificada. No final, os compósitos foram expostos ao envelhecimento natural, ciclos de lavagem e secagem, e ciclos de congelamento e descongelamento para verificar a durabilidade de endurecimento e a fibra natural dentro da matriz cimentícia.

Abstract of Thesis presented to COPPE/UFRJ as a partial fulfillment of the requirements for the degree of Doctor of Science (D.Sc.)

DESIGN AND CHARACTERIZATION OF STRAIN HARDENING CURAUÁ
FIBER CEMENT-BASED COMPOSITES

Bartosz Żukowski

December/2017

Advisors: Romildo Dias Toledo Filho
          Flávio de Andrade Silva

Department: Civil Engineering

This work presents the application of the theoretical model to design the strain hardening cement-based composite reinforcement with natural curauá fiber. The work investigates the properties of curauá fiber and the influence of hot water washing cycles and alkaline treatments on fiber strength. The fiber-matrix bond is investigated by pull-out tests. The collected data is implemented into the theoretical model for minimum fiber volume needed to achieve strain hardening behavior. The influence of fiber length on mechanical performance of the composite is investigated. In the final stage, the composites were exposed to natural weathering, wetting and drying cycles, and freeze and thaw cycles to verify the durability of the strain hardening behavior as well as the curauá fiber in the cement-based matrix.

SUMMARY

1   THESIS STRUCTURE

1.1   OBJECTIVE

The new composites based on cement matrices are in development in various research facilities all over the world. With new materials, new technologies and science development cement composites are designed to fit better the construction purposes in various environmental conditions. Nowadays the requirements emphasize the ecological aspects of material used and the terms like ecological impact, sustainable material, and environment-friendly seem to be linked with future cement composites. The search for natural substituents of synthetic materials is one of the ways to make the product more environment-friendly. This work presents the application of natural curauá fiber in Strain Hardening Cement Composites. The purpose of this work is to verify the possibility of creating a cement composite presenting SHCC properties with natural short fiber instead of synthetic fiber. The benefits of this composite may include low cost, low environmental impact, and high accessibility of the composite for various applications. The natural fiber used in this research was the curauá (*ananas comosus* var. *erectofolius*). Various tests in the literature prove the high tensile strength of curauá fiber among natural fibers, which was one of the indicators to replace PVA fiber (TOMCZAK, 2007). Other motives were based on local access (Brazil) and a movement to increase the demand on natural fibers from Amazon region to enhance the curauá plantations as a reasonable source of income for agricultural regions in Brazil (ADRADE et al., 2011).

One of the most challenging aspects of this work was the fiber-matrix bond. To obtain the multiple-cracking behavior with the limited crack width various conditions have to be fulfilled. One of them includes a satisfactory bond between matrix and fiber. In the case of PVA fibers, the bond is even weakened to prevent the fiber from rupture (YANG; LI, 2010). In case of natural fibers, the bond is noticeably lower than PVA that is why the challenge was to improve the bond. Various treatments (hot water washing, alkaline immersion) were tested on fibers during the initial stage of this research to verify fiber-matrix bond improvement to obtain the desired composite.

The presented results help in better understanding of the design process of SHCC with natural fiber as well as its durability challenges.

1.2 THESIS ORGANIZATION

The brief description of chapters and visual representation of the thesis:

Chapter 1: Thesis structure

The objective and thesis structure are presented with research benefits.

Chapter 2: Literature review

The literature review presents the information about Strain Hardening Cement-based Composites, also state of the art of SHCC with natural fiber. This chapter presents information about natural fiber properties, and includes the challenges of natural fiber's durability in cement-based matrix.

Chapter 3: Materials

This chapter presents information about materials and testing procedures used during this research.

Chapter 4: The Influence of hot water washing cycles on curauá fiber tensile properties

This chapter presents the dimensional changes and strength characterization of fibers submitted to washing cycles. Determination of 3 hot water washing cycles was the first criterion for fiber's treatment selection, which was used in the composite.

Chapter 5: Design of Strain Hardening Cement-based Composites with alkali treated natural Curauá fiber

This chapter presents the design procedure of SHCC with the support of theoretical model. The influence of alkaline treatment on fiber tensile properties is presented, as well as on fiber pull-out behavior. The results are implemented into the model for critical fiber volume prediction for strain hardening behavior. The importance of fiber alkaline treatment on critical volume is presented. The influence of fiber length for SHCC tailoring and composite properties is presented for 20, 30 and 40 mm alkali treated curauá fibers.

Chapter 6: Natural weathering of Strain Hardening Cement-based Composites with alkali treated natural Curauá fiber.

This chapter presents the results of durability studies on composites exposed to natural weathering. The chapter contains the information about weather conditions, composite performance over time periods of 3, 6, 9 and 12 months with the study of matrix and fiber pull-out behavior changes. The chapter presents the challenges for natural fiber to endure in a cement matrix.

Chapter 7: Laboratory controlled wetting and drying cycles.

This chapter presents the influence of wetting and drying cycles on composite performance as a comparison to natural weathering exposure.

Chapter 8: Summary

This chapter presents the short summary of the carried research with indication for future investigation.
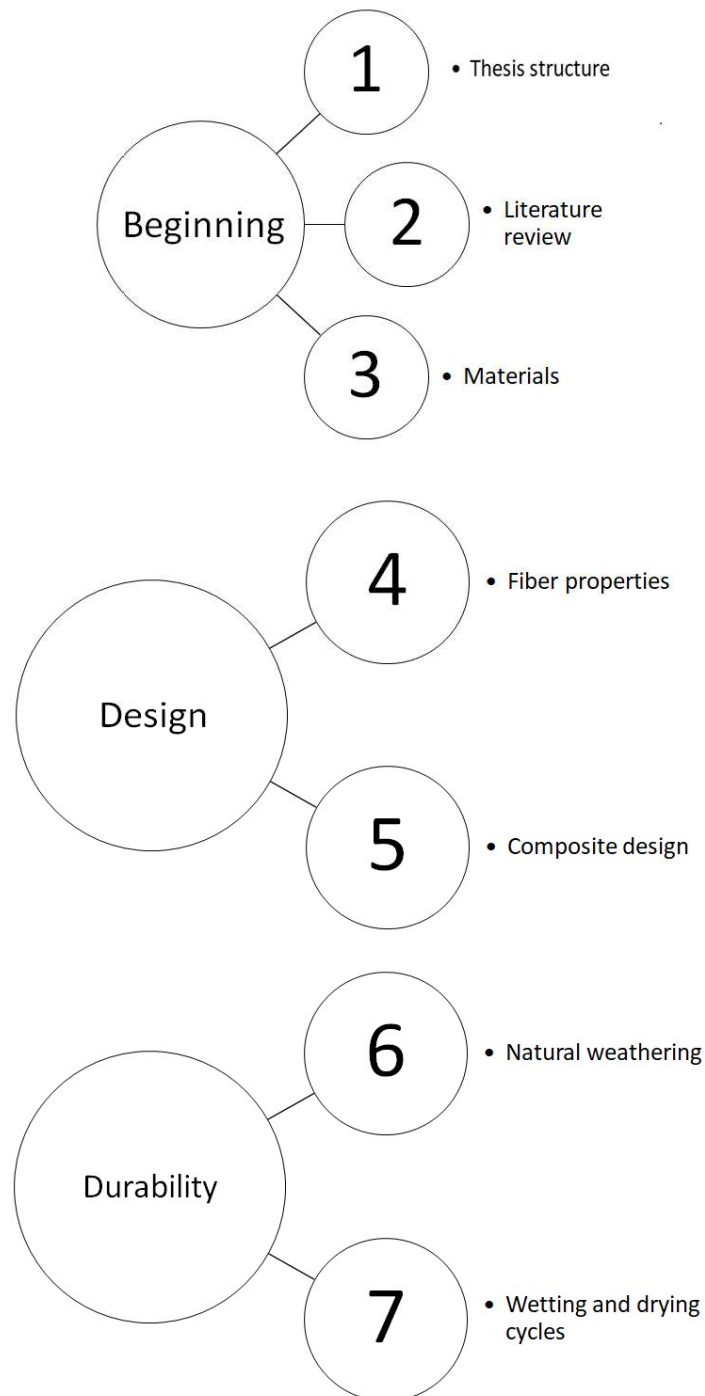
Figure 1-1 Graphical representation of the thesis chapters.

1.3 RESEARCH BENEFITS

Author thanks previous researchers who contributed to this work. Especially Professor Romildo Dias Toledo Filho for creating the basis for a calcium hydroxide free matrix which was later modified by Saulo Rocha Ferreira as a matrix with the possibility for natural fiber to endure. The research carried by Thiago Melo Grabois on cement-based materials fracture behavior was essential for matrix parameters used in model prediction. The works of Adriana Paiva de Souza and Maria Ernestina Alves Fidelis, which served as inspiration for durability tests and at the end to Andrielli Morais which testing methods used in research on ECC with PVA were adapted to composites with curauá fiber. This work is a continuation of a long process with various researchers on its way, but as I hope it puts a piece of new information, which will be with a benefit for future studies.

1.3.1 SHCC with natural fiber

This work presents the conceptual design of strain hardening composite reinforced with natural curauá fiber. This research benefits from previous studies on natural fiber properties and fiber treatments. It establishes 3 hot water washing cycles as sufficient for fiber cross-section reduction and improvement of strength properties. Also, it applies the alkaline treatment as a superficial deposition of Calcium on fiber surface to improve the fiber-matrix bond. The research finds the solution for strain hardening to occur for 20 mm chopped fiber (washed and alkali treated). The further investigation presents the influence of fiber length on strain hardening behavior.

1.3.2 Modelling approach for strain hardening behavior with short natural fiber

This work combines matrix, fiber, and fiber-matrix bond properties into a theoretical model for critical fiber volume prediction. The model developed for synthetic fiber was slightly adapted because of natural fiber shape irregularity. The minor modification which used fiber perimeter calculated at ImageJ software for fiber-matrix bond calculation and the application of maximum frictional bond into model data. The modification was used to reach maximum adequacy with critical fiber volume prediction. Parallel to this study the iterative method of SHCC with natural fiber was presented (SOLTAN et al., 2017). Modeling approach presented in this work is probably the first trial to predict critical fiber volume needed for strain hardening with short curauá fiber.

1.3.3 Durability studies

Due to the special matrix, free of Calcium hydroxide, which should prevent the natural fiber from petrification in cement-based composite this work investigates durability aspects. Sadly, the strain hardening behavior is lost with time, but the fiber endures. It presents insights on natural fiber behavior in the matrix (swelling and shrinking) which reduce the fiber-matrix bond efficiency and causes loss of the multiple-cracking behavior. The research provides additional information on durability challenges which hopefully will be overcome and durable strain hardening cement composite with natural fiber will be created.

2 LITERATURE REVIEW

2.1 STRAIN HARDENING CEMENT MATERIALS

The recent progress in composite materials goes along with new requirements and challenges stated by the modern industry. These requirements cannot be fulfilled by natural materials and one way to accomplish new goals is to use composite materials with tailored properties, designed especially for given implementation. These properties depend on an element and its role in construction starting from the high strength and low deformability through low weight and high insulation properties, up to enhanced toughness and temperature resistance (BRANDT, 2009). There is also a cost in design consideration included. In civil engineering usually the large volumes of material are used and the unit price is crucial, but there are several areas where the small volume of expensive high-performance material provides safety and reliability of the construction (bridge joints, beam-column joints in seismic structures, beams, lining reparation of damns and tunnels).

One of the high-performance fiber-reinforced cement-based composites (HPFRCC) is a group of composites named Strain Hardening Cement Composites (SHCC), also called Engineered Cement Composites (ECC) due to the tailoring process of the components with the support of micromechanical model. The SHCC composites are designed to demonstrate an extraordinary mechanical behavior by tensile strain-hardening behavior with multiple fine cracks below 100 μm. The SHCC present moderate tensile strength (3-8 MPa) and strain capacity (up to 3% and more) (WITTMANN et al., 2011).
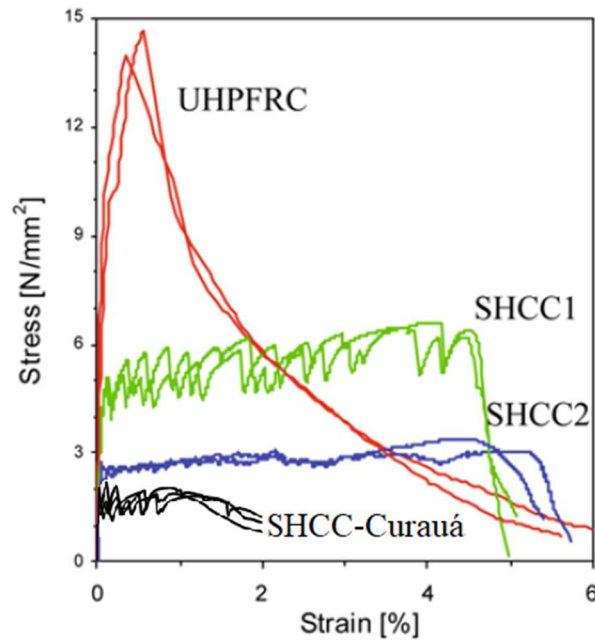
Figure 2-1 Uniaxial tensile behavior of classes HPFRCC compared to SHCC-curauá (40 mm fiber) adapted from (VAN ZIJL, 2009)

The strength and crack pattern formation in the SHCC differs from the Ultra-high performance fiber-reinforced concretes (UHPFRC), which present the high tensile and flexural strength with high compressive strength as well (180-240 MPa) but the cracks are localized in areas of weakness, where in SHCC they are distributed along the pseudo-plastic zones (VAN ZIJL, 2009). Figure 2-1 presents the classes of high-performance fiber-reinforced cement-based composites proposed by Van Zijl with the result of this research achieved for 4% of 40 mm curauá fiber.

2.1.1   Strain Hardening and Strain Softening behavior

In fiber reinforced composites, fibers' role starts after the first crack, they bridge across the cracked matrix. They are used for two main reasons. First, they can increase the composite strength by the load transfer across the crack (fiber is a mean which connects two separated matrix parts and transfer load from one part to another). This can cause ascending stress-strain curve after first cracking and it is called strain hardening behavior. Second, fibers used in composite increase its toughness, by providing the energy absorption mechanisms (deboning and fiber's pull-out across the cracks) and stress-strain

curve descending after the first crack called strain softening (NAAMAN; REINHARDT, 2003). The two behaviors are presented in Figure 2-2.
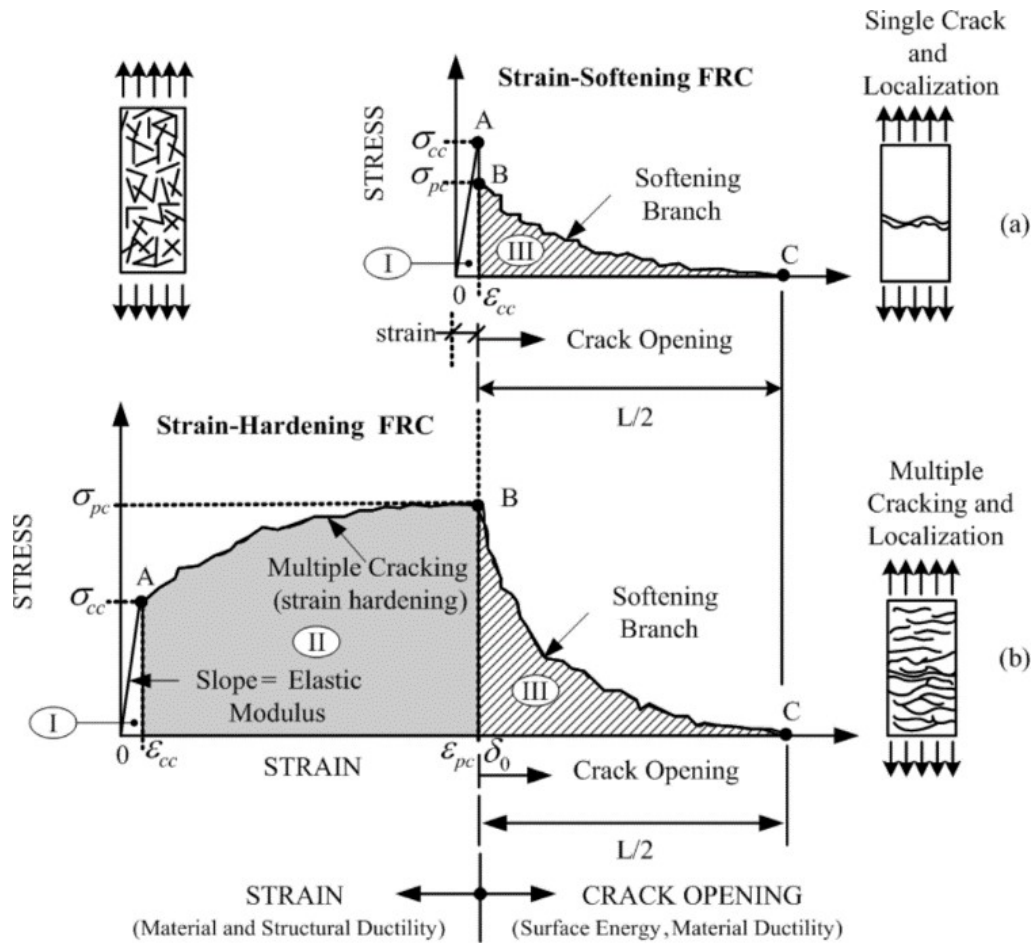
Figure 2-2 Strain-Softening (a) and Strain-Hardening (b) behavior of High Performance Fiber Reinforced Cement Composites (NAAMAN; REINHARDT, 2003).

Composite behavior after the first crack (softening or hardening) depends on the sequence of events. When a crack occurs the loads are transferred to fibers. To prevent composite failure, fibers load-bearing capacity (left side of the equation 1.1) should be greater than the load on the composite at first crack (right side) (BENTUR; MINDESS, 2007).

$$\sigma_{fu}V_f > E_m\varepsilon_{mu}V_m + E_f\varepsilon_{mu}V_f \tag{1.1}$$

When the condition is fulfilled (which means fiber volume is sufficient) the first crack will not lead to a catastrophic failure but will result in a redistribution of loads between matrix and fibers. Additional loading will cause additional cracks dividing matrix into segments connected by cracks, which is known as multiple cracking mechanism.

8

2.1.2 Tailoring strain hardening behavior with short fiber

The micromechanical model applied to the evaluation of data was developed at the University of Michigan. The model is designed for randomly oriented and discontinuous synthetic fibers in brittle matrix composites. The modeling approach is used for critical fiber volume prediction, which is sufficient for strain hardening to occur. The model combines properties of matrix, fiber, and fiber-matrix interface. It is a useful tool for composite design and provides information on particular constituents influence on critical fiber volume. The model application is used to find an optimal composition of fiber, matrix and interface properties to achieve maximum tensile ductility at the minimum amount of fiber (YANG; LI, 2010).
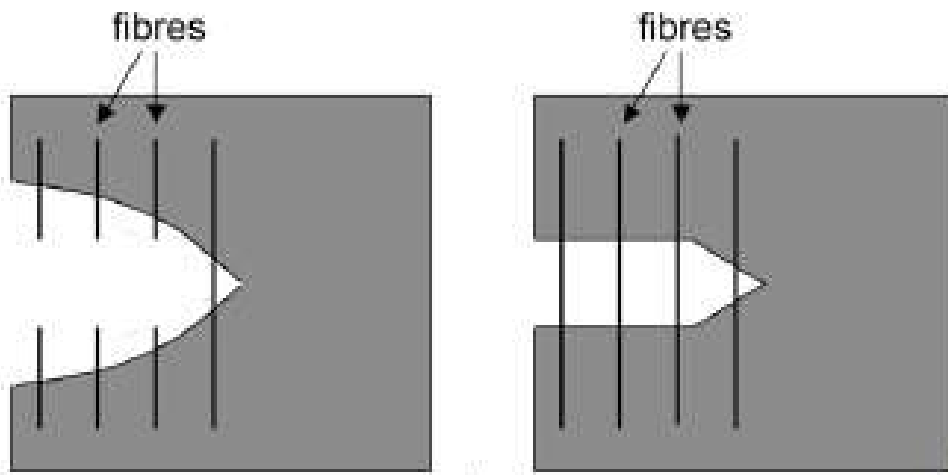
Figure 2-3 Griffith type of crack (left) versus steady-state crack (right) (SIERRA-BELTRAN, 2011).

The pseudo strain-hardening in composite appears along with multiple cracking, which divides matrix into segments connected to each other by fibers. To multiple cracking behavior occur the steady-state flat crack formation under tension is needed (Figure 2-3). This requires the crack tip toughness (J_{tip}) to be less than the complementary energy (J'_b). The two values are calculated from the bridging stress (σ) versus crack opening (δ) curve (MARSHAL; COX, 1988).
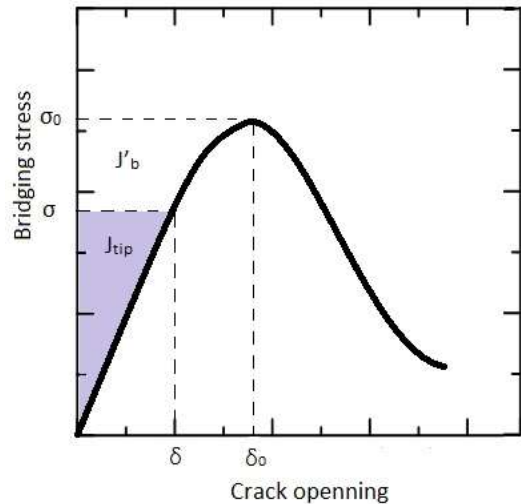
Figure 2-4 Crack tip opening curve with complementary energy (J'$_b$) and maximum bridging stress (σ$_0$) for corresponding maximum crack opening (δ$_0$).

The concept of energy criterion is presented in Figure 2-4. It involves external energy (work) with crack tip energy absorption (matrix toughness) and cracks flank energy absorption (fiber-matrix bond). This energy criterion determines the crack propagation mode (steady-state or Grifith crack). The crack width (δ) should be below maximum crack opening that fibers can bridge (δ_0), to maintain the stress level below the bridging capacity of fibers (if stress will be above δ_0 tension softening with the crack opening will occur).

2.1.3 SHCC with short natural fiber

Various polymer fibers have found application in SHCC among them: polyvinyl alcohol (PVA), polyethylene (PE), aramid or high-tenacity polypropylene (HTPP) and there is a movement to add natural fiber to this group. Here is the brief description of the two research groups working on natural fiber implementation in SHCC.

2.1.3.1 SHCC with flax and hemp fiber

The group at Ghent University (Belgium) tried to create Strain Hardening Cement-based Composite with flax and hemp 20 mm fibers with the objective to obtain a composite with self-healing properties due to controlled multiple cracking behavior. They studied various chemical treatments on fibers:

- silane primer saturation,

- soaking in a solution of benzoyl peroxide in acetone,
- mercerization in sodium hydroxide solution,
- soaking in acetic acid solution.

They used 2% of fiber by volume in their composites with presoaking the fibers for better mix workability. The realized four-point bending tests on composites verified the multiple cracking behavior under flexural load. The results presented some promising treatments for both flax and hemp fibers, especially mercerization in 2% solution of sodium oxide for 24 h worked well. The composites with fibers after mercerization presented deflection hardening behavior and average crack width lower than 30 μm for flax and 85 μm for hemp. The applied drying and wetting cycles proved self-healing properties of the composites and for cracks smaller than 30 μm healing was complete. The cracks in a range from 50 to 150 μm were healed only partially and larger cracks did not present healing (SNOECK; SMETRYNS; BELIE, 2015).

2.1.3.2   SHCC with Curauá

The very interesting approach of SHCC design with short Curauá (10-20 mm) is carried out at the University of São Paulo, where the iterative procedure lead to curauá critical fiber volume prediction of 4.4% presented in Figure 2-5 (similar to critical volume predicted by the micromechanical model used in this work).
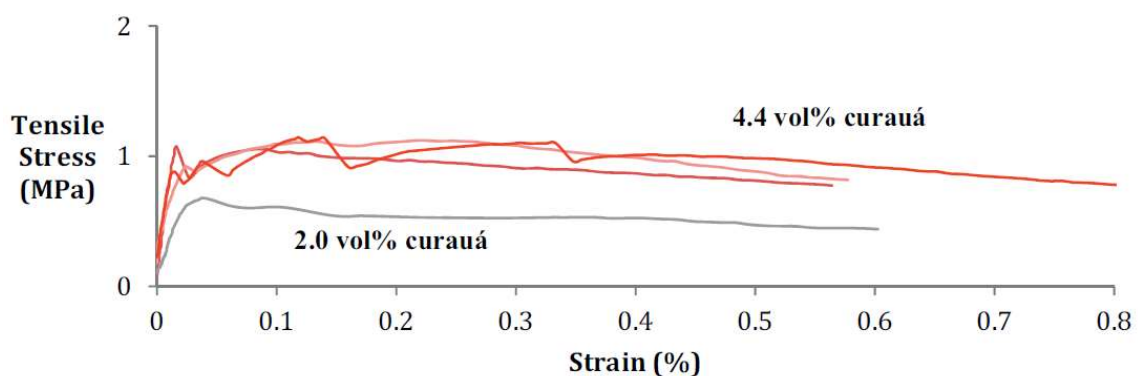
Figure 2-5 Results of iterative method for critical fiber volume prediction for 10-20 mm curauá fiber SHCC (SOLTAN et al., 2017).

The São Paulo group also used washing and drying cycles as well as combing for fiber separation from bundles. However, the technique used for fiber-matrix bond improvement was different. The silane coupling agent dosed to the matrix improved the

bonding. The strain hardening behavior was confirmed in tensile tests for various silane agent amounts, but especially the 1% admixture presented remarkable results, where the strain reached 0.8 % with the first crack strength of 1.6 MPa and ultimate strength of 2.2 MPa. The final matrix composition used for their composites included Type I Portland Cement (Alpena Lafarge Plant), along with Class F Fly Ash and Microsilica (Silica Fume) Grade 955, Vinyltrimethoxysilane (VS) coupling agent and Grace ADVA 190 water reducing agent. The application of Microsilica (Figure 2-6) was motivated as improvement of composite compressive and tensile strength, but with reduction of strain capacity (SOLTAN et al., 2017).
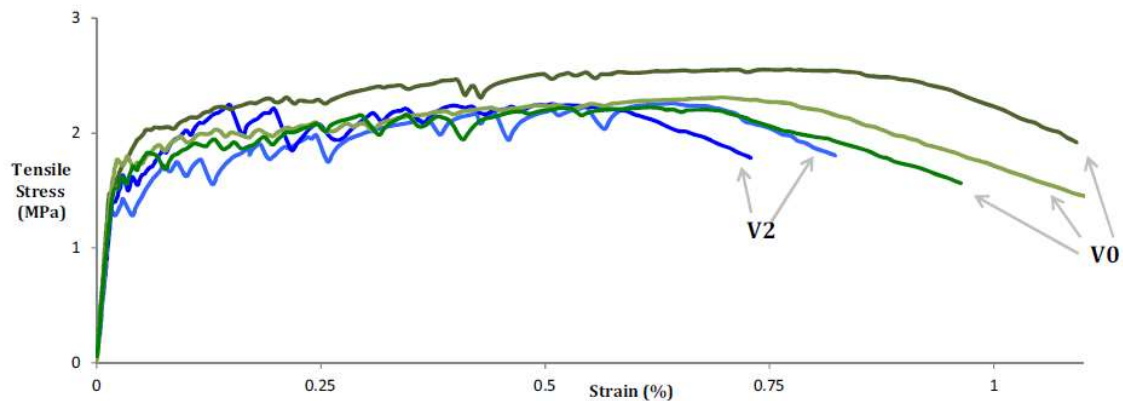
Figure 2-6 The influence of microsilica application in matrix on tensile strain capacity of SHCC with short curauá fiber and 1% of silane coupling agent, V0: no microsilica admixture, V2: 20% of microsilica admixture (SOLTAN et al., 2017)*.*

The interesting point of the comparison of São Paulo research and this work is that the two have found a solution for Strain Hardening Cement-based Composite designed with short curauá fiber. There are some similarities in fiber preparation (washing and drying or combing), but the whole procedure is different and the matrices are different. The dosage of coupling agent presented by (SOLTAN et al., 2017) presents a promising solution, a simple treatment to improve the fiber-matrix bond. This research applied alkaline treatment for calcium deposition on the fiber surface, which also improved bonding properties and reduced critical fiber volume. This research investigated the influence of fiber volume and went beyond 20 mm studying composite performance for 30 and 40 mm fiber lengths and composite durability. The durability is the most important part of the composite future application. The author roots for São Paulo group, that their composites will present durable strain hardening behavior. Sadly for this research, the

strain hardening behavior occurs for laboratory cured specimens for 28 days. The exposure to moisture movements (natural weathering, wetting and drying cycles, freeze/thaw cycles) caused fiber-matrix bond problems and strain capacity reduction.

2.1.4   SHCC application

When SHCC material used in a place of concrete, its properties lead to better control of failure mechanism, deformation capacity and damage degree of reinforced elements. As a cement-based material, SHCC can be used in various shapes adapting to formwork. SHCC finds application in structural elements like bridge decks, columns, beams and building dampers to repair material of concrete dams, water channels and retaining walls. Here are selected application of SHCC.

Building dampers

The shock absorber, a short span reinforced column with SHCC material (Figure 2-7). Used at multi-story buildings in Japan. Damper, by energy absorption and deformation capacity, increases structural safety reducing the floor drift in case of an earthquake (FUKUYAMA, 2006).
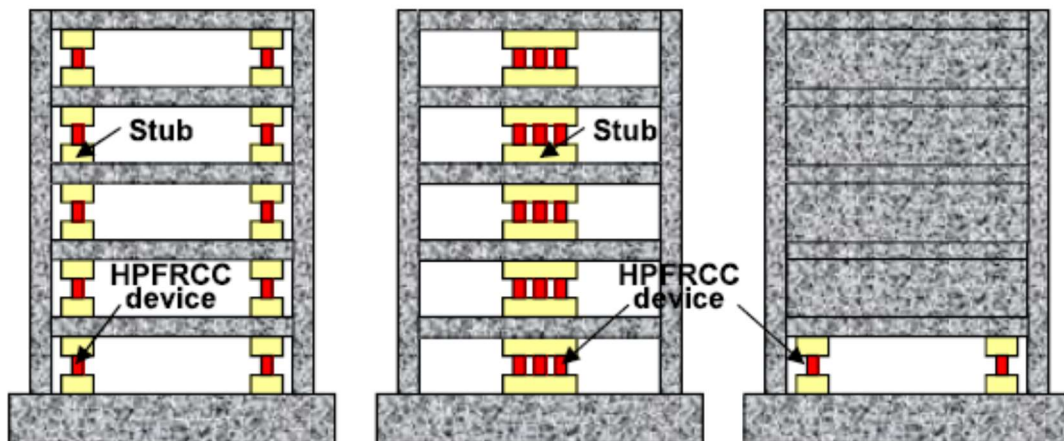
Figure 2-7 Example of SHCC material application as a dumper in design of structures with earthquake risk (FUKUYAMA, 2006).

SHCC-Reinforced beams

Reinforced members with SHCC layer or only with SHCC material are used to protect steel bars from corrosion (Figure 2-8). The multi-cracking mechanism can prevent inner reinforcement from corrosion progress due to micro-cell formation instead of macro-cell and a large anode/cathode area ratio (JAPAN SOCIETY OF CIVIL ENGINEERS, 2008).
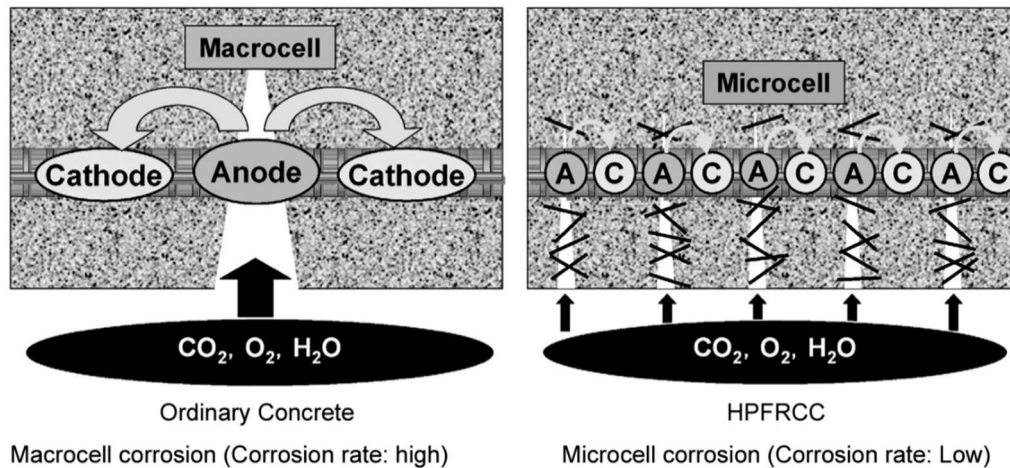
Figure 2-8 Corrosion cell pattern differences by crack development mode
(JAPAN SOCIETY OF CIVIL ENGINEERS, 2008).

Tunnel lining

SHCC material is used in retrofitting of tunnels which suffered damages (cracks, concrete flaking). SHCC material layer is applied on existing structure with additional reinforcement. Solution minimizes flaking and de-lamination of concrete. SHCC layer provides tensile resistance with a small thickness (50-70 mm), which is about a half of conventional solutions. This method was used in Ten-nou tunnel recovery after Niigata Chuetsu Earthquake (YAMAMOTO et al., 2005).

Bridge Steel Floor Deck

The Mihara Bridge in Ebetsu in Japan was constructed with SHCC layer (Figure 2-9). Intense traffic, heavy vehicles and fatigue damage was a reason to increase a thickness of reinforcement of steel floor deck with SHCC layer. The structure increased fatigue resistance due to stress reduction by a hybrid combination of steel deck and SHCC layer (MITAMURA et al., 2005).

Figure 2-9 The Mihara Bridge (RISOMIRU, 2010).

Surface Protection against Carbonation

SHCC layer can be used when paint lining type materials are applied for reinforced structures exposed to carbonation (viaducts). Paint lining materials are influenced by cracks formation in concrete member. The bigger and deeper cracks the higher risk of carbonation. SHCC works as a protective layer and increases durability by crack width control and multiple-crack pattern (MITAMURA et al., 2005).

Irrigation channel

A sprayable SHCC material was used in channel construction as a structural lining highly impermeable improving durability and water conservation. Can be easy repaired if damaged by spraying the new layer on existing one (LI; FISHER; LEPECH, 2009).

Dam reparation

SHCC material was used as an overlay layer an aged concrete surface of Sanko dam, Japan (KOJIMA et al., 2004).

2.2 Natural Fiber

2.2.1 Introduction

Natural vegetal fibers are a broad group of fibers and the main division is based on the origin as in Figure 2-10 (KICIŃSKA-JAKUBOWSKA; BOGACZ; ZIMNIEWSKA, 2012). The most common type of fiber used in cement composites is a plant type fiber. Regards the type of the plant and part it has been taken the fibers can vary in properties like tensile strength, elongation, modulus of elasticity.
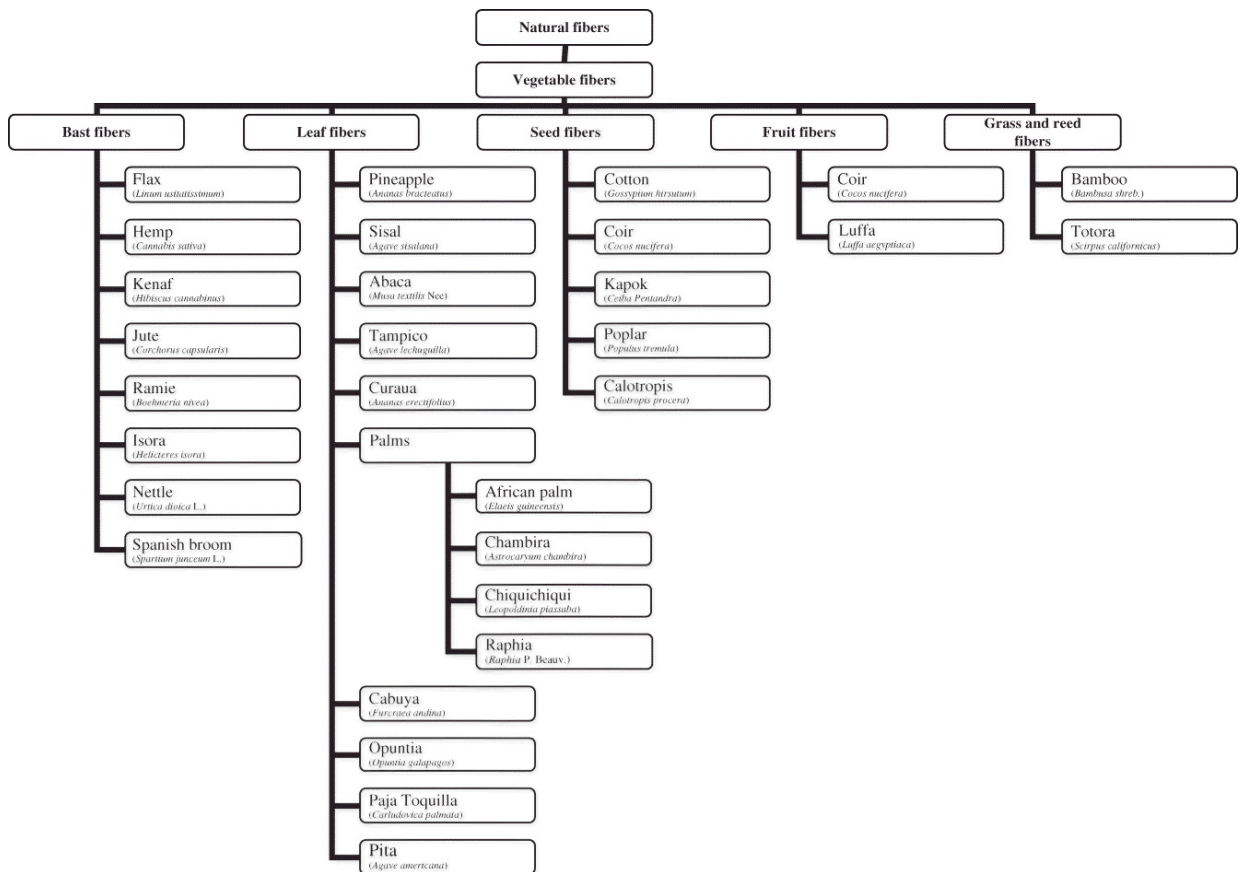
Figure 2-10 Natural vegetable fibers

(KICIŃSKA-JAKUBOWSKA; BOGACZ; ZIMNIEWSKA, 2012)..

Natural fiber is a combination of fibrils with layered structure (primary cell wall and secondary wall divided into three layers around the lumen) as in Figure 2-11. The middle layer of the secondary cell walls determines the mechanical properties of fiber (fiber strength is correlated with the microfibril angle and cellulose content). The microfibril angle is the angle between the axis of the fiber and microfibrils. Smaller the angle higher the strength and stiffness, larger angle higher ductility (DEFOIRDT et al., 2010).
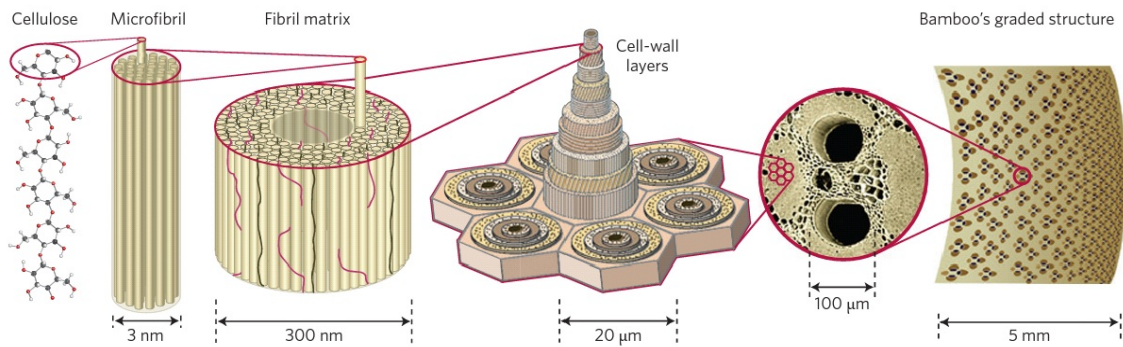
Figure 2-11 Hierarchical structure of natural fiber on bamboo fiber example from
(WEGST et al., 2015).

The natural structure differs between particular plants, for example, sisal fiber has a visible lumen, when curauá fiber present more squeezed structure. Also within the leaves are differences, where fibers can have a different shape, for example horseshoe and star shape in case of curauá. The extraction process can deform the fiber. Mechanical properties will also depend on leaf section they were extracted as well as plant environment conditions (Table 2-1) (DITTENBER; GANGARAO, 2012).

Table 2-1 Influence factors on natural fibers quality adapted from
(DITTENBER; GANGARAO, 2012).

Stage	Factors
Cultivation	Plant species, Cultivation, Localization, Climate, Insolation.
Harvest	Fiber maturity (Whole plant or selected leaves).
Fiber extraction	Chemical processes, Mechanical extraction.
Supply	Transport conditions, Storage conditions, Age of fiber

Mechanical properties vary among different natural fibers. Some of the fibers are considered low performance when the tensile strength is low (below 600 MPa). The other called high performance present better tensile strength (above 600 MPa) and seems to have much more chance to find application in cement composites as reinforcing fibers (SILVA; CHAWLA; TOLEDO FILHO, 2008). Here are selected examples from

17

literature of various types of fibers and their mechanical properties. Table 2-2 presents clearly that steel fiber properties are far beyond the capacity of natural fiber, but PVA fiber is not so far and exists a possibility for substitution of synthetic PVA by natural fiber.

Table 2-2 General properties of selected fiber.

Fiber	Specific gravity (g/cm³)	Tensile Strength (MPa)	Elastic Modulus (GPa)	Deformation (%)	Source
Hemp	1.48	550 - 900	70	1.6	(LI; TABIL; PANIGRAHI, 2007)
Bamboo	1.38	720 - 910	33	2.9	(DEFOIRDT et al., 2010)
Jute	1.39	300 - 400	26	1.6	(DEFOIRDT et al., 2010)
Sisal	1.33	230 - 860	17	2.8	(SILVA, 2008)
Curauá	1.44	490 - 770	38	2.1	(FERREIRA, 2016)
PVA	1.30	1200 - 1600	40	-	(NYCON, 2016)
Steel	7.85	1050 - 2000	210	-	(SAHIN; KOKSAL, 2011)

2.2.2 Natural fiber composition

Natural fibers are mainly composed of cellulose, lignin, and hemicellulose. Other components are pectin, oil, and waxes (JOHN; THOMAS, 2008). All the chemical components are formed thanks to photosynthesis in the leaves (SWAMY, 1988). The table 2-3 presents the chemical composition of selected fibers.

Table 2-3 Chemical composition of selected natural fibers.

Fiber	Cellulose (%)	Hemicellulose (%)	Lignin (%)	Source
Sisal	73	10	7.6	(SYDENSTRICKER et al., 2003)
Jute	65	17	14	(WANG; CAI; YU, 2008)
Curauá	58.8	23.8	14.7	(FERREIRA, 2016)

Cellulose, natural polymer built with carbon, hydrogen, and oxygen, is the most important structural component of natural fiber. It is resistant to alkalis, dilute acids and oxidizing agents, but is susceptible to chemical treatments. The higher amount of cellulose in fiber the higher is tensile strength and the modulus of elasticity of fiber (YOUNG et al., 1998). Hemicelluloses are lower molecular weight polysaccharides and they are a cementing factor between cellulose microfibrils (AZWA et al., 2013). Hemicellulose is soluble in alkalis and presents high water absorption capacity. Hemicellulose has an amorphous

structure and is prone to degradation by dilute acids and alkali (JACOBSEN; WYMAN, 2000).

Lignin is a complex hydrocarbon polymer and is responsible for plant's rigidness (bonding between cells) and water transport (it has hydrophobic nature). Lignin is also responsible for yellowish color and does not improve fibers strength, however, it is resistant to most microorganisms attack. It is soluble in alkali solutions and can be removed in the bleaching process (BENTUR; MINDESS, 2007).

Wax and oil's function is the fiber protection and they are present on the fiber surface (WONG; YOUSIF; LOW, 2010). They can be removed with impurities present on fiber surface by immersion in alkali solution (TOLEDO FILHO et al., 2000).

It is considered that the natural fibers with higher cellulose content, the higher degree of polymerization, longer cell length and lower microfibril angle has higher mechanical performance (strength).

Derfordt correlated fibers (coconut, bamboo, and jute) tensile strength with cellulose content as the main factor. The microfibril angle is proportional to deformation capacity (microfibrils tend to align before the break, smaller the angle less capacity to align, smaller elongation) and elasticity modulus is proportional to cellulose content and invert proportional to microfibril angle (DERFORDT et al., 2010).

2.2.3 Natural fiber durability

Application of natural fibers in cement composites is related to higher risk of fiber degradation in comparison to synthetic fibers. A comparison example of PVA fiber, which is considered chemically stable and presets high strength retention in acid solutions and organic solvents. The estimation based on tests carried by (HOSHIRO; NISHIYAMA; YAMAMOTO, 2006) which correlated tensile strength variation and UV absorption of PVA fibers immersed in hot alkaline water, shows the tensile strength retention of 100% in 60 years and 97.5% in 120 years. This opens an important chapter in PVA fiber substitution by natural fiber, which is durability. The natural fiber degradation depends on the environment condition. The Figure 2-12 presents the fiber's components susceptible to the environmental hazard.

Figure 2-12 Compounds responsible for natural fiber properties adapted from

(AZWA et al., 2013).

In composite natural fibers are susceptible to: natural weathering due to moisture movement, degradation in the alkaline environment, and biological attack and mineralization in a cement matrix. Ultraviolet radiation seems to have an influence on fiber mostly during the production process (fibers dry outdoor exposed to sun). Natural fibers which present higher mechanical performance (the higher cellulose content, the higher degree of polymerization, the longer cell length and lower microfibril angle) probably will be also more durable in cement matrix in comparison to low-performance natural fibers.

2.2.3.1 Humidity

The water movement occurs along a fiber, from a matrix to fiber and from fiber to matrix. Because of that movement fiber can swell or shrink in a matrix, which can have influence on fiber-matrix bond. It is considered that fibers tend to "steal" water from the mix, but after they put it back to matrix, and they play role of water residue in composite. This phenomenon is used in design of self-healing cement materials at TU Delft. The moisture absorption of natural fibers is related to hemicellulose content (METHACANON et al., 2010). The higher hemicellulose content the higher absorption of water. Moisture content in fiber influence the degree of crystallinity, crystalline orientation, tensile strength, swelling behavior and porosity of fibers as well as increase the possibility of biodegradation by the microbial attack (JOHN; THOMAS, 2008). Fibers absorption capacity can be reduced by alkaline treatment (i.e. potassium hydroxide (KOH) or sodium hydroxide (NaOH)). Alkaline treatment is used to decrease hydrogen bonding capacity of cellulose and eliminate open hydroxyl groups which tend to bond with water molecules. Alkaline treatment dissolves hemicellulose, which reduce moisture absorption capacity of fiber (DITTENBER; GANGARAO, 2012).

After mentioning the importance of moisture on natural fibers it is reasonable to consider that in composite fibers durability will depend on humidity. With higher humidity, fibers lose stiffness and become more ductile. Their strength decreases and they may reach higher ultimate strain, but there is a reduction of elasticity modulus when compared to dry fibers (UZOMAKA, 1976) and (MAI; HAKEEM, 1984).

In dry composites, natural fibers present a fragile failure mechanism (there is a characteristic sound of fiber rupture related to rapid energy release). Saturated composites present fiber pull-out mechanism. The interfacial transition zone (ITZ), the vicinity of fiber in matrix, is a zone where fiber and matrix influence each other. The matrix elements can penetrate fiber, connect to fiber when water, waxes, oils from fiber can influence matrix. The denser interfacial transition zone, the higher possibility of fiber fracture (matrix-fiber bond stronger than fiber tensile strength). When vicinity of fiber is more porous pull-out behavior is more likely to occur. In other words the denser matrices can difficult multi cracking behavior of composite, or will require more resistant natural fiber to prevent fiber fracture before pull-out. Interfacial transition zone properties change with time, where aged matrix tend to compress/squeeze fibers by continuing precipitation of hydration products around the fiber. The moisture movement can result in mineralization

of fiber leading to deposition of calcium hydroxide in lumen and voids of fiber cells as in Figure 2-13 where coconut fiber-matrix ITZ was compared after 28 days to specimen subjected to 25 cycles of wetting and drying (TOLEDO FILHO et al., 2000).
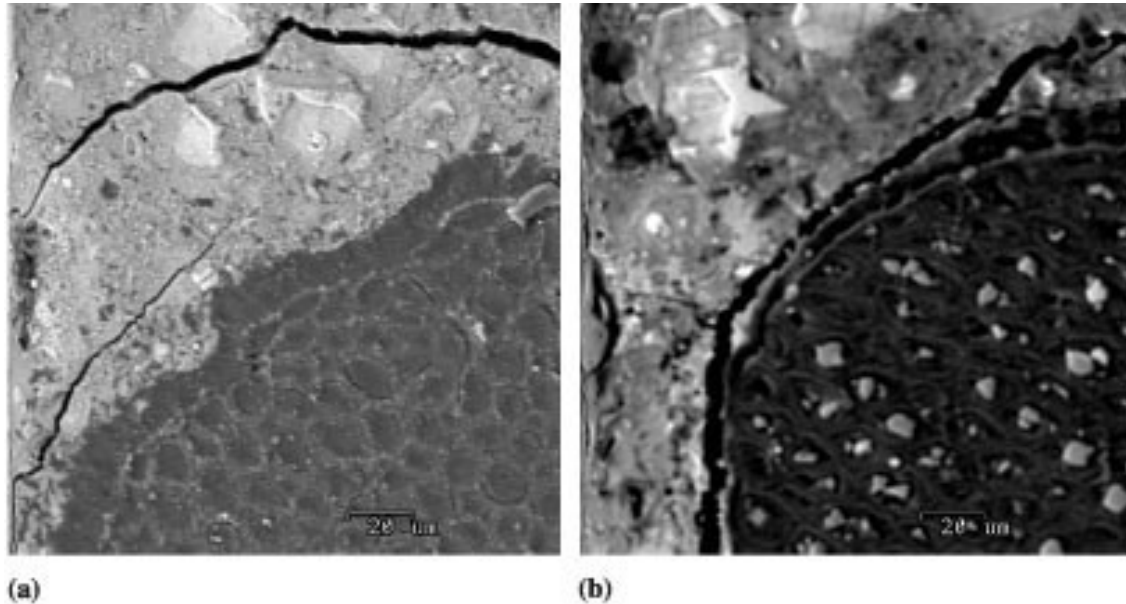
Figure 2-13 Fiber-matrix ITZ: (a) coconut fiber–mortar interface zone for a specimen 28 days old; (b) coconut fiber–mortar interfacial zone for a specimen subjected to 25 cycles of wetting and drying (TOLEDO FILHO et al., 2000).

2.2.3.2 Thermal resistance

Cellulose and lignin are two components most important to fire degradation. The higher cellulose content the higher flammability. The more lignin the more char formation. From fibers structure point of view, high crystallinity and lower polymerization improve fire resistance. Most of the natural fiber decomposition (60% of the mass fraction) occurs in temperature between 215-310° C (MELO FILHO; SILVA; TOLEDO FILHO, 2013). The thermal decomposition of natural fibers was divided into three stages by various authors, the Table 2-4 presents the collected data.

Table 2-4 Stages of natural fiber thermal decomposition.

Stage 1	Stage 2	Stage 3	Reference
50–100° C: Evaporation of moisture in the fibers	200–300° C: Decomposition of hemicelluloses	400–500° C: Weight loss due to lignin and cellulose degradation	(ARAÚJO; WALDMAN; PAOLI, 2008)
300° C: Corresponds to the thermal decomposition of hemicellulose and the glycosidic links of cellulose	360° C: Corresponds to the thermal decomposition of α-cellulose	200–500° C, max 350° C: Lignin peak is wider and appears superposed on the other two peaks	(MANFREDI et al., 2006) (ALVAREZ; VÁZQUEZ, 2004)
250–300° C: Characteristic of low molecular weight components, such as hemicelluloses	300–400° C: Corresponds to the thermal degradation of cellulose	Near 420° C: Due to lignin decomposition	(LEE; WANG, 2006)
220–315° C: Pyrolysis of hemicelluloses	315–400° C: Pyrolysis of cellulose	160–900° C: Pyrolysis of lignin	(SUARDANA; KU; LIM, 2011)

2.2.3.3 Chemical degradation

Two major degradation mechanisms of natural fiber in an alkaline environment are peeling off and alkaline hydrolysis. Peeling off mechanism (in temperatures below 75° C has reduced influence on fiber) is a liberation of end groups of the molecular chain due to reducing end groups and OH- ions. Alkaline hydrolysis influences most hemicellulose and lignin reduces the degree of polymerization by dividing molecular chain. Both components are mostly in the walls of fibers, so degradation breaks the link between individual fiber cells and reduces their reinforcing efficiency (Figure 2-14 and 2-16). Alkaline influence is less significant in pulp fibers, where the middle lamellae is removed (lignin and hemicellulose) in chemical treatment (GRAM, 1983) and (GRAM, 1986)
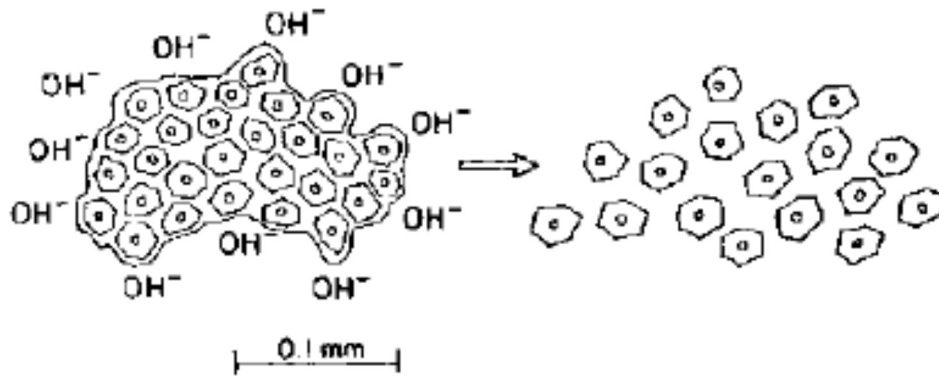
Figure 2-14 Degradation of sisal fibers in concrete environment, by the decomposition and dissolution of the middle lamellae in the alkaline pore water (GRAM, 1983).

In cement composite natural fiber degradation mechanism are fiber mineralization and degradation of fiber components. Mineralization is caused by precipitation of calcium hydroxide in fiber cell and on the fiber surface. Degradation of cellulose, hemicellulose, and lignin occurs due to calcium and hydroxyl ions adsorption (Figure 2-15). Degradation process begins rapidly and after 10 cycles of wetting/drying and the composite flexural behavior is modified (MELO FILHO; SILVA; TOLEDO FILHO, 2013).
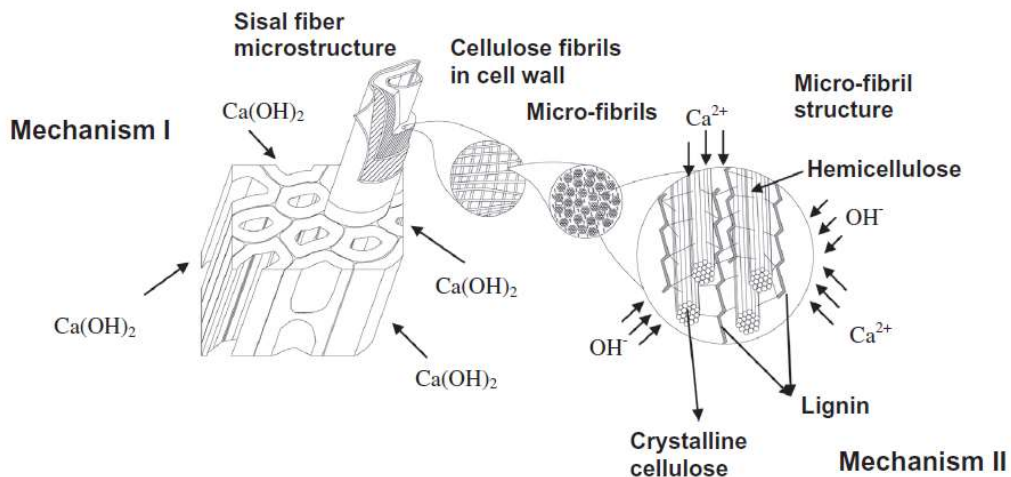
Figure 2-15 Natural fiber degradation mechanisms inside cement matrix
(MELO FILHO; SILVA; TOLEDO FILHO, 2013).

One of the possibilities to prevent the fiber from degradation is the immersion of fibers in silica fume slurry before casting (TOLEDO FILHO et al., 2003). Another fiber treatments can improve fiber durability such as water repellant agents (formine and

stearid acid) or polymer coating. The latter seems to be an interesting possibility of fiber protection from matrix environment as well as improve the fiber-matrix bond.

NUMATS.PEC0355   2015/10/09   A L   D11.3 x250   300 um
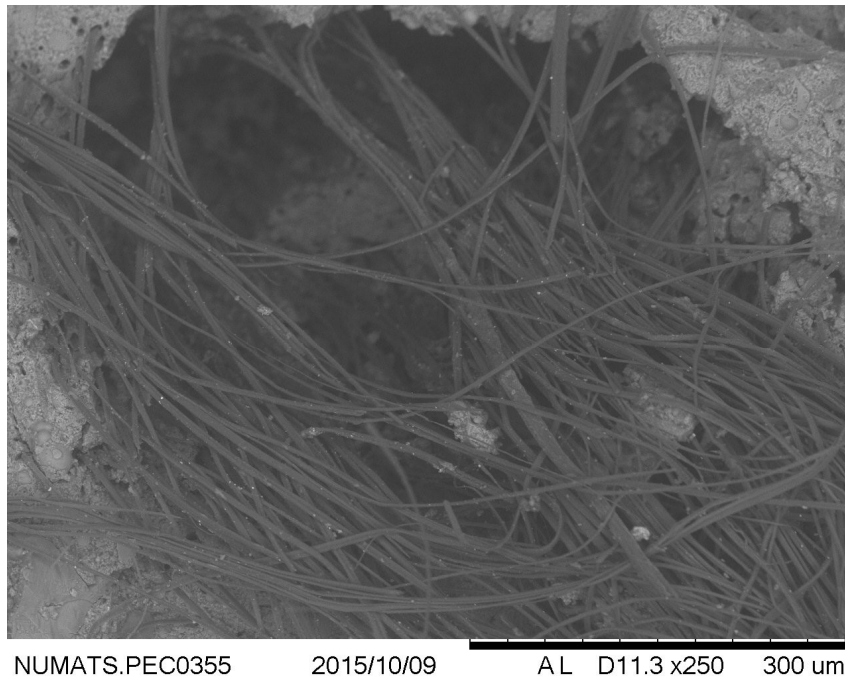
Figure 2-16 Fiber defibrillation after exposure to highly aggressive alkaline environment (80° C and alkali solution for 6 hours).

There is also a possibility of matrix modification and cement replacement by silica fume to improve the durability of natural fibers because of matrix alkalinity reduction (fly ash is not effective). Another possibility is to use alumina cement matrix, but the cost could overcome benefits. One of most promising matrix modification is partial replacement of cementitious matrix by calcined clays to reduce calcium hydroxide content in composite (TOLEDO FILHO et al., 2009), (SILVA et al., 2010).

2.2.3.4   *Biological degradation*

Bacteria and fungi can grow in the humid environment. They can attack fiber in the natural state when stored in improper conditions (no ventilation, humid storages) as well as in composite when wetting and drying occurs in a warm climate. The matrix alkaline nature seems to prevent composite from biological risk (UZOMAKA, 1976). However, matrix alkalinity reduction could increase the risk of biological attack.

2.2.4 Curauá Fiber

The curauá, *Ananas comosus* var. *erectifolius* (L. B. Smith), is a type of pineapple plant with a small fruit mostly cultivated for the leaves. It has unarmed and straight erected leaves. When ready to harvest a leaf reaches about 1.5 m length and about 83 grams of weight. There are two most common types of curauá in cultivation. The first with green leaves called white curauá. The second with reddish-purple leaves called purple curauá. Curauá is an easy cultivation plant, which needs hot and humid climate to grow but is very susceptible to cold weather (REIS; LAMEIRA; CORDEIRO, 2004). It can be cultivated on sandy and sandy-clay soils. It has been seen that curauá can grow along the paricá tree (Figure 2-17) and can be used in reforestation areas. In Brazil, it is cultivated in the North, the native area of curauá.

Figure 2-17 Curauá plant with paricá tree plantation.

Curauá plant has been discovered by the native people of Amazonia, where the leaves were used to reinforce boats (canoes) and to make hammocks. The bromelain present in the leaves is used in medicine to heal wounds (SILVA et al., 2014). However, the most promising application is fiber extracted from leaves. Fiber production starts one year after plantation with a break in 5-6 years due to the lifecycle of a pant. Each harvest is manual (leaf by leaf) and gives 12-25 leaves from one plant, which is about 2 kg of fiber (RAMALHO, 2005), (ADRADE et al., 2011).

(a)   (b)   (c)

Figure 2-18 Curauá fiber extraction, (a) machine used to fiber separation from leaves, (b) mucilage (residue after fiber extraction, (c) curauá fiber drying in the sun.

Fibers are extracted by a mechanical process as illustrated in Figure 2-18. After extraction, the fibers are washed to remove residues and impurities. This residue is called mucilage (sap and fiber pieces) and is used as a nutrition component for animal or organic fertilizer after water dilution. Mucilage can be also used with fiber in recycled paper production (BRAGA et al., 2010). The washing process is important for fiber properties because residues can cause fungus growth on fibers and reduce their resistance. After washing, fibers are dried for 48 hours in natural conditions and then tied into bundles ready to distribution for future use.

The demand on curauá fiber has been growing since it was used in automotive industry as an ecological alternative to glass fibers. With a low initial capital, it is considered as a possibility to improve the economic condition of agriculture states in Brazil (ADRADE et al., 2011). That is why there is been a wide movement to increase curauá plantation among farmers in the state of Pará. Another reason is to decrease deforestation of Amazon rainforest by providing an alternative plant that could grow along with other species and

will provide an additional income (CORDEIRO et al., 2009) . Curauá plant tolerates the soil with low pH and low fertility and does not require high initial cost and qualified workforce. The fiber production reaches of 800 kg per hectare (LOPES, 2015).
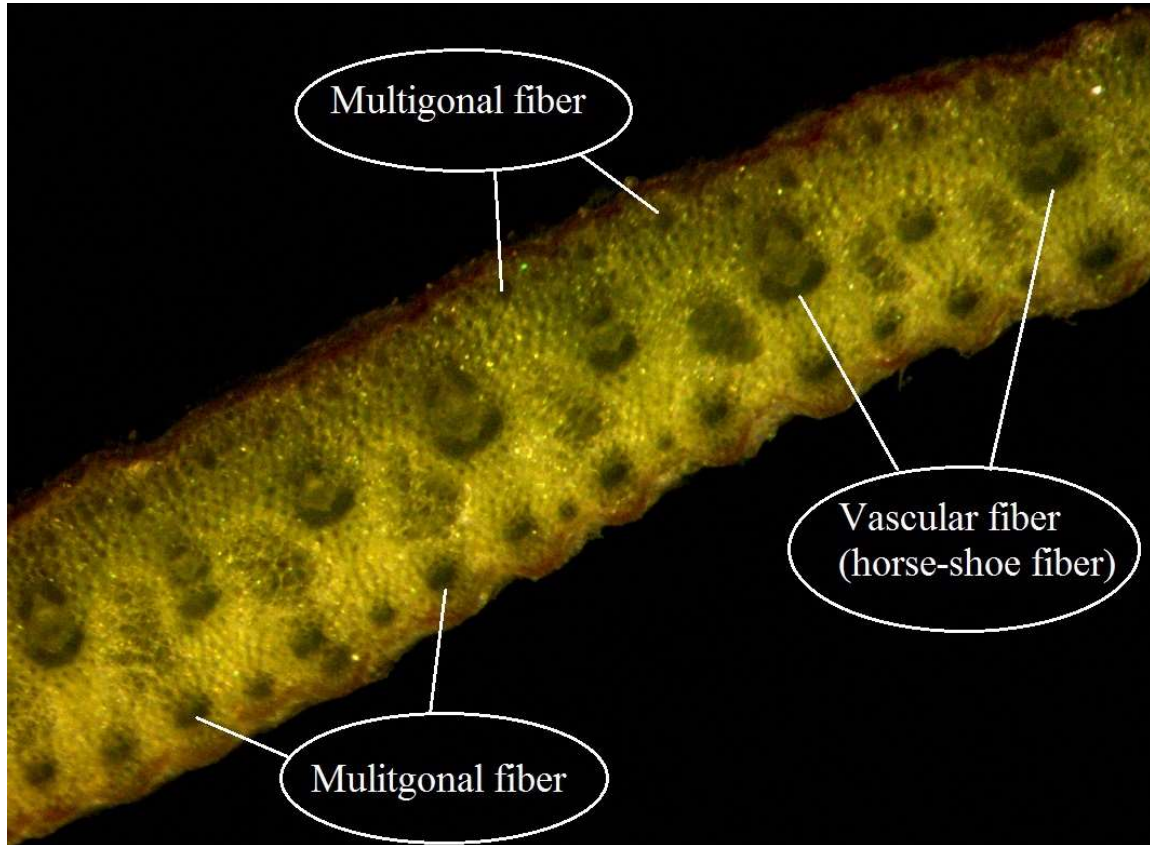
Figure 2-19 Curauá leaf cross-section under optical microscope.

The leaf contains two types of fibers (Figure 2-19 and 2-20). The first, polygonal fiber (located at both leaf edges) provides stiffness and strength. The second, arch or horse-shoe fiber, also called the vascular fiber, is located in the middle of the leaf cross-section and is responsible for water and nutrients transportation (OLIVEIRA et al., 2008) The diameter of the curauá fiber varies 60 to 120 μm.

(A) Multigonal fiber 200μm   (B) Vascular (horse-shoe fiber) 200μm
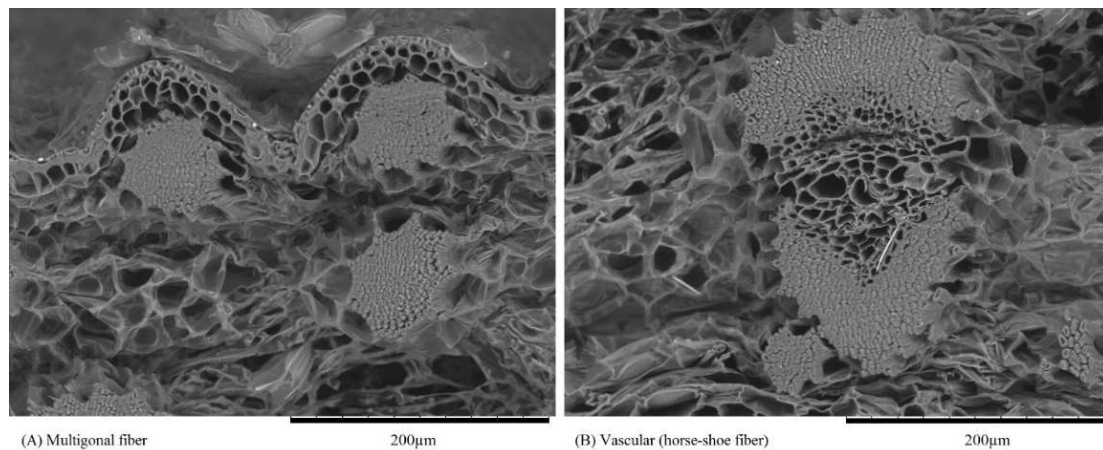
Figure 2-20 Two types of curauá fibers in a leaf: (A) polygonal, (B) vascular (horse-shoe) fiber.

This variety of fiber in one leaf could explain why in the literature properties of curauá fiber vary so much. From a research point of view it could be interesting to compare the strength of vascular and polygonal fiber also the comparison between polygonal fiber from internal and external leaf's part but at this point, it is beyond the scope of this work. Even if one type of fiber will present better mechanical properties, the process of extraction makes difficult to separate selected group of fiber and it will include an effort to do so which could cut economic benefits of using the natural fiber.
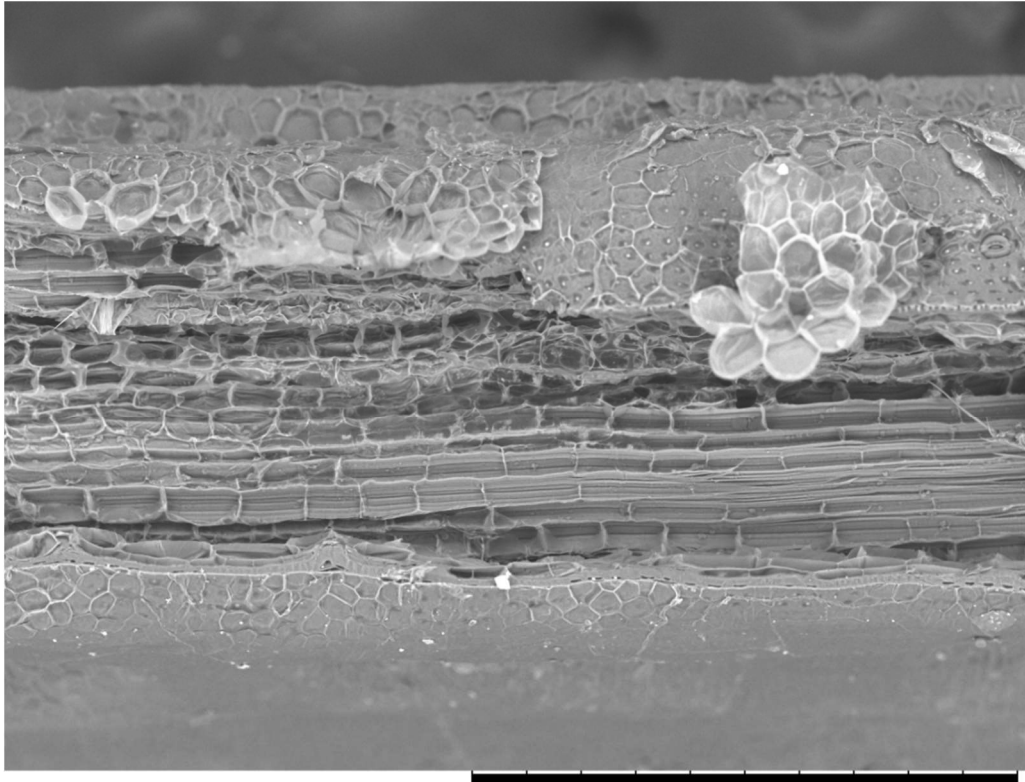
Curauá fiber in the leaf   0.5mm

Figure 2-21 Curauá fiber in a leaf with visible wrinkles on its surface.

The curauá fiber surface has characteristic wrinkles or ribs which are imprints of plant cells connected to the fiber (Figure 2-21). The curauá fiber surface could remind the ribbed steel bars. The ribbed surface of curauá fiber could be beneficial for pullout properties. The ribs working as anchors in the matrix during pullout process should increase frictional bond. From the other hand, the ribs created from hemicellulose are definitely soft part of fiber so the impact of wrinkled structure could be much more related to deposition of matrix products between ribs of the fiber surface.

3 MATERIALS

3.1 MATRIX

3.1.1 Materials

Materials used during this research were characterized at Laboratory of Structures and Materials (Labest) of COPPE/UFRJ. The chemical composition of binders was determined by spectrometry analysis of X-ray diffraction (EDS) at Shimadzu EDX 720. The specific gravity of materials was determined by helium pycnometer from Micrometrixs (AccuPyc 12340).

The Cement Mauá CP II F 32 used for this research was produced by Holcim-Lafarge. According to Lafarge specification, this type of cement contains limestone filler, which helps regulate physical properties. The Cement Mauá is recommended for structural and conventional concretes, mortars, concrete injections, and prefabricated elements. Specific gravity was estimated as 3.10 g/cm^3.

Metacaulim HP Ultra produced by Metacaulim do Brasil and was used to provide effective pozzolan reaction with calcium hydroxide Ca(OH)$_2$. Specific gravity was estimated as 2.29 g/cm^3

Fly ash produced by company PozoFly (Tubarão in Santa Catarina, Brazil of the specific gravity estimated as 2.81 g/cm^3.

The results of chemical analysis of cement, fly ash and metakaolin used in this research are presented in Table 3-1.

Table 3-1. Chemical composition in % of Cement (CP II F-32), Fly ash (PozoFly), Metakaolin (Metacaulim HP Ultra).

Oxide	CP II F-32	Fly Ash	Metakaolin
SiO_2	13.643	51.580	51.857
Al_2O_3	3.776	28.240	41.692
Fe_2O_3	-	-	1.915
K_2O	0.386	3.390	1.895
SO_3	3.968	1.510	1.091
V_2O_5	-	-	0.048
ZrO_2	-	-	0.039
Ta_2O_5	-	-	0.025
Cr_2O_3	-	-	0.019
Rb_2O	-	-	0.080
Ag_2O	-	-	0.007
MnO	0.064	1.510	0.006
ZnO	0.050	-	0.006
SrO	0.299	-	0.003
NbO	-	-	0.002
Y_2O_3	-	-	0.002
Ga_2O_3	-	-	0.002
TiO_2	0.299	1.300	-
CaO	73.090	1.940	-
CuO	0.019	-	-

River sand of 2.70 g/cm^3 specific gravity was used for composite casting, sieved on the 212 μm sieve (Figure 3-1). The sieve process was applied to eliminate the bigger grains and provide more fine sand, beneficial for fracture propagation in composite.
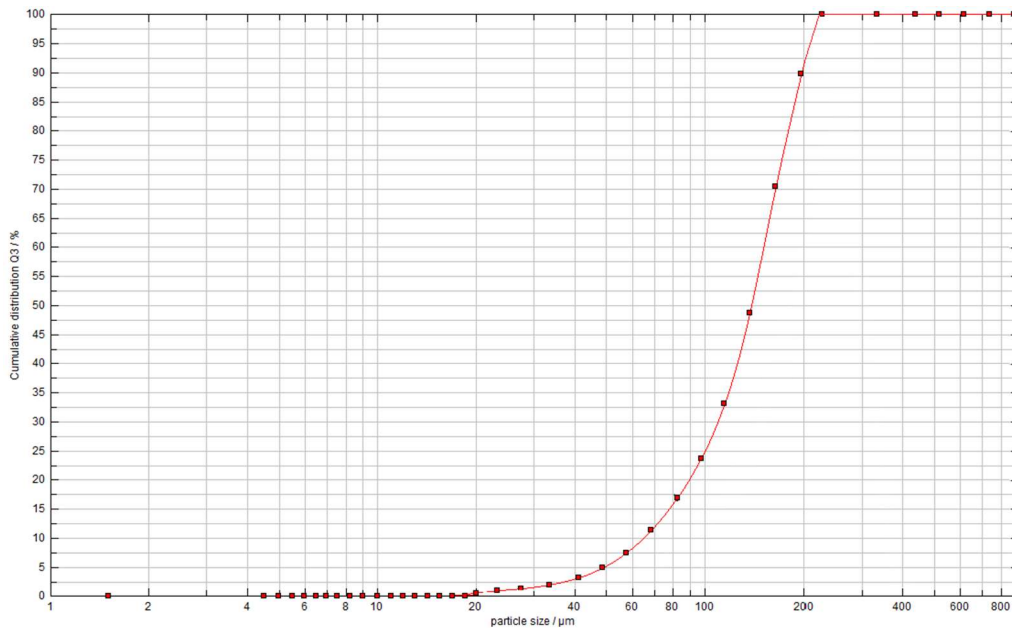
Figure 3-1. Granulometry result for sand used for composite casting.

3.1.2 Composition

The matrix used for this research was designed as a calcium hydroxide free matrix due to improvement of natural fiber durability in a cement matrix environment (petrification prevention). The mix proportions by weight were estimated at 1:0.5:0.4 (binder : sand : water/binder ratio). The binder was composed of 33% of Portland Cement CP II F-32 with 27% of metakaolin and 40% of fly ash. Superplasticizer Glenium 51 (type PA) with solids content of 31% was used. To cast composites, a viscosity modifier Rheomac UW 410(manufactured by BASF) at a dosage of 0.87 kg/m^3 was used in order to avoid segregation and bleeding during molding. The matrix composition for 1 m^3 is presented in Table 3-2.

Table 3-2. Matrix composition for 1 m^3.

	Cement	Metakaolin	Fly Ash	Sand	Water	Glenium	Rheomac
kg/m^3	361.85	289.85	434.22	542.78	417.97	24.67	0.87

3.2 FIBER

3.2.1 Fiber supply and storage

The fiber used for this research was provided by Pematec (Santarem, Pará). The company which works with individual farmers providing seedlings for curauá cultivation and collects fiber bundles for commercial use. The raw fibers used in this work were stored in a closed room prepared for natural fiber storage (dry condition of 40º C). The fibers in bundles were stored in paper boxes as it came from a provider and removed in amounts that served research purposes.

3.2.2 Hot water washing cycle

The dry fiber in bundles is added to tap water at room temperature and heated (the temperature during the boiling stage reaches 80º C and is maintained for three hours in stainless steel pot. After three hours, the heating is off and fiber with water cools down in room temperature for 3-5 hours to be maneuvered manually to the dryer. The drying occurs for 24 hours at 40º C. This procedure is considered as one cycle of washing and drying.

3.2.3 Fiber combing and cutting

After washing cycles, the fiber is combed to separate single fibers from a bundle. The process was carried out manually at the timber board with nails used as a comb. All fibers tested for properties passed combing phase as a necessary condition for future implementation in composite and to prevent fiber agglomeration. There is no certainty about the influence of combing process on fiber properties. From one hand, it should separate the strong fibers from the weak ones (which stay at the comb). From the other hand, it introduced a tension on fiber bundle during combing, which could cause microdamage in fibers (which was not investigated in this study). The residue after combing can be used in gardening works in mat form, or shredded in pieces and mix with soil to improve aeration and water retention. For the price of 1-1.5 USD for 1 kg of fiber in a bundle (SOLTAN et al., 2017), there is 600 g of combed and chopped fiber ready to use in composite and 400 g of residue which can be reutilized. After combing the fiber was manually cut by scissors to desired lengths. The fiber before and after the combing and cutting is presented in Figure 3-2.

Figure 3-2 The fiber preparation: fiber bundle (left), cut fiber (middle), residue (right).

3.2.4 Alkaline immersion

The alkaline immersion was the second stage treatment on curauá fiber. The washed fiber (after combing and cutting) was immersed into alkali solution of Calcium hydroxide with water for 60 minutes. After that time water was removed and fiber was dried at 40º C for 24 hours and used for casting. Due to the possibility of calcium penetration inside the fiber with time, the procedure was controlled to avoid different times of exposure to the alkaline solution or drying periods which could have an effect on fiber properties. The time of the exposure, time of drying was not the subject of this study. These parameters ware based on research carried at COPPE, UFRJ (FERREIRA et al., 2015).

3.3 COMPOSITE

3.3.1 Casting

The procedure of composite casting was divided into following steps:

- 30 seconds of dry ingredients mixing.
- 30 seconds of admixture of water during mixing.
- 60 seconds of admixture of 50% superplasticizer with increased speed of mixing.
- 30 seconds of adding of 50% superplasticizer with reduced speed of mixing.
- 60 seconds of mixing.
- 60 seconds of rest.
- 120 seconds of fiber addition.
- 60 seconds of mixing.
- Casting into molds.
- 30 seconds at vibrating table.

3.3.2 Curing

The composites curing was carried at closed plastic bags with inner wet paper towels as a moisture provider. The composites were stored in the chamber of $21°$ C temperature for 28 days then they were taken out of the bags and adjusted for machine set up dimensions before the tests. In case of the dog bone and plate specimens, the surface was polished. In case of the cylinders, the bases were polished to provide the uniform surface for applied load.

4 THE INFLUENCE OF HOT WATER WASHING CYCLES ON TENSILE PROPERTIES OF CURAUÁ FIBER

Chapter 4 presents the influence of hot water treatment on the tensile strength of natural curauá fibers and its dimensional changes. In this chapter, the monotonic tensile behavior of natural and treated curauá fibers have been studied. Tensile tests were performed on a microforce testing system using four different gage lengths: 10, 20, 30 and 40 mm. The cross-sectional area of the fiber was measured using scanning electron microscope (SEM) micrographs and image analysis. The measured Young's modulus was corrected for the machine compliance. Weibull statistics were used to quantify the degree of variability in fiber strength at the different gage lengths. Furthermore, the time length of the hot water treatment was investigated. The fibers were divided into three groups: reference, 9 hours and 18 hours of treatment in hot water (80° C) with water being changed every 3 hours. This process was applied to remove the wax, impurities and plant residues from the surface of the fibers. The used treatment increased the tensile strength of the fibers and, after 18 hours, caused a notable cross-sectional area reduction.

The results gathered in this chapter were presented as an oral presentation at 17th International Conference on Non-Conventional Materials and Technologies "Construction for Sustainability Green Composites & Technologies", NOCMAT XVII, November 26-29th, Mexico, 2017.

4.1 TENSILE TESTING

Curauá fibers were investigated at different gage lengths 10, 20, 30 and 40 mm (see Figure 4-1). The fibers were glued to paper frames for given gage lengths. Before the test fibers were dried for 24 hours at the 40º C and transported to the laboratory, where they were tested at room temperature. The test was performed according to ASTM-C1557 (ASTM, 2014).
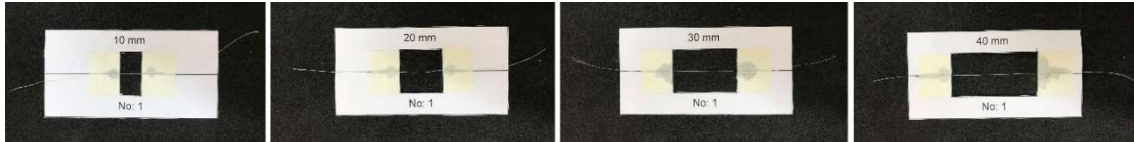
Figure 4-1 Specimens for fiber tensile strength verification for 10, 20, 30 and 40 mm gage lengths.

The tensile tests were performed in a microforce testing machine Tytron 250 at the strain rate of 0.00008 s^{-1} and load cell of 50 N (Figure 4-2).
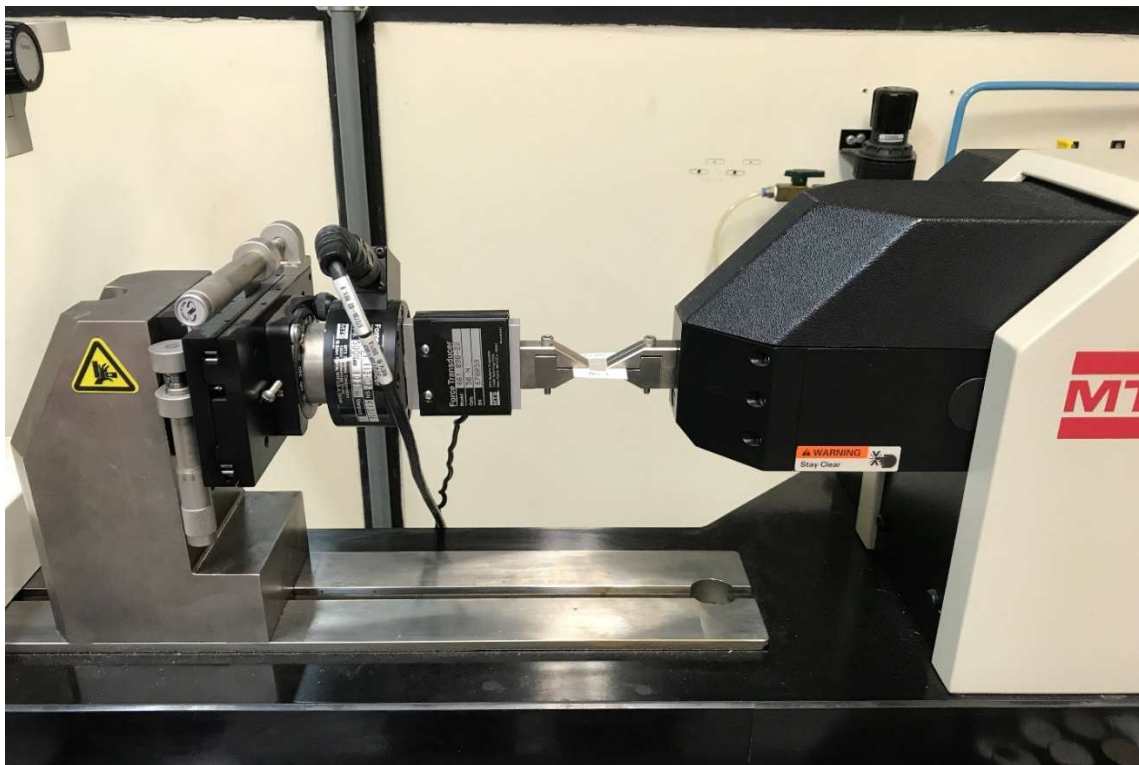
Figure 4-2 Tytron 250 microforce testing machine with fiber specimen set up ready for tensile test.

The tensile test steps are presented in Figure 4-3. After specimen is assembled in the machine's grips, the paper frame is cut. The one grip moves and the force is measured by Tytron 250 up to fiber rupture. The data was collected and analyzed for tensile strength and strain calculation.

| Specimen assembling | Paper frame cutting | Testing |
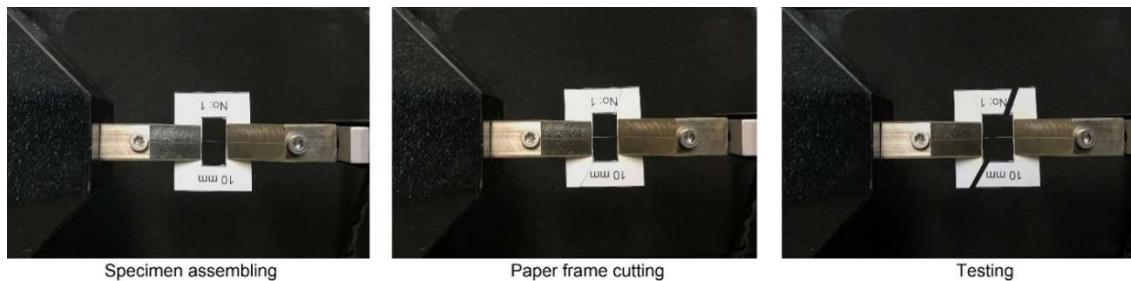
Figure 4-3 Paper frame used to support fiber before test.

The fiber's microstructure was investigated using a SEM (TM 3000) at 25kV of accelerating voltage. The images obtained were processed using the software package ImageJ for measuring the cross-section of each fiber at the two external points of the sample. A contour line was interactively drawn to delineate the irregular fiber cross-section and then the area was measured and compared with the circular model (Figure 4-4).

Circular model and real fiber cross-section   100 µm
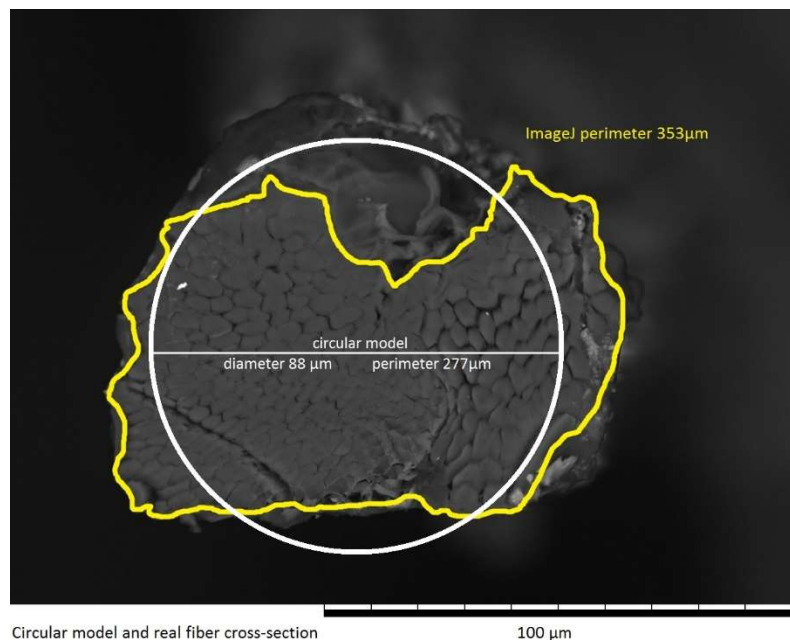
Figure 4-4 Curauá fiber cross-section at SEM and ImageJ analysis: yellow presents the contour line, white the approximation to circular model diameter.

The compliance of the loading and gripping system was determined by obtaining the force versus displacement behavior of the fiber at various gage lengths (10, 20 and 30 mm) following the methodology used by Silva (SILVA; CHAWLA; TOLEDO FILHO, 2008) and Chawla (CHAWLA; KERR, 2005). The total cross-head displacement during fiber testing δ_t can be expressed by:

$$\frac{\delta_t}{F} = \left[\frac{1}{EA}\right] l + c \tag{4.1}$$

Where: c = the machine compliance, F = the applied force, E = the Young's modulus of the fiber and A = the cross-sectional area of the fiber.

Thus, a plot of δ_t/F versus gage length, l, yields a straight line of slope $1/EA$ and intercept c, the compliance of the load train (Figure 4-5: Left).
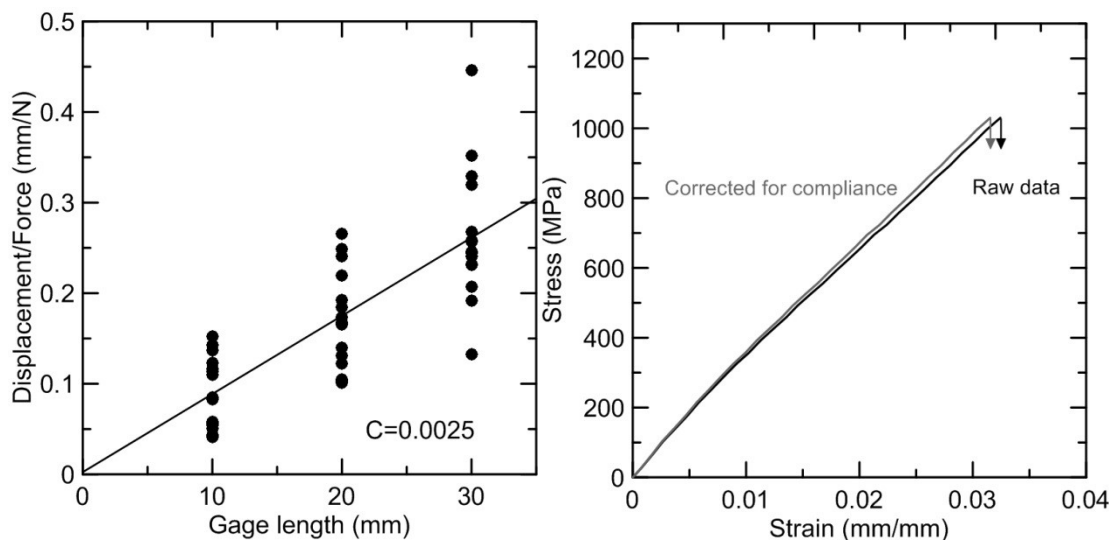
Figure 4-5 Determination of the machine compliance (Left): displacement/force versus gage length. The machine compliance, given by the intercept (c = 0.0025), was determined from the plot. (Right): stress-strain behavior of a curauá fiber tested at 10 mm gage length, showing the raw data compared with the data corrected for compliance.

4.2 RESULTS AND DISCUSSION

Tables 4-1, 4-2, and 4-3 present the tensile test results of the curauá fibers for the different gage lengths at different time exposure to hot water treatment called cycles. Each cycle contains 3 hours of washing followed by 24 hours of drying. Young's modulus was calculated in the elastic portion of the stress-strain curve and then corrected for compliance. The gage length does not seem to influence Young's modulus of the fibers and the variability of modulus values are related to the microstructure of the curauá fibers and possible damages during the extraction process, as reported by (FIDELIS et al., 2013). However, the tensile strength seems to decrease with the increase in the gage length. For all groups of fibers tested the highest strength is for the shortest gage length. This can be caused due to the increased probability of fiber damage with the fiber length.

For untreated fibers, the obtained average tensile strength values varied from 991 to 688 MPa with standard deviation oscillating around 150 MPa.

Table 4-1 Summary of average tensile test results and standard deviation for curauá fibers with no exposure to hot water treatment.

Fiber length (mm)	Area (mm^2)	Diameter (μm)	Strain to failure (%)	Force at rupture (N)	Strength (MPa)	Young's modulus (GPa)	Weibull modulus
10	0.00483 (0.00066)	78.21 (5.34)	3.54 (0.50)	4,78 (0.96)	991.18 (156.25)	27.33 (3.38)	4.61
20	0.00590 (0.00112)	85.92 (8.62)	2.57 (0.45)	4.44 (1.41)	735.19 (150.73)	28.71 (3.10)	5.69
30	0.00576 (0.00143)	84.55 (10.97)	2.15 (0.35)	3.93 (1.18)	688.83 (133.72)	32.55 (3.55)	3.55
40	0.00506 (0.00072)	79.87 (5.69)	2.22 (0.32)	4.54 (0.98)	928.51 (194.17)	41.67 4.73	2.74

Graphical representation of results and calculated average for curauá in nature (without hot water cycles) presents specimen results and calculated average (Figure 4-6).
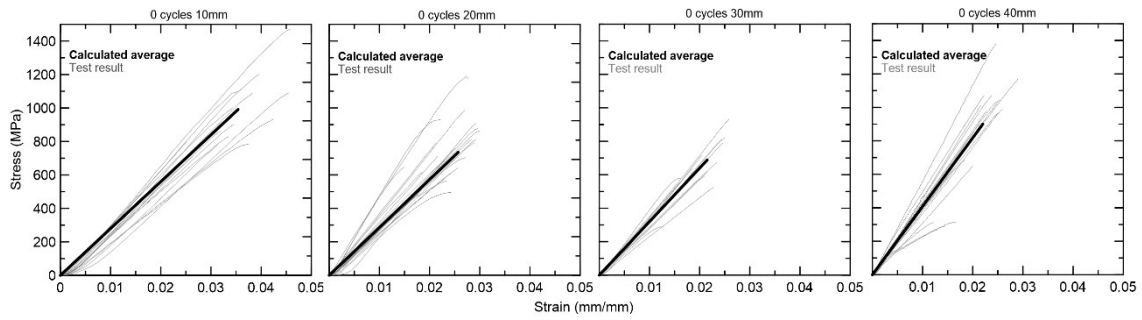
Figure 4-6 Graphical representation of tensile test results for Curauá fiber without treatment.

The group of fibers after 9 hours of hot water treatment presented higher tensile strength ranging from 1328 to 895 MPa with the standard deviation ranging from 117 to 300 MPa.

Table 4-2 Summary of average tensile test results and standard deviation for curauá fibers after 9 hours of exposure to hot water treatment.

Fiber length (mm)	Area (mm²)	Diameter (μm)	Strain to failure (%)	Force at rupture (N)	Strength (MPa)	Young's modulus (GPa)	Weibull modulus
10	0.00489 (0.00096)	78.33 (7.24)	4.44 (0.34)	6.12 (0.78)	1328.84 (300.54)	35.43 (5.81)	3.78
20	0.00461 (0.00113)	75.88 (8.88)	3.21 (0.38)	4.95 (1.05)	1096.72 (142.81)	35.92 (5.92)	6.33
30	0.00507 (0.00086)	79.99 (6.80)	2.80 (0.33)	5.10 (0.97)	1006.62 (117.73)	37.92 (5.43)	6.77
40	0.00572 (0.00098)	84.88 (7.15)	2.78 (0.21)	5.04 (0.87)	895.40 (138.85)	22.99 (3.25)	4.41

Graphical representation of results and calculated average for curauá after 3 cycles of hot water treatment are presented in Figure 4-7.

Figure 4-7 Graphical representation of tensile test results for Curauá fiber after 9 hours of hot water treatment.

The group of fibers after 18 hours of hot water treatment presented more uniform tensile strength between 1110 to 935 MPa with the smallest standard deviation values ranging from 64 to 108 MPa.

Table 4-3 Summary of average tensile test results and standard deviation for curauá fibers after 18 hours of exposure to hot water treatment.

Fiber length (mm)	Area (mm²)	Diameter (µm)	Strain to failure (%)	Force at rupture (N)	Strength (MPa)	Young's modulus (GPa)	Weibull modulus
10	0.00402 (0.00123)	70.18 (10.53)	3.31 (0.36)	4.44 (1.30)	1110.88 (64.10)	41.11 (4.98)	13.12
20	0.00384 (0.00072)	69.54 (6.57)	2.52 (0.23)	3.85 (0.77)	1003.72 (108.10)	44.26 (5.39)	8.41
30	0.00326 (0.00067)	63.80 (6.71)	2.40 (0.22)	2.95 (0.57)	920.65 (92.28)	39.45 (6.40)	7.56
40	0.00397 (0.00093)	70.43 (8.38)	2.18 (0.17)	3.65 (0.78)	935.24 (92.19)	44.13 (7.28)	7.50

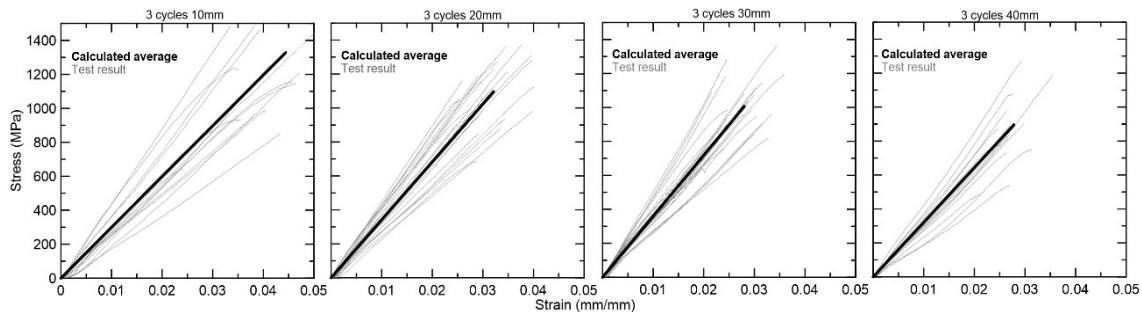Graphical representation of results and calculated average for curauá fiber after 18 hours of exposure to hot water treatment are presented in Figure 4-8.
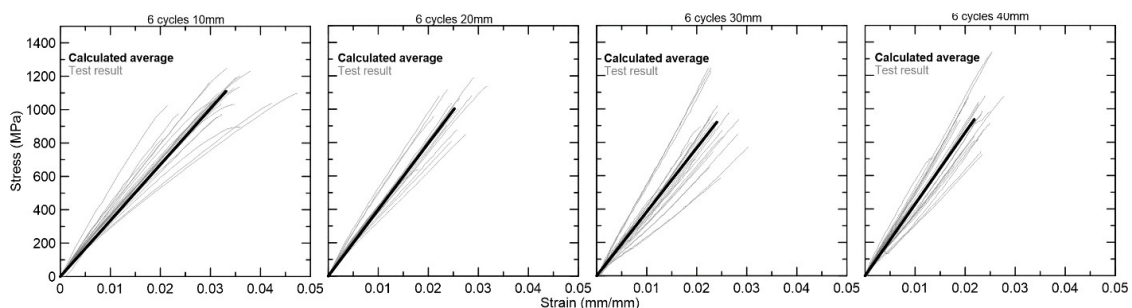
Figure 4-8 Graphical representation of tensile test results for Curauá fiber after 18 hours of hot water treatment.

The strain-to-failure seems to decrease when increasing the gage lengths with a significant difference between 10 and 20 mm gage lengths.
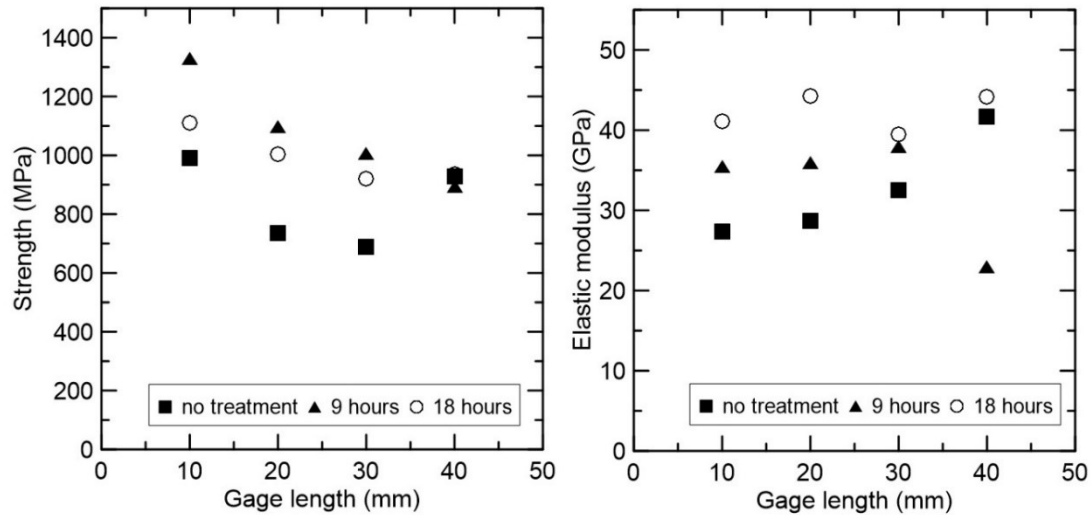
Figure 4-9 (Left) Tensile behavior of the curauá fiber correlated with gage length and time of hot water treatment. (Right) Young's modulus of the curauá fiber correlated with the gage length and time of hot water treatment.

The tensile behavior of curauá fibers can be classified as a high-performance fiber according to Silva (FIDELIS et al., 2013). The untreated curauá fibers presented strength higher than 600 MPa with the modulus greater than 27 GPa. The hot water treatment increased the value of the fiber tensile strength to more than 1000 MPa and Young's modulus to 35 GPa (and even to more than 40 for 18 hours of treatment) (Figure 4-9: Left). The increased strength seems to be correlated with the dimensional changes. The hot water treatment reduces the area of the fiber. This change can be shown as a diameter reduction of 6% for 9 hours and 15% after 18 hours in comparison to the untreated fiber (Figure 4-10). The dimensional change can be due to the wax and impurities removal and reduction of hemicellulose and lignin content.
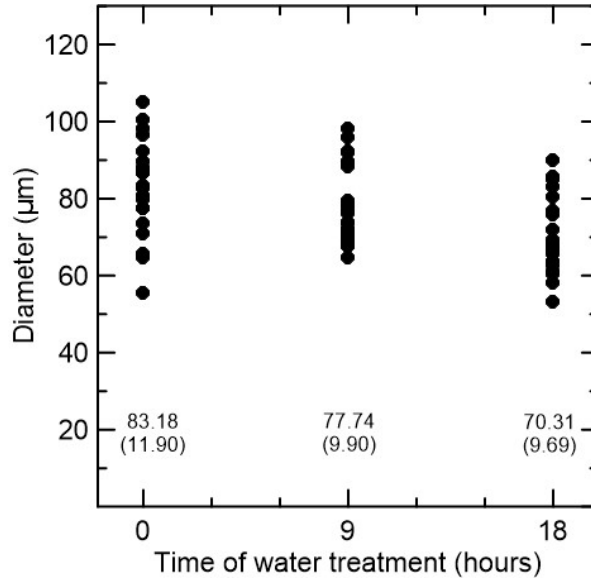
Figure 4-10 Dimensional changes (circular diameter in μm) as a function of the hot water treatment time.

The application of Weibull distribution on the fibers tensile strength is described by several authors (SILVA; CHAWLA; TOLEDO FILHO, 2008), (CHAWLA; KERR, 2005). In this study, the form presented by Silva et al. (SILVA; CHAWLA; TOLEDO FILHO, 2008) was used. According to the Weibull analysis, the probability of survival of a fiber at a stress σ, is given by:

$$P(\sigma) = exp\left[-\left(\frac{\sigma}{\sigma_0}\right)^m\right] \tag{4.2}$$

Where:

σ = the fiber strength for a given probability of survival, m = the Weibull modulus, σ_0 = the characteristic strength, which corresponds to $P(\sigma) = 1/e = 0.37$.

The higher is the value of m the lower is the variability in strength. Ranking of the fiber strengths is performed by using an estimator given by:

$$P(\sigma)_i = 1 - \frac{1}{N+1} \tag{4.3}$$

Where:

$P(\sigma)_i$ = the probability of survival corresponding to the *i-th* strength value;

N = the total number of fibers tested.

Substituting Eq. (4.3) into Eq. (4.2) yields:

$$\ln \ln \left[\frac{N+1}{N+1-i}\right] = m \ln \left(\frac{\sigma}{\sigma_0}\right) \tag{4.4}$$

Thus, a plot of *ln ln((N+1)/N+1-i))* versus *ln(σ/σ₀)* yields a straight line with the slope of *m*. Figure 4-11:(Left) shows the variability of Weibull modulus among the group of fibers (after 9 hours of hot water treatment) for the different gage lengths. Figure 4-11:(Right) presents the variability of the Weibull modulus for three groups of curauá fibers which were verified. The Weibull modulus increased with the time exposure to hot water treatment showing the less variability of strength after treatment. According to Weibull modulus, 18 hours of hot water treatment reduced the variability of strength between the fibers.
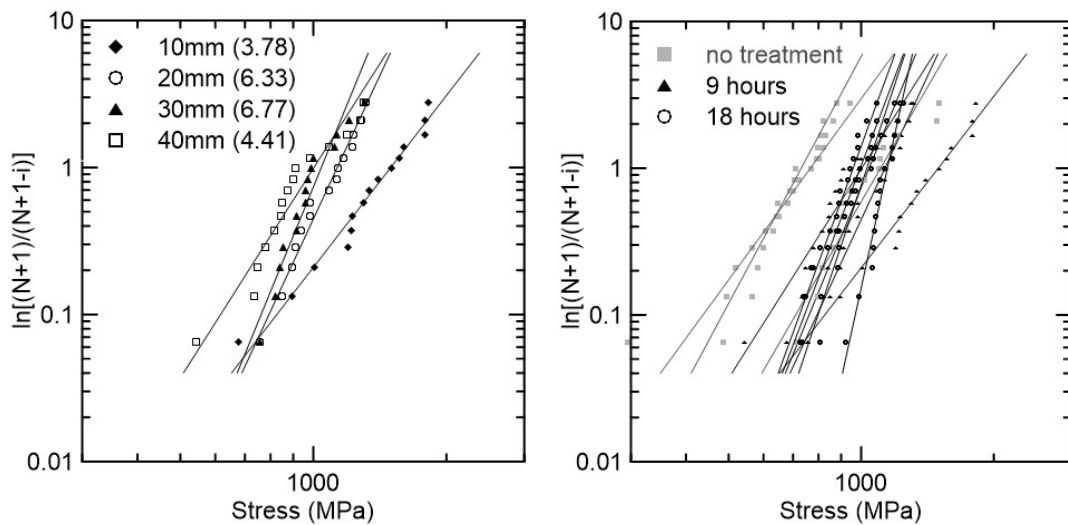
Figure 4-11 Weibull distribution of the (Left) curauá fiber strength for different gage lengths after 9 hours of hot water treatment. (Right) curauá fiber tensile strength for different gage lengths and different time of hot water treatment.

4.3 CONCLUSIONS

The curauá fiber is a high-performance natural fiber. Its tensile strength presents higher values in comparison to other high-performance natural fibers like Jute and Sisal. From the present work the main findings are presented below:

- The gage length has influenced the measured tensile strength of the fiber: the higher the gage length, the smaller the measured tensile strength.

- The hot water treatment reduced the area of the fibers.

- The hot water treatment decreased the data scatter which is shown in higher Weibull modulus representing the lower variability of measured strength.

- The hot water treatment improved the mechanical properties of the fibers encouraging their application as a reinforcement in cement-based composites.

5 DESIGN OF STRAIN HARDENING CEMENT-BASED COMPOSITES WITH ALKALI TREATED NATURAL CURAUÁ FIBER

Chapter 5 presents the design process of Strain Hardening Cement-based Composite reinforced with natural curauá fiber. The matrix fracture energy and matrix-fiber bond were studied and implemented into the theoretical model for critical fiber volume prediction, which was verified by mechanical tests for tensile, bending and compression strength. The influence of matrix-fiber bond on critical fiber volume is presented. The fiber properties are improved by two-stage treatment. Firstly, hot water (80° C) washing in water changed every 3 hours. Secondly, immersion in 1% solution of calcium hydroxide $Ca(OH)_2$ with water for 60 minutes for calcium deposition on fiber surface to increase bond properties. The critical fiber volume calculated by the model was 4% for 20 mm treated curauá fiber. Strain hardening behavior occurred under tensile load (1.75 MPa maintained over 0.4 – 0.8% strain along new cracks formation). The 4-point bending test on plate specimens confirmed flexural hardening behavior. After the determination of critical fiber volume, the influence of fiber length is investigated on the model prediction and composite properties. The collected data compare the mechanical properties obtained for the composites reinforced with 4% of 20, 30 and 40 mm alkali treated fibers.

5.1 METHODOLOGY

5.1.1 Matrix properties

5.1.1.1 Compressive strength

Compressive strength was verified on cylindrical specimens (50x100 mm) at Shimadzu, with the load cell of 100 kN and 0.3 mm/min velocity (Figure 5-1).

Figure 5-1 Compression test on cylinder specimen with deformation measured by LVDT.

5.1.1.2 Matrix fracture

The aim of the fracture test is to determinate the fracture energy (G_c). The analysis is based on simplification, where hardened cement paste is considered as homogeneous material and a crack is straight. The sand grains can deviate the crack from straight line creating a more tortuous path and increase energy demand for crack's formation (RADJY; HANSEN, 1973) so the fine sand of maximum grain diameter lower than 212 μm was used. To determine fracture mechanics parameters, wedge loaded compact tension

specimens are suggested, as they allow crack development in a simple manner (HILLEMEIER; HILSDORF, 1977). In this work, the fracture toughness of brittle material was estimated on Tapered Double Cantilever Beam (TDCB) specimens that allow the stable crack growth (VASUDEVAN et al., 2017). The TDCB specimens were cast and tested at age of 28 of days under tensile load in electromechanical testing machine from Shimadzu with a load cell of 1 kN at stroke displacement rate 0.01 mm/min. The specimen's geometry is presented in Figure 5-2.
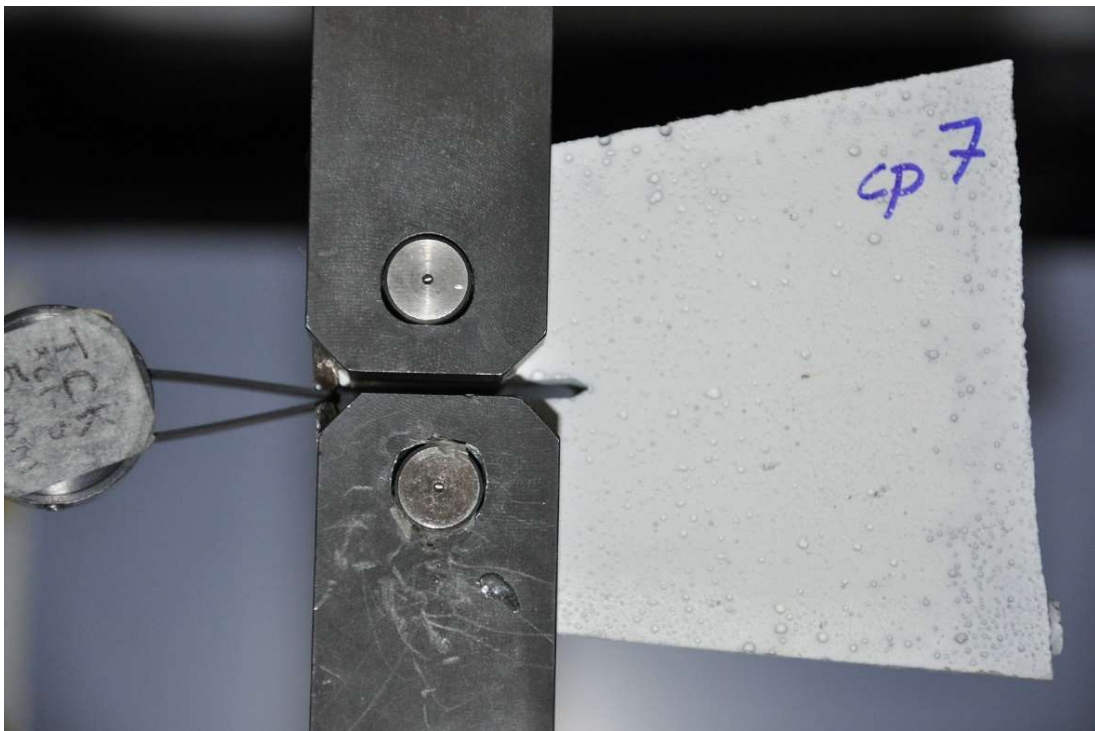
Figure 5-2 TDCB specimen for matrix fracture testing with crack opening controlled by clip gage.

After specimen assembly in testing set-up, grips started movement opening initial crack, which dimension was controlled by clip gage. The matrix fracture testing method was based on (VASUDEVAN et al. 2017), where the crack propagation in cement pastes with Finite Elements Method support was investigated. The method presented in his thesis was applied to the matrix used in this research for fracture parameters estimation. For the three specimens, the curves of force versus crack opening were drawn and one with the most planar fractured surface was chosen as a representative curve for the group.

5.1.2   Fiber-matrix bond properties

To ensure a proper envelope of fiber in the matrix the PVC molds were used. PVC mold is a tube with a given depth which corresponds to embedment length (Figure 5-3). In these tests, the 10, 15 and 20 mm tubes were used corresponding to halves of gage lengths 20, 30 and 40 mm used for tensile tests. Fiber is placed in the middle of a tube, fixed from the bottom by acrylic frame and closed by paper tape to prevent matrix leakage. Then matrix is poured inside the tube and top frame closes the specimen providing the straight and central position of fiber in a specimen. After 24 hours specimens were separated from the frames and stored in a plastic bag with humid inner (wet paper towels) to provide conditions similar to composite's curing. After 28 days fibers were tested to verify pull-out behavior in microforce machine Tytron 250 with 50 N load cell.
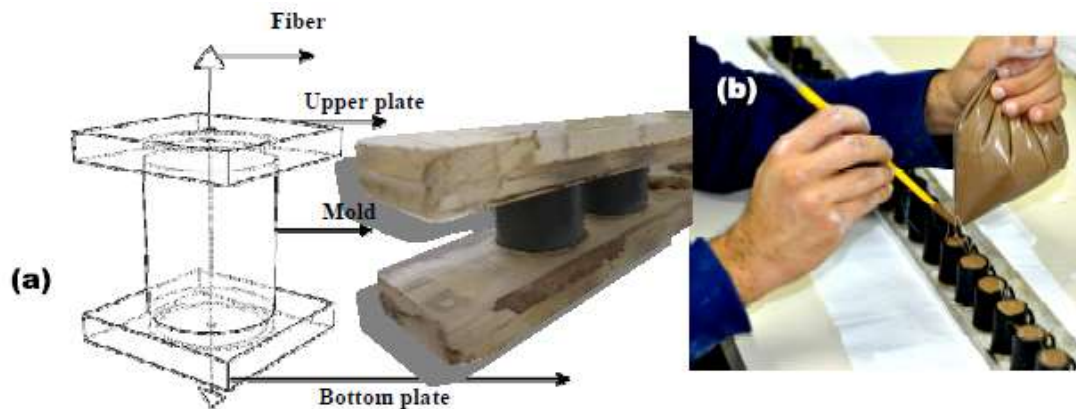
Figure 5-3 Pull-out specimens preparation after (FERREIRA et al., 2017).

The pull-out test starts with the tube placed in the iron ring and clenched by screws to prevent specimen's movement during the test. The fiber is pulled out from the specimen and the data of force and displacement are collected by Tytron 250 (Figure 5-4).

Pull-out test | Completely pulled out fiber
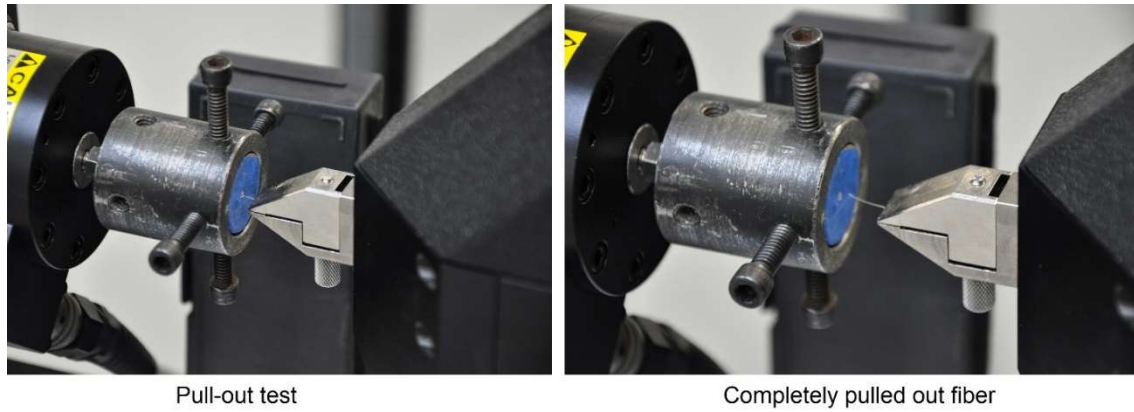
Figure 5-4 Pull-out test stages: fiber being pulled out (left), completely pulled out fiber (right).

The collected data were analyzed according to the modified model of (LIN; KANDA; LI, 1999), where the values of chemical debonding energy (G_d), frictional bond strength on the onset of fiber slippage (τ_0), maximum frictional bond (τ_{max}) were calculated (Figure 5-5).
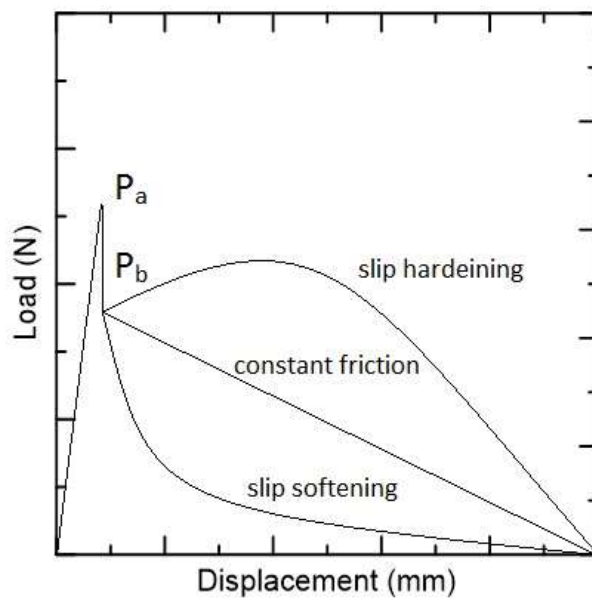
Figure 5-5 General profile of single fiber pull-out.

The proposed model was used for PVA fiber in the design process of SHCC (ECC) composite and combineS properties important FOR composite design (chemical bond and initial bond strength). It is worth to mention, that it is a trial to adapt model successfully used for PVA fiber to natural fiber which is characterized by much more variety in dimension and properties.

$$G_d = \frac{2(P_a - P_b)^2}{E_f A_f Perimeter} \qquad (5.1)$$

Where:

G_d - Chemical bond,

P_a - Peak load of single fiber pull-out curve,

P_b - Load after sudden drop fallowing P_a,

E_f - Fiber modulus of elasticity,

A_f - Fiber area measured in ImageJ software.

$$\tau_0 = \frac{P_b}{l_f Perimeter} \qquad (5.2)$$

Where:

τ_0 - initial frictional bond strength,

l_f - fiber embedment length,

5.1.3   Modelling approach

Equation 5.3 presents the concept of energy balance during crack formation. It involves external energy (work) with crack tip energy absorption (matrix toughness) and crack flank energy absorption (fiber-matrix bond). This energy criterion determines the crack propagation mode (steady-state or Grifith crack). The crack width (δ) should be below maximum crack opening that fibers can bridge (δ_0), to maintain the stress level below the bridging capacity of fibers (if stress will be above δ_0 tension softening with the crack opening will occur)(YANG; LI, 2006).

$$G_c \equiv J_{tip} \leq \sigma_0 \delta_0 - \int_0^{\delta_0} \sigma(\delta) d\delta \equiv J_b' \qquad (5.3)$$

Where: σ_0 – the maximum bridging stress, corresponding to the maximum crack opening that fibers can bridge (δ_0).

The stress-crack opening curve $\sigma(\delta)$ is derived by combining analytic tools of fracture mechanics and micromechanics (LIN; KANDA; LI, 1999). It takes into account the interface chemical bond between fiber and matrix (G_d) and frictional bond (τ). To calculate complementary energy formula is used:

$$J_b' = \frac{V_f \tau^2 L_f}{6 d_f^2 E_f} - \frac{2 V_f G_d L_f}{d_f} + \frac{8 V_f G_d}{3\tau}\sqrt{\frac{2 E_f G_d}{d_f} - \frac{2 V_f E_f G_d^2}{\tau^2 L_f}} \tag{5.4}$$

Simplified to:

$$J_b' = V_f \frac{L_f}{d_f}\left(\frac{\tau^2 E_f^2}{6 d_f E_f} - 2G_d\right) \tag{5.5}$$

The second criterion is related to first cracking strength (σ_{fc}) which must be lower than maximum bridging stress (σ_0) to control initiation of cracks.

$$\sigma_{fc} < \sigma_0 \tag{5.6}$$

After calculation of δ_0 by formula:

$$\delta_0 = \frac{\tau L_f^2}{d_f E_f} - \frac{2G_d}{\tau} \tag{5.7}$$

Calculation of maximum bridging stress which corresponds to δ_0 is given by:

$$\sigma(\delta) = \begin{cases} 2V_f\sqrt{(2G_d + \tau\sigma)\dfrac{E_f}{d_f}} - \dfrac{V_f E_f \delta}{L_f} & \delta \leq \delta_c \\[2ex] \dfrac{4V_f \tau}{L_f d_f}\left(\dfrac{L_f}{2} - \delta\right) & \delta_c \leq \delta \leq \dfrac{L_f}{2} \end{cases} \tag{5.8}$$

Satisfying both criterions leads to strain-hardening behavior. If they are not fulfilled tension-softening occurs (LIN; KANDA; LI, 1999) (LI; LEUNG, 1992). Imperfections can influence a behavior of composite that is why a large margin between criterion values is recommended, which can be represented by the pseudo strain-hardening performance index (PSH) (KANDA, 1998).

$$PSH_{energy} = \frac{J_b'}{J_{tip}} \tag{5.9}$$

$$PSH_{strength} = \frac{\sigma_0}{\sigma_{fc}} \tag{5.10}$$

Graphical representation of model presents the important role of initial frictional bond in composite strain-hardening design. The higher the value the lower fiber volume critical needed to achieve desired behavior. It also proved that alkaline treatment on fibers is a step ahead to achieve the desired behavior by improving fiber-matrix bond and lowering critical volume needed.

5.1.4 Composites

Molding was proceeded by mixing all dry ingredients (cement, fly ash, metakaolin, sand, and viscosity modifier) followed by addition of water and superplasticizer similar to standard ECC mixing sequence (ZHOU et al., 2012). At the end dry fiber, 20 mm of two-

stage treated at 4% of volume, was added to mix maintaining maximum separation possible which could be achieved by manual dosage. Composites were cast into steel formwork and stored for 48 hours to be disassembled. Next, the specimens were stored in plastic bags with wet inner (wet paper towels) to provide a humid condition for curing up to 28 days, when they were tested.

The most important characteristic of SHCC is the tensile performance (strain-hardening stress-strain behavior and crack width control). The three major material properties: tensile strength, strain capacity, and maximum crack width, are defined to describe SHCC properties. The tensile test provides information to determine the first two and sample observation provide data for crack analysis. The crack width was defined by visual observation of cracks formed followed by indirect estimation of crack's width based on a number of cracks and tensile strain according to (JAPAN SOCIETY OF CIVIL ENGINEERS, 2008).
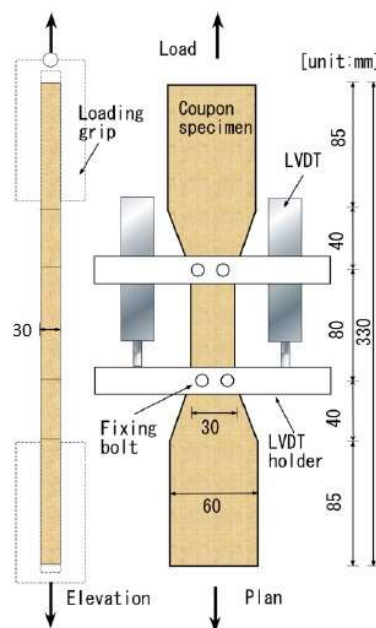
Figure 5-6 Tensile test set up after
(JAPAN SOCIETY OF CIVIL ENGINEERS, 2008)*.*

The tensile test specimens were cast in dog bone forms of 330 mm length with 80 mm of the clear span with the cross-section of 30 mm by 30 mm (instead of 30 mm by 12.7 mm as in JSCE recommendation) as presented in Figure 5-6. Tensile tests were carried at Shimadzu (Figure 5-7), with load cell of 100 kN and 0.1 mm/min velocity (MAGALHÃES, 2013).
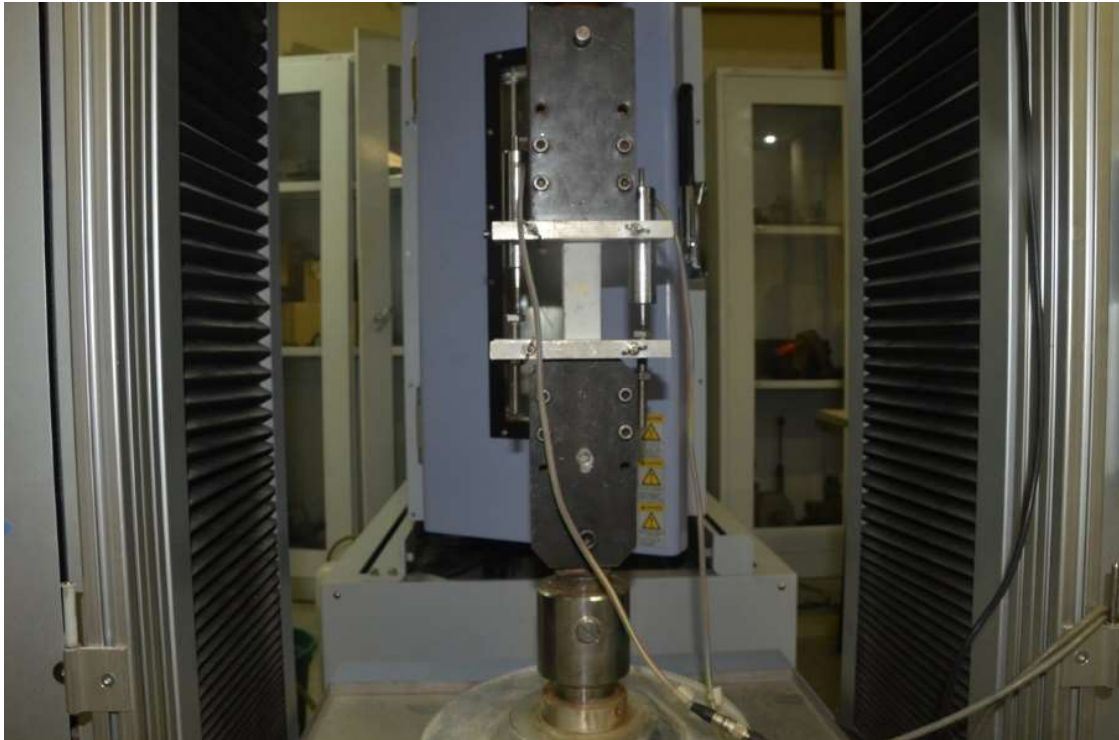
Figure 5-7. Tensile test carried at Shimadzu machine for dog bone specimens.

The collected data was used for plotting the graph of tensile stress versus strain. The values of first crack strength, maximum strength were calculated according to the formula:

$$\sigma = \frac{Tensile\ Force}{Area} \tag{5.11}$$

And the strain by formula:

$$\varepsilon = \frac{\Delta L}{L} \tag{5.12}$$

Where ΔL is the average of the two LVDT measurements and L is the specimen span (80 mm).

The example of tensile stress versus strain curve is presented in Figure 5-8. The first crack strength, maximum strength, and estimated strain are presented.
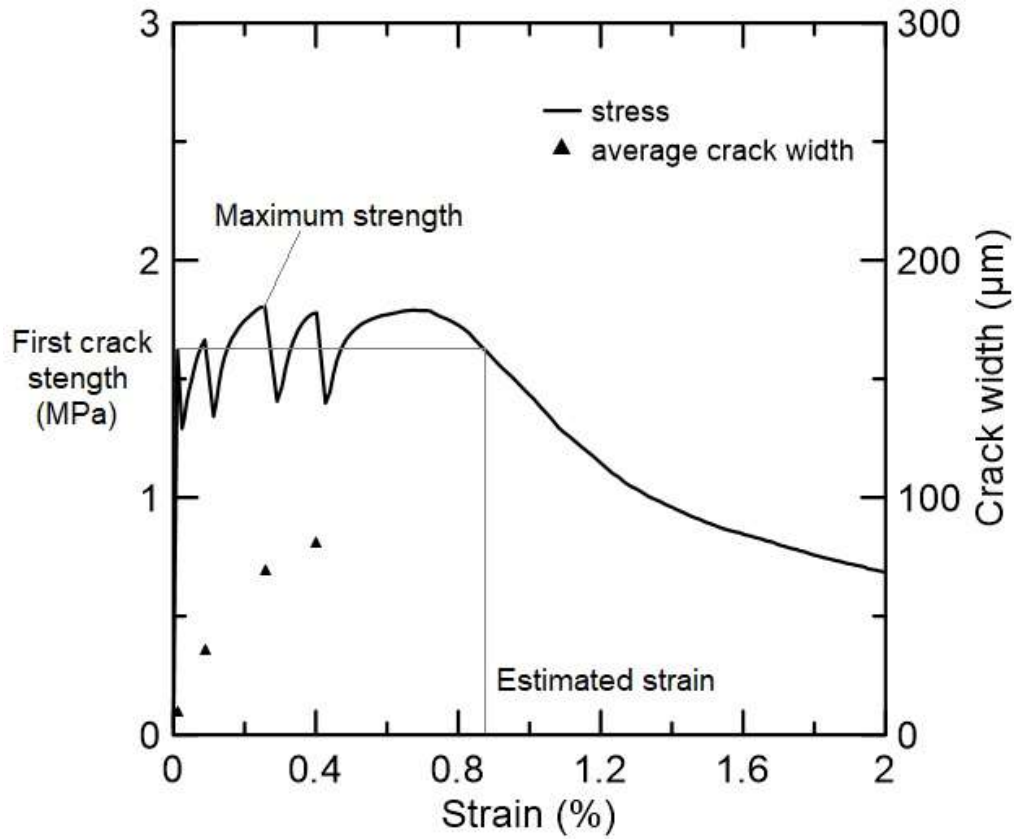
Figure 5-8 Example of tensile stress versus strain curve obtained during the test with marked properties used for composites evaluation.

Flexural strength was verified at 4 point bending test on plates with dimensions 400x60x15 mm (carried at Shimadzu, which load cell of 50 kN and 0.3 mm/min velocity). The span between supports was equal to 255 mm (Figure 5-9). The first crack flexural strength and maximum flexural strength were calculated according to the formula:

$$\sigma_{flexural} = \frac{FL}{bd^2} \tag{5.13}$$

Where: F - applied force, L – the span between the supports, b – specimen width, d - specimen thickness.

After the tests the specimens were dried to constant mass and presented mass loss of 15%.

Figure 5-9 The 4-point bending test with the middle span deformation span controlled by LVDT, camera image used for crack pattern analysis.

5.2 RESULTS AND DISCUSSION

5.2.1 Matrix fracture properties

Figure 5-10 presents a representative curve of three specimens. The area below the curve of applied force (F) versus crack mouth opening (δ) was adapted to a rough estimation of fracture energy equal to 15 J/m^2 which was applied for model prediction. In comparison to the fracture energy of 5 J/m^2 used for the tailoring the SHCC with PVA and PP fiber (YANG; LI, 2006) this results presents higher value. From the other hand the values of fracture energy for mortars vary depending on the materials used and their size distribution, as well as testing method (KARIHALOO; CARPINTERI; ELICES, 1993). The fracture energy values in range of 5 J/m^2 determined on cylindrical specimens in 3 point bending were reported for cement pastes (DELA; STANG, 1997). Higher values were reported to mortars 60 J/m^2 (LI; MAALEJ, 1996).
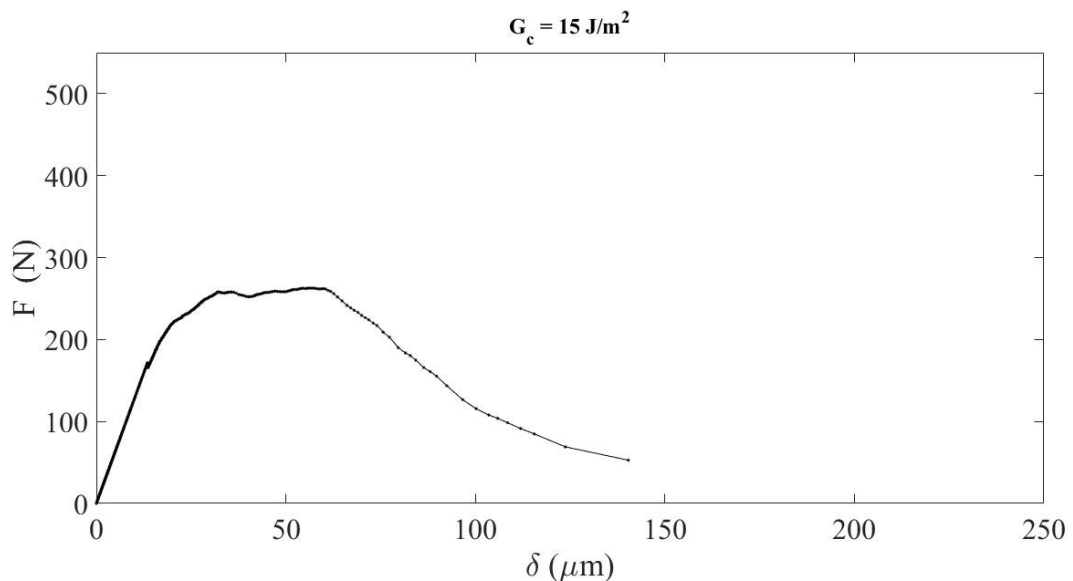
Figure 5-10 Representative curve of crack mouth opening vs load for applied matrix.

5.2.2 Influence of treatment stages on fiber tensile properties

First stage treatment despite impurities removal influenced the average fiber cross-section area represented by circular model diameter from 85.92 to 75.88 μm. The cycles of wetting and drying reduced the size of lumens and increased strength value without changing significantly force at rupture 4.44 N for natural curauá versus 4.95 N after washing cycles. The fiber cross-section reduction provides greater fiber aspect ratio

(length/diameter) from 232 for natural fiber to 263 after washing cycles. The higher the aspect ratio the lower critical volume is needed for strain hardening to happen. Washed fiber presented higher strain to failure (3.21% versus 2.57% for natural fiber) with higher strength values (1096.72 MPa versus 735.19 MPa for natural fiber) and higher value of Young's modulus (35.92 GPa versus 28.71 GPa).

Second stage, the alkali immersion after washing cycles decreased fiber force at rupture (3.36 N versus 4.95 N), which influenced the tensile strength drop as well (697.19 MPa versus 1096.72 MPa), without any significant difference in cross-section area represented by the circular diameter (77.70 μm versus 75.88 μm). The lower strain value (2.01% versus 3.21%) suggests that fiber increased its brittleness and lost the deformation capacity. However the there is no significant difference in Young's modulus between compared groups. After Gram the reduction of strength should be caused by hemicellulose and lignin degradation and destruction of links between fiber cells (GRAM, 1983). Despite tensile properties reduction and more fragile behavior, alkaline treatment increased Young's modulus which is beneficial for critical fiber volume prediction to obtain strain-hardening behavior. Data from the tensile tests properties are presented in Table 5-1.

5.2.3   Influence of treatment stages on pull-out behavior

The alkali treatment increased significantly debonding (disconnection) force (2.22 N versus 1.10 N), also maximum force reached during the pull-out test (2.47 N versus 1.37 N), which impacted maximum friction (0.59 MPa versus 0.41 MPa). This improvement is related to calcium deposition on the fiber's surface and its increased roughness of fiber surface. Moreover, alkali immersion increased chemical bond between fiber and matrix (0.13 J/m^2 versus 0.02 J/m^2), providing better interaction between fiber and matrix. The chemical bond improvement could be related to the matrix pozzolanic activity with the calcium from the fiber's surface.

Table 5-1. Pullout test results done on selected stages of fiber treatment with 10 mm embedment length.

Description	Area (μm²)	Perimeter (μm)	P_a (N)	P_b (N)	P_max (N)	G_d (J/m²)	τ (MPa)
1 stage treatment	8256	388	1.10	0.86	1.37	0.02	0.41
Hot water washing cycles	(4968)	(141)	(0.92)	(0.85)	(0.95)	(0.05)	(0.52)
2 stage treatment	12549	442	2.22	1.88	2.47	0.13	0.59
Immersion in alkali solution	(7245)	(148)	(0.90)	(0.70)	(0.78)	(0.15)	(0.21)

Figure 5-11 presents the graphical representation of pull-out tests for both treatments. With a red color the ruptured and discarded results are presented. The benefits of alkaline treatment are visible on the graph by the highest disconnection force as well as higher friction during pull-out phase.
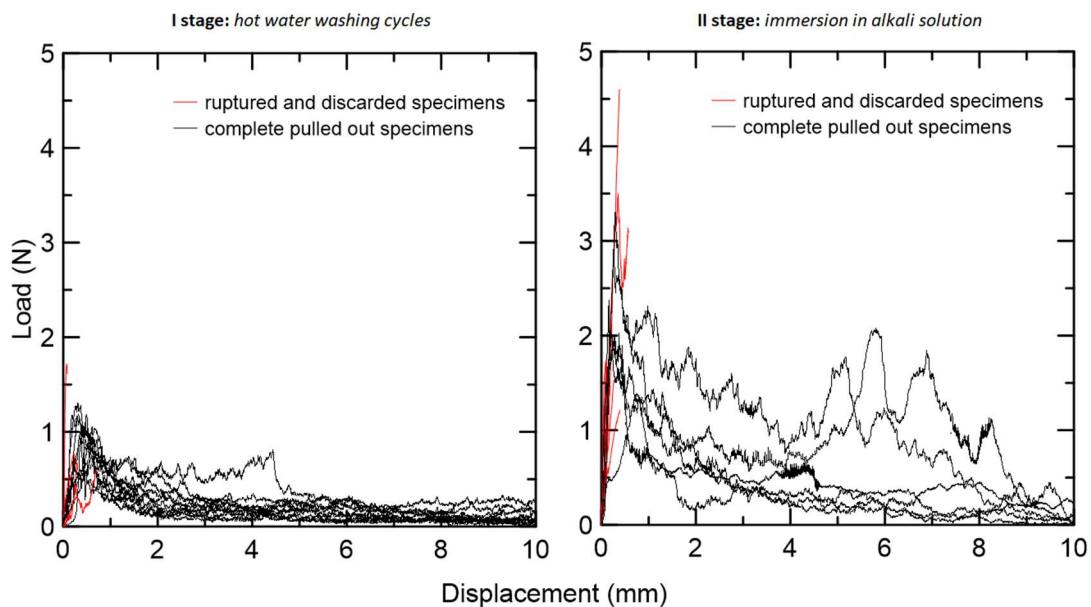
Figure 5-11 Pull-out results for two stages of fiber treatment

5.2.4 Micromechanical model prediction

Table 5-2 presents values collected from the matrix, fiber and fiber-matrix properties analysis. The fiber length used for model prediction is equal to 20 mm. The model prediction presents the difference between washed fiber and fiber, which after washing was alkaline treated. The first crack strength of matrix is equal to 1.75 MPa, which is the first crack strength of the composite verified on dog bone specimens. The matrix fracture energy of 15 J/m² is used. The two stage treated fiber present lower critical volume needed for strain hardening behavior for strength criterion (6.5 versus 4.5%) as well as energy

criterion (4.2% versus 4.0%). Strength pseudo strain hardening index higher for two stage treated fiber (3.49 versus 2.47) as well as energy index (5.07 versus 2.85), which presents beneficial aspect of alkaline treatment on probability of strain hardening to occur. However, the critical volume should be taken into special consideration and should work, only as an indication of a range of fiber needed to strain hardening behavior to occur instead of detailed prediction. First of all, the pull-out model test considers the constant cross-section of fiber which is an assumption used for calculation. The curauá fiber presents not symmetrical corrugated surface. The second assumption is based on the fact that all fiber surface is in contact with matrix. The fiber swelling and shrinking along moisture movement could create gaps between fiber-matrix. Further investigation would provide more understanding about interfacial transition zone, but it is out of a scope of this work. The snubbing factor related to fiber inclination is not evaluated in this model, so the assumption is made that all fibers are perfectly aligned with the plane of composite, perpendicular to the tensile force. Also the assumption of fiber uniformly distributed along composite is made. Finally, the micromechanical model is a useful tool to predict the range of critical fiber volume needed to obtain the strain hardening and to narrow the process of composite design to selected volume fractions.

Table 5-2. Theoretical model values for stages of curauá fiber treatment.

Treatment	Fiber			Interface		Strength criterion			Energy criterion			Critical Volume	
Stage	L_f	d_f	E_f	G_d	τ	σ_0	σ_{fck}	$PSH_{strength}$	J_{tip}	$J^{'}_b$	PSH_{energy}	$V_{strength}$	V_{energy}
	mm	μm	GPa	J/m^2	MPa	MPa	MPa		J/m^2	J/m^2		%	%
Washing cycles	20	76	36	0.02	0.41	4.32	1.75	2.47	15	42	2.85	6.5	4.2
Alkali solution	20	77	39	0.13	0.59	6.11	1.75	3.49	15	76	5.07	4.5	4.0

Figure 5-12 presents graphical representation of model prediction. Marked green circle presents the area of critical volumes which could provide strain-hardening behavior with model accuracy for natural fiber and the economic principle for a search of minimum volume needed. The predicted critical volume for two-stage treated curauá fiber varies from 4% for energy criterion to 4.5% for strength criterion. The higher fiber volume the lower mix workability, which could influence the outcome of the tests so volume 4% was applied for verification.
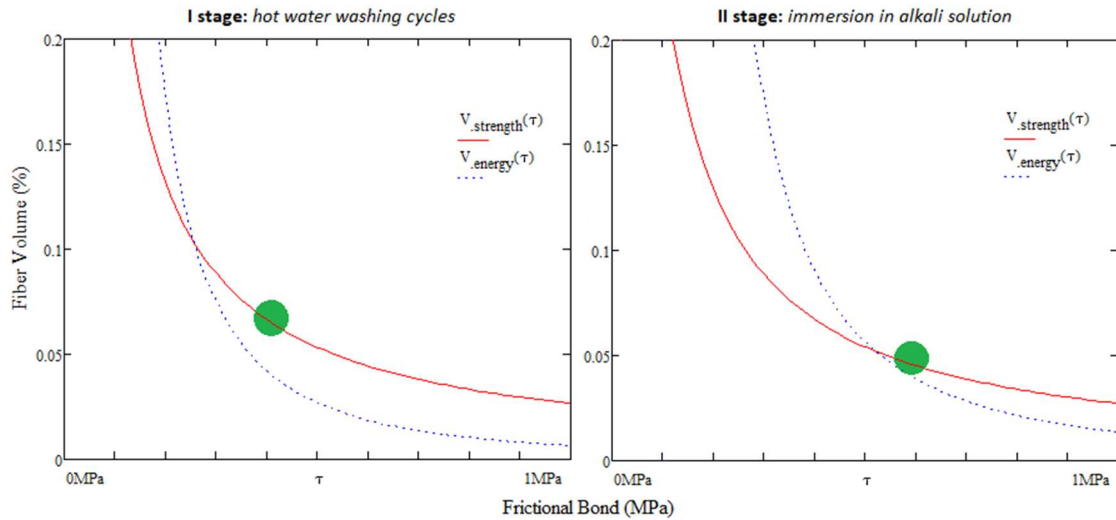
Figure 5-12 Comparison of model predictions for I and II stage of 20mm curauá fiber treatment. Green area represents possibility of strain-hardening behavior.

5.2.5   Composite performance

Figure 5-13 presents result of tensile tests of 3 specimens with average crack width analysis. The composite with 4% of two-stage treated curauá fiber presented multiple cracking pattern (2-4 cracks), strain higher than 0.4% and increase average strength value about 9%.
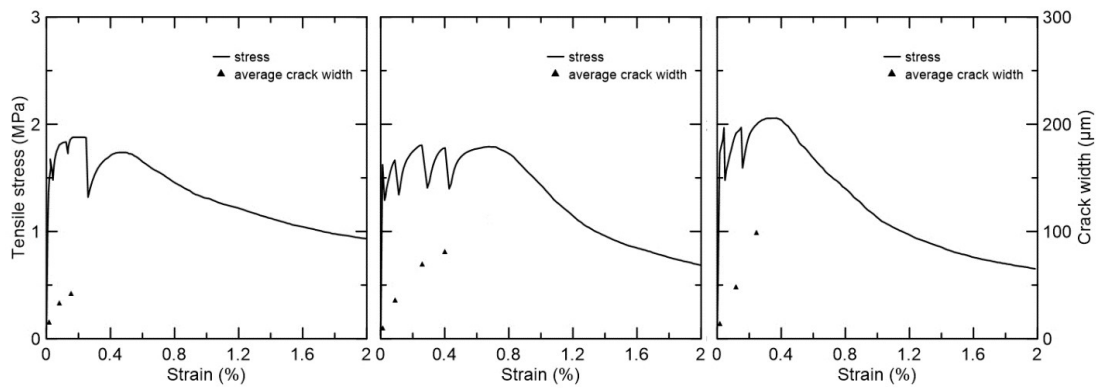
Figure 5-13 Results of tensile tests on dog bone specimens reinforced with 4% of 20mm two-stage treated curauá fiber.

Figure 5-14 presents crack formation (marked with white color) during the tensile test. The first two cracks remain their width and a new crack appears between them. Then another one in the middle of the specimen and this is the last new crack formed. Along with the test, the crack at the bottom is opening to material failure.
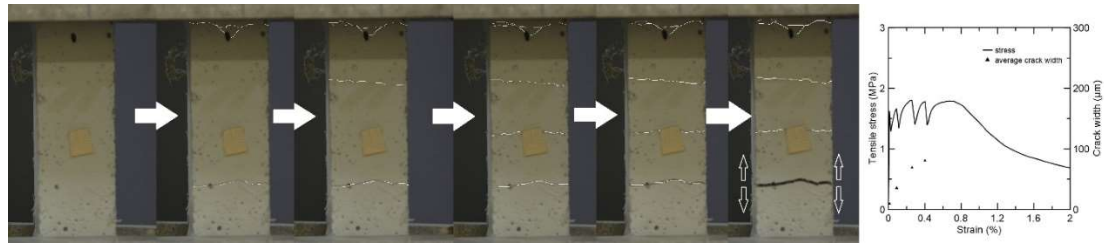
Figure 5-14 Multiple-cracking pattern formation for dog bone specimen under tensile load.

Composites presented deflection hardening behavior with multiple-cracking pattern (2-3 cracks) with 2% increase in bending strength. Figure 5-15 presents bended specimen with two cracks formed corresponding to two peaks on the flexural strength versus deformation diagram. The results are presented in Table 5-3.
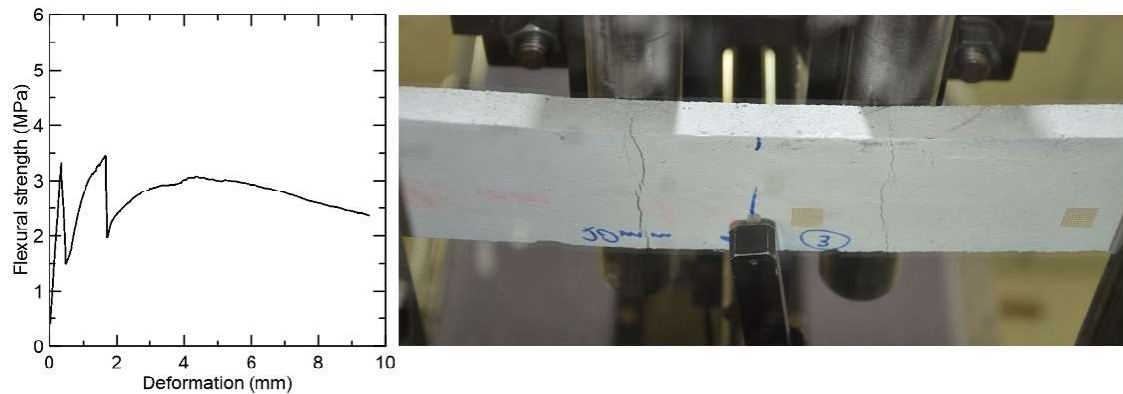
Figure 5-15 Example of composite plate reinforced with 4% of 20 mm two-stage treated curauá fiber behavior under 4 point bending test.

Compression strength verified on cylinders (50 mm x 100 mm) presented strength reduction caused by fiber addition from 40.75±2.34 MPa for pure matrix to 20.23±0.78 MPa for matrix with 4% fiber volume.

Table 5-3. Composite properties obtained from tests for two staged treated curaua fiber with 4%.

Test mode	First crack strength (MPa)	Maximum strength (MPa)	Strength growth (%)	Strain (%)	Number of cracks
Direct tension	1.75 (0.19)	1.91 (0.13)	9	0.4 – 0.8	2 - 4
4-point bending	3.26 (0.19)	3.34 (0.16)	2	-	2 - 3

5.3 STRAIN CAPACITY IMPROVEMENT BY THE FIBER LENGTH MODIFICATION

5.3.1 Tensile properties of curauá fiber

The tensile tests were performed on single fibers according to the methodology presented in chapter 4 and are collected in Table 5-4.

Table 5-4. Tensile strength of two-stage treated curauá fiber for 10, 20, 30 and 40 mm gage length.

Fiber length (mm)	Area (mm^2)	Diameter (µm)	Strain (%)	Force at rupture (N)	Strength (MPa)	Young modulus (GPa)
20	0.00482	77.70	2.01	3.36	697.19	39.01
	(0.00103)	(8.23)	(0.37)	(0.92)	(153.74)	(7.02)
30	0.00626	87.83	1.84	4.07	630.75	36.38
	(0.00184)	(13.26)	(0.51)	(1.78)	(164.43)	(4.28)
40	0.00574	85.56	1.71	3.93	615.22	36.11
	(0.00162)	(9.13)	(0.49)	(1.48)	(146.77)	(4.05)

The gage length has influence on fiber performance at tensile test. The longer the length the lower tensile strength and force at rupture. This could be explained by the higher risk of fiber flaws and micro damages which increase with fiber length. There is no significant difference in elastic modulus except the standard deviation which decreases with length.

5.3.2 Comparison of fiber-matrix interaction for 10, 15 and 20 mm pull-out specimens

The specimens of 10, 15 and 20 mm of embedment length were prepared and tested to verify the fiber-matrix interaction. The lengths 10, 15 and 20 mm are the halves of the 20, 30 and 40 mm fiber's length used in composite. The graphical results are presented in Figure 5-16.
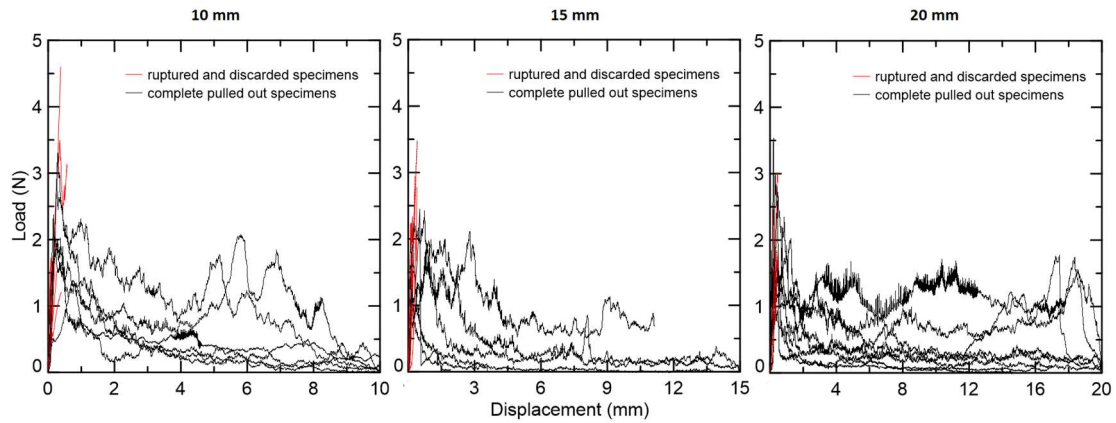
Figure 5-16 Results of pull-tests on two-stage treated curauá fiber for 10, 15 and 20 mm of embedment length (red color is marked for ruptured and discarded fibers).

The increase of embedment length caused greater percentage of ruptured fiber during analysis. The data based on completely pull-out fiber shows that bond properties decreased with embedment length. This could be caused by higher interaction between fiber and matrix and higher risk of fibers rupture than pull-out. In other words fibers which presented completely pull-out behavior were less bonded to the matrix. The complete pull-out behavior is welcome for strain-hardening composite design, because of continuous interaction between fiber and matrix, without fiber failures.

Table 5-5. Results of pull-out tests for two-stage treated curauá fiber which presented complete pull-out behavior for embedment lengths 10, 15 and 20 mm.

Length (mm)	Area (μm^2)	Perimeter (μm)	P_a (N)	P_b (N)	P_{max} (N)	G_d (J/m^2)	τ_{Pa} (MPa)	τ (MPa)	Complete (ruptured)
10	12549 (7245)	442 (148)	2.22 (0.90)	1.88 (0.70)	2.47 (0.78)	0.13 (0.05)	0.52 (0.21)	0.59 (0.21)	13 (7)
15	11049 (6161)	436 (146)	1.99 (0.77)	1.57 (0.92)	2.72 (1.38)	0.10 (0.19)	0.32 (0.12)	0.42 (0.15)	11 (9)
20	12616 (6315)	435 (115)	1.56 (0.88)	1.12 (0.47)	2.11 (1.31)	0.09 (0.20)	0.18 (0.10)	0.26 (0.11)	10 (10)

The results provided by pull-out test (Table 5-5) were applied for theoretical model to verify fiber critical volume for strain-hardening to occur for fiber lengths 20, 30 and 40 mm.

5.3.3 Model prediction

Investigating the natural fiber and its application to theoretical model one should have in mind that the values are not sharp and there is a dispersion of results for single fiber tests which could provide confusing data for model prediction. That is why a caution is recommended for the results and prediction. The model provides a volume range of interest for critical fiber volume which is a base for experimental program verification. The model does not combine the influence of molding process which have influence on fiber performance (ZHOU et al., 2012). Table 5-6 presents data collected for model prediction and critical fiber volumes necessary for filling strength and energy criterions.

Table 5-6. Theoretical model values for different curauá fiber length.

Fiber					Interface		Strength criterion		Energy criterion			Critical Volume
L_f	d_f	E_f	G_d	τ	σ_0	σ_{fck}	$PSH_{strength}$	J_{tip}	J'_b	PSH_{energy}	$V_{strength}$	V_{energy}
mm	μm	GPa	J/m²	MPa	MPa	MPa		J/m²	J/m²		%	%
20	80	39	0.13	0.59	6.11	1.75	3.49	15	76	5.07	4.56	4
30	80	39	0.10	0.42	6.32	1.75	3.61	15	124	8.28	4.47	4
40	80	39	0.09	0.26	5.69	1.75	3.25	15	111	7.46	4.36	4

Graphical representation of the model combines two criterions for strain-hardening providing information about critical fiber volume necessary and indicates the influence of corresponding factors. Figure 5-17 presents the frictional bond influence on critical fiber volume for given fiber lengths 20, 30 and 40 mm. The green area represents the range of critical volume which could be investigated in experimental program (model accuracy issue and laboratory conditions such as manual separation of fibers and molding in small scale without pressuring the specimens).
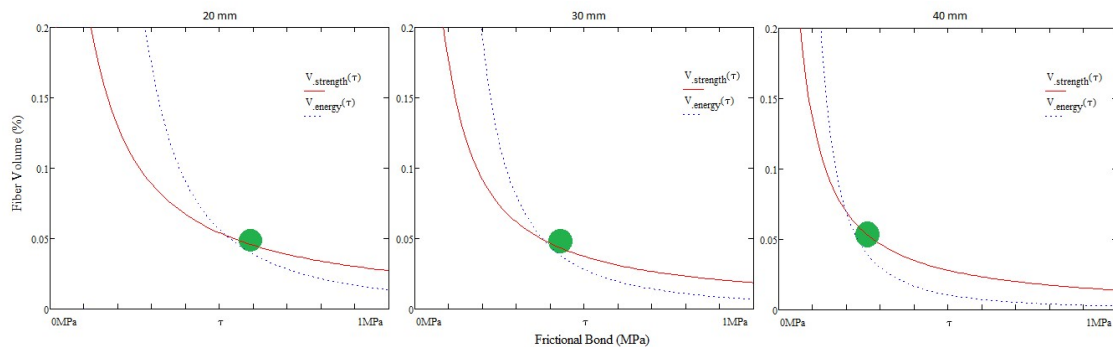

Figure 5-17 Graphical model representation for critical fiber volume for 20 30 and 40 mm two-stage treated curauá fiber.

Marked green circle represents real possibility of strain hardening behavior for 20, 30 and 40 mm two-stage treated curauá fibers. The predicted critical volume is 4% for energy

criterion and oscillates around 4.5% for strength criterion. The interesting fact is that the greater fiber length did not reduced critical volume prediction which is associated with decreasing bond properties for completely pull-out fibers. For experimental program the lower value of critical fiber volume was applied, because of workability issue with that amount of fiber and model accuracy.

5.3.4 Experimental verification

Table 5-7 presents the comparison of the tensile tests carried on composites for selected fiber lengths.

Table 5-7. Results of tensile tests carried on dog bone samples on composites reinforced with 4 % of two-stage treated curauá fiber of 20, 30 and 40 mm lengths.

Fiber length (mm)	First crack strength (MPa)	Maximum strength (MPa)	Strength growth (%)	Average crack width (μm)	Maximum strain (%)
20	1.75 (0.19)	1.91 (0.13)	9.40 (4.40)	Below 100	0.8
30	2.57 (0.05)	2.57 (0.05)	-	-	0.7
40	2.01 (0.33)	2.19 (0.24)	4.32 (4.67)	100 - 150	1

The all groups presented multiple cracking pattern under tensile test. Specimens reinforced with 20 and 40 mm fibers presented strain-hardening behavior with strength growth (9 and 4% respectively) after first crack occurred. Specimens reinforced with 30 mm presented strain-softening behavior which is correlated with high first crack strength in comparison with other groups. This could be caused by any difference in molding process or fiber properties variation. This also shows the importance of first crack strength and provides an idea about fiber bridging capacity. In other words in this set of matrix, fiber and fiber-matrix properties we can influence strain capacity of composite or number of cracks to be formed by choosing the fiber length but all this is going to happen around real fiber bridging capacity close to 2 MPa (Figure 5-18).
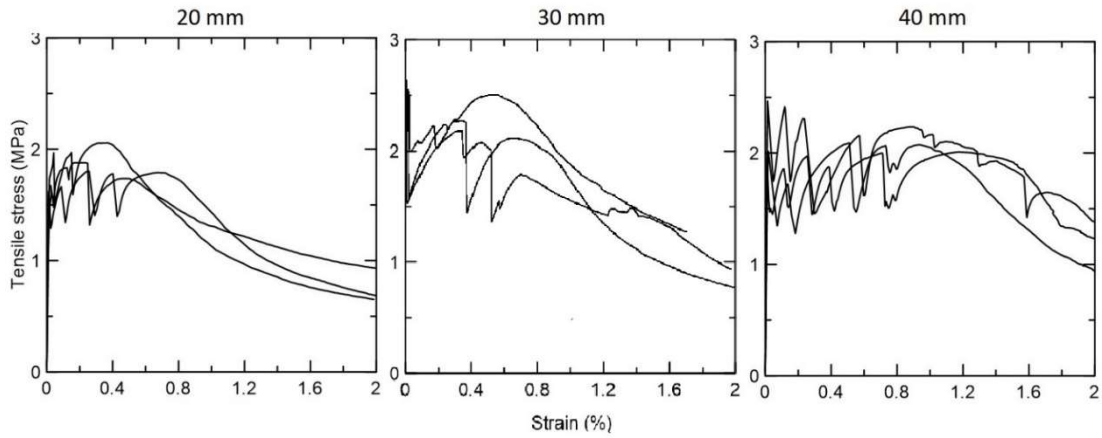
Figure 5-18 Results of tensile tests carried on composites reinforced with 4% of 20, 30 and 40 mm two-stage treated curauá fiber.

Figure 5-19 presents crack formation of composite reinforced with 4% of 40 mm fiber. There is a clear new crack formation pattern up to 4th crack where one of the crack started opening. However the failure is not rapid and fibers still connect fissured composite.
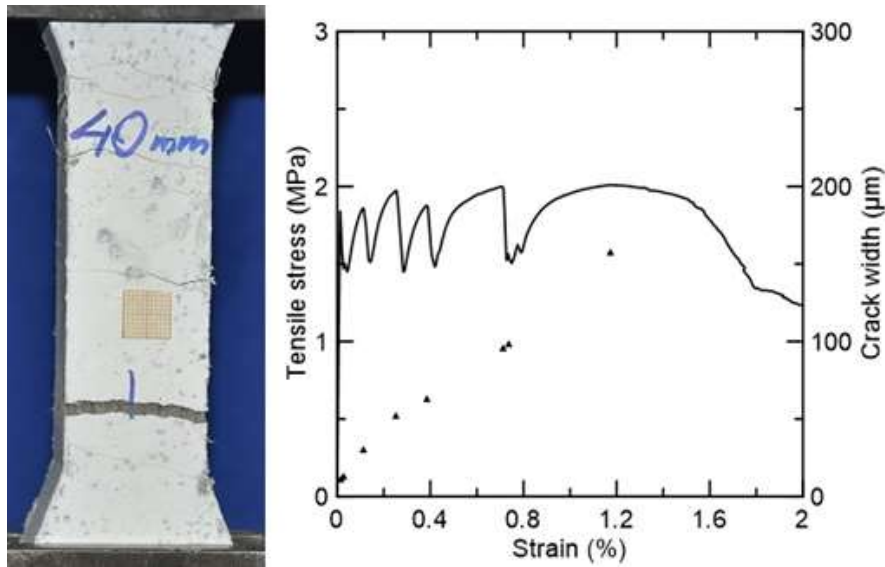
Figure 5-19 Crack formation for composite reinforced with 4% of two-stage treated curauá fiber of 40 mm length.

Table 5-8 presents the results of 4-point bending tests for the composites with selected fiber lengths.

Table 5-8. Results of 4 point bending test carried on composites reinforced with 4% of two-stage treated curauá fiber with 20, 30 and 40 mm fiber length.

Fiber length	First crack strength	Maximum strength	Strength growth	Number of cracks
(mm)	(MPa)	(MPa)	(%)	
20	3.26 (0.19)	3.34 (0.16)	2	2 - 3
30	3.50 (0.05)	3.84 (0.31)	10	4 - 8
40	3.82 (0.30)	4.14 (0.68)	8	4 - 9

All groups presented deflection-hardening behavior with multiple cracking pattern. The fiber's length has influence on number of cracks to be formed (the longer was the fiber, the more cracks appeared). This could be related to the scale effect and greater efficiency of crack bridging by longer fiber.
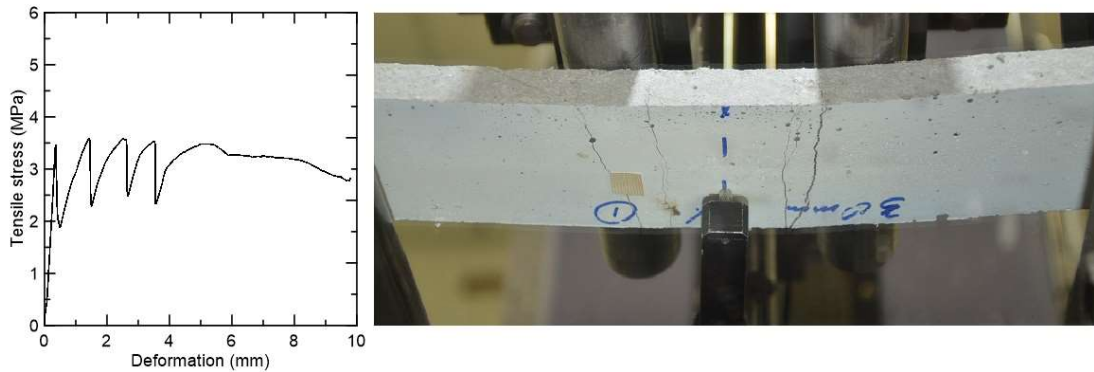
Figure 5-20 Crack formation under 4 point bending test over composite reinforced with 4% of 30 mm two-stage treated curauá fiber.

Composites reinforced with 4% of 30 mm two-stage treated curauá fiber presented 10% growth of strength after first crack and multiple cracking pattern of 4 to 8 cracks (Figure 5-20). The fiber bridging was much more effective in this case and many cracks were formed during the test.
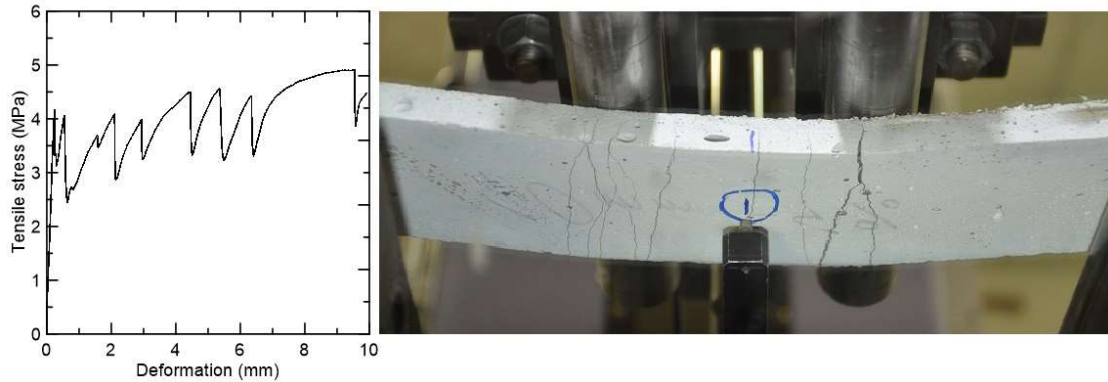
Figure 5-21 Crack formation under 4 point bending test over composite reinforced with 4% of 40 mm two-stage treated curauá fiber.

Composites reinforced with 4% of 40 mm two-stage treated curauá fiber presented strength growth of 8% and multiple cracking pattern of 4 to 9 cracks during the test (Figure 5-21). This group presented the most promising behavior under bending and as well under tension and is going to be investigated in future tests for durability verification. Compressive strength verified on cylinders (50x100 mm) showed strength reduction caused by 4% of volume fiber addition from 40.75±2.34 MPa for pure matrix to 20.23±0.78 MPa for 20 mm, 17.95±0.99 MPa for 30 mm and 19.72±1.54 MPa for 40 mm fiber reinforced specimens. The addition of 4% fiber reduced compressive strength about a half, which was related to added volume not the length of the fiber.

5.4 CONCLUSIONS

This chapter presented the process of data collection for micromechanical modeling of critical fiber volume needed for strain hardening to occur in cement based matrix. The matrix fracture was tested. The fiber properties were investigated along with washing cycles influence on fiber size. The beneficial influence of alkaline treatment on fiber-matrix was evaluated. All data was implemented into micromechanical model for critical volume prediction, which was verified on direct tensile, 4-point bending and compression tests. Summarizing the investigation the fallowing conclusions are made:

- The Tapered Double Cantilever Beam (TDCB) specimens were used successfully for matrix fracture energy verification as a first step of micromechanical design. The value of 15 J/m^2 obtained for the matrix composed of (Cement, Fly Ash, Metakaolin), evaluated as the area under the curve of applied force versus crack opening was used in model prediction.

- Cycles of washing and drying improved fiber aspect ratio from 262 to 280 more by the area decrease.

- The second stage (alkali treatment) improved bond between fiber and matrix which was beneficial for critical fiber volume reduction needed to strain-hardening occur.

- Addition of 4% of 20 mm of two-stage treated fiber was sufficient for obtaining pseudo strain hardening behavior with multiple cracking pattern.

Fiber length has influence the strain capacity of strain-hardening cement composites reinforced with two-stage treated curauá fiber.

- The longer the fiber length more cracks are formed and strain capacity is increased.

- The positive influence of fiber length was also visible during bending, the longer the fiber more deflection capacity was observed with more crack formation.

- The fiber application reduced the compressive strength of the composite in comparison to pure matrix. This phenomenon is related to added volume and no significant difference was observed between cylinders reinforced with different fiber length but the same volume.

- For durability studies the composites reinforced with 4% and 40 mm fibers were chose as they presented the highest deformation capacity with various cracks under tensile and bending stress.

6 NATURAL WEATHERING OF SHCC REINFORCED WITH ALKALI TREATED CURAUÁ FIBER

Chapter 6 is a continuation of research program on strain hardening cement composites with Brazilian two-stage treated natural curauá fiber. After investigation of fiber critical volume needed for strain hardening behavior and influence of fiber length on composite's strain capacity this chapter focus on the durability of composites exposed to natural weathering conditions. The sets of:

- *5 dog bone specimens reinforced with 4% of 40 mm two-stage treated curauá fiber,*
- *7 TDCB specimens,*
- *40 pull-out specimens,*

were exposed to natural weathering for periods of 3, 6, 9 and 12 months. Along the composite's performance, the matrix changes and fiber-matrix interaction were analyzed. The observation of the composite under optical microscope provided visual data on fiber-matrix interaction.

6.1 METHODOLOGY

6.1.1 Location

The test location was laboratory roof at Cidade Universitaria, Federal University of Rio de Janeiro on Ilha do Fundão, Rio de Janeiro, Brazil with coordinates 22° 51' 39.666" S, 43° 13' 52.904" W (SunEarthTools.com).

Figure 6-1 Location of natural weathering tests with sun path and specimens exposition on the roof (SunEarthTools.com).

Specimens were placed on the metallic roof, which is surrounded by a wall. The metallic surface could increase the temperature level of specimens that is why they were located on a plastic cage to provide good ventilation and reduce heat transfer from metallic roof to specimens. The Figure 6-1 presents the exact roof location with sun path on 24.01.2017 with underlined the shortest day (top black line) on 21st of June and the longest day (bottom black line) on 21st of December. The yellow filling represents the range of sun movement during the whole year period.

6.1.2 Weather analysis

Climate zone in state Rio de Janeiro is described as Tropical Brazil Central according to (NIMER, 1979). On the official web page of Rio de Janeiro metropolitan area climate is described as tropical hot and humid with local variations due to altitude, vegetation and ocean proximity. Annual medium temperature is about 22° C with higher medium

temperatures during summer (30 - 32° C) from December to March and is characterized by long luminous days with short rainfalls during evenings (PREFEITURA DO RIO DE JANEIRO, 2009). Weather conditions were measured by weather station from BIOWIN connected by radio frequency with PC "Easyweather software" for data analysis. The range of station's working temperature is -40 to 65° C with precision 0.5° C. The humidity range from 1 to 99% with 5% precision. The data was collected in periods of 30 minutes and average values are presented in Table 6-1.

Table 6-1. Weather data averages collected for natural weathering location from June 2016 to May 2017.

	Jun	Jul	Aug	Sep	Oct	Nov	Dec	Jan	Feb	Mar	Apr	May
Minimum temperature (°C)	18.7	18.4	17.9	16.6	17.7	17.1	20.0	22.8	22.0	22.6	18.5	16.9
Average temperature (°C)	21.8	21.4	21.8	24.5	25.2	26.4	27.7	30.4	30.3	30.3	26.1	25.0
Maximum temperature (°C)	35.9	34.9	38.9	40.5	40.9	41.2	41.7	43.1	43.0	41.2	40.6	35.5
Monthly rainfall (mm)	61	40	33	45	39	133	100	109	126	132	172	62
Days with rainfall (>1mm)	6	4	5	7	7	9	11	15	12	9	10	6
Minimum relative humidity (%)	17	18	16	29	20	27	20	21	26	24	27	17
Average relative humidity (%)	77	77	67	67	66	67	63	58	64	69	67	77

6.1.3 Testing methods

6.1.3.1 Composite tensile strength

The tensile dog bone specimens of 330 mm length with 80 mm of the clear span with the cross-section of 30 mm by 30 mm. Tensile tests were carried at Shimadzu, with the load cell of 100 kN and 0.1 mm/min velocity (MAGALHÃES, 2013).

6.1.3.2 Compact tension

The TDCB specimens were tested under tensile load in testing machine Shimadzu AG-X with a load cell of 1 kN at displacement rate 0.01 mm/min. The area below the curve of applied load versus crack opening (measured by clip gage) was used for matrix toughness calculation.

6.1.3.3 Pull-out tests

The 10 mm tube specimens were tested to verify pull-out behavior in micro force machine Tytron 250 with 50 N load cell. Pull-out specimen consist the fiber which is protected by the matrix and a part which is exposed to external hazards. Due to the risk of exposed fiber damage, the set of 40 pull out specimens was prepared for each natural weathering period. The results presents only the specimens which were mountable in the machine (the exposed fiber survived environmental stress).

6.1.3.4 Verification of matrix pH

The pulverized specimen of 500 mg was mixed with 10 ml of deionized water. The suspension was stirred by a sonic mixer for 10 minutes. The pH analysis was carried at pHmeter (NOVA) by the electrode in the water system.

6.1.3.5 X-ray diffraction

X-Ray diffraction was carried at Bruker D8 Focus Advance Eco (Cu-kα tube, λ= 1.5418 Å, 40kV and 35 mA). Operating range was from 4° to 104° of 2θ, with increment of 0.010°

6.1.3.6 Thermogravimetric analysis

Thermogravimetric analysis was carried at TGA Q-500, TA Instruments. The test started with the initial temperature of 35° C, which was maintained for 1 hour before constant heating with the rate of 20° C/minute up to 950° C. Nitrogen was used as purge gas. The analysis was done specimen of 10 mg.

6.1.3.7 Visual observations

The rectangular specimens were selected from the tensile region of dog bones and broken into halves to make visual observation of fiber-matrix interaction (Figure 6-2). The surface of the fractured specimens was observed under an optical microscope.

Figure 6-2 Preparation of the specimens for visual observation of fiber-matrix interaction.

6.1.3.8 Fiber reinforcement pull-out work indicators for composites

After methodology applied to cement-based textile composites by (BUTLER; MECHTCHERINE; HEMPEL, 2009) also used by (FIDELIS et al., 2016) the fiber pull-out work was calculated and used in composites durability studies comparison.
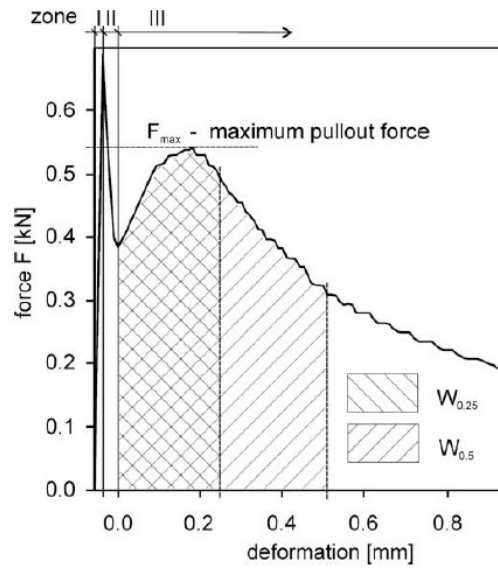
Figure 6-3 Schematic representation of load-deformation curve with calculated indicators F_{max}, $W_{0.25}$, and $W_{0.5}$ (BUTLER; MECHTCHERINE; HEMPEL, 2009).

Figure 6-3 presents the schematic representation of load-deformation curve for double pull-out specimens reinforced with a textile. The zone I (not-cracked specimen) and zone II ("snap-back", the force drop after cracking) are discarded in analysis. The only zone III (originally yarn pull-out, in this study fibers pull-out) is investigated and indicators of the maximum force (F_{max}), fiber pull-out work ($W_{0.25}$) and ($W_{0.5}$) at crack widths of 0.25 mm and 0.5 mm are calculated.

Due to only one crack formation of the dog-bone composites submitted to durability studies they worked as a double pull-out specimens similar to presented methodology. The same indicators were calculated and representative curves for the natural weathering, wetting and drying cycles, and freeze and thaw cycles were drawn. The results were compared to the indicators calculated for composites reinforced with 4% of 40 mm curauá fiber despite the multi crack formation. The presented methodology was used to verify the fiber bridging capacity and the work was used as a parameter.

6.2 RESULTS AND DISCUSSION

6.2.1 Weather variations

Collected data presents the temperature and humidity variations over monthly periods (Table 6-1). The weather measurements presented the difference between maximum and minimum temperatures in the range of 24° C. However, the temperature measured at the specimen's surface during daylight presented values even higher about 10° C. This difference is related to insolation of composite's surface, where the weather station's thermometer is located in a plastic box protected from direct sunbeams. This information helps to understand that the composites were exposed to higher temperature stress when compared to weather station data. The collected data presents the weather fluctuation which occurred in an environment around the composite. Figure 6-4 presents the data collected during April 2017, where the day-night temperature variations are visible (left). The temperature/humidity cycles are visible for the week 18-24 of April 2017. Finally, the micro cycles on the 23rd, when the morning small rain was followed by the temperature increase about 5° C, then another rain and temperature decreased to once again there was rain. To summarize exposure to natural weathering could be compared to exposure to the combination of temperature and humidity macrocycles and microcycles.
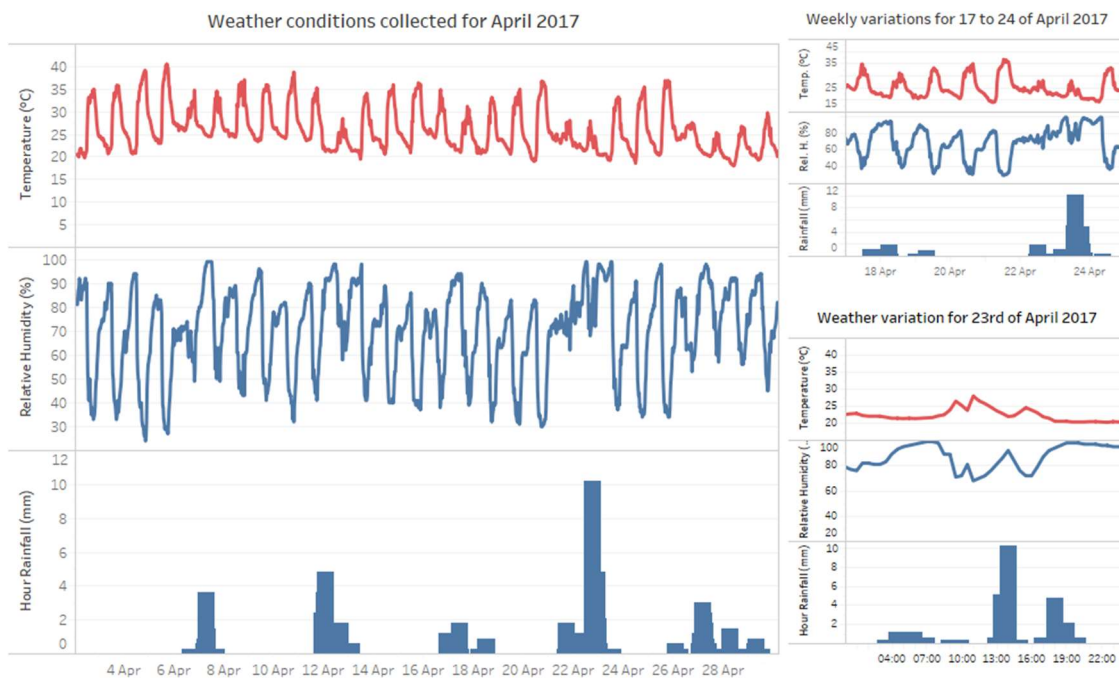

Figure 6-4 The weather variations measured by weather station over one month (left), one week (top right), one day (bottom right).

Such a combination of cycles could be difficult to reproduce in laboratory controlled conditions which make the results unique for a given set of specimens and period of exposure.

6.2.2 Composite durability

The dog bone specimens tested under tensile load did not present strain hardening nor multiple cracking pattern after natural weathering exposure (Figure 6-5). The first group exposed to 3 months presented results out of expectation (the first crack strength lower about a half in comparison to 28 days composites), which could be related to an improper molding process where fiber bundled together and the matrix did not present sufficient continuity. The groups exposed to 6, 9 and 12 months presented strain softening behavior with visible work of fibers in the composite, but not sufficient to bridge the crack for another to occur. The composites presented the first crack strength equal to 1.75 MPa for 6 months, 2.06 MPa for 9 months and 2.03 MPa for 12 months of exposure so there is no deterioration of composite's tensile strength over verified time periods.
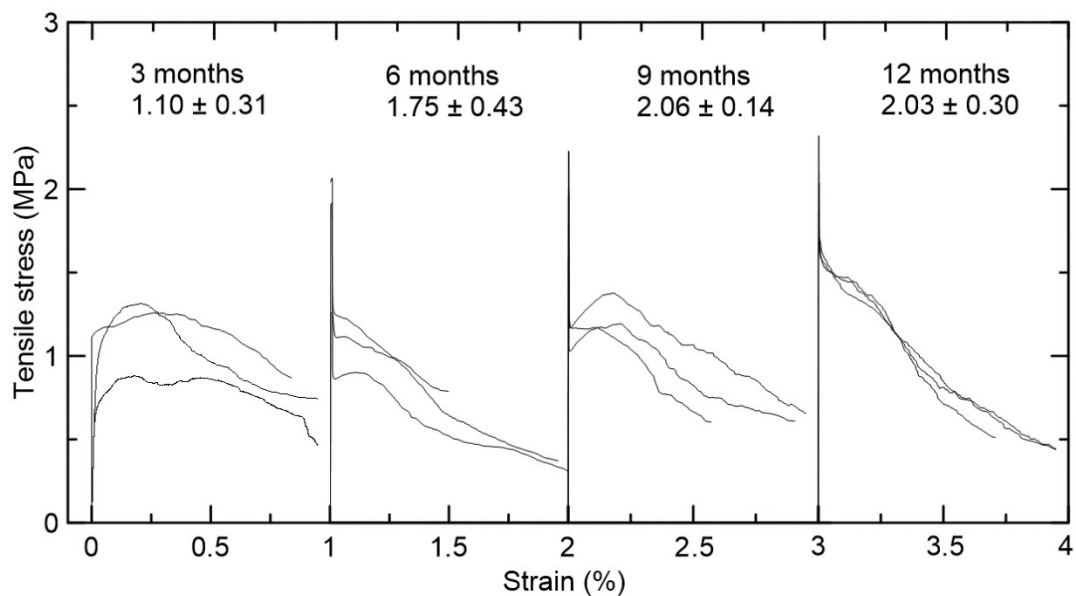
Figure 6-5 Results of tensile strength test carried on dog bone specimens exposed to 3, 6, 9 and 12 months of natural weathering.

The descending stress-stress curve during tensile test means that fiber survived in the matrix environment for the whole period, but the interaction between fiber and matrix deteriorated. This could be the result of the matrix and fiber properties changes.
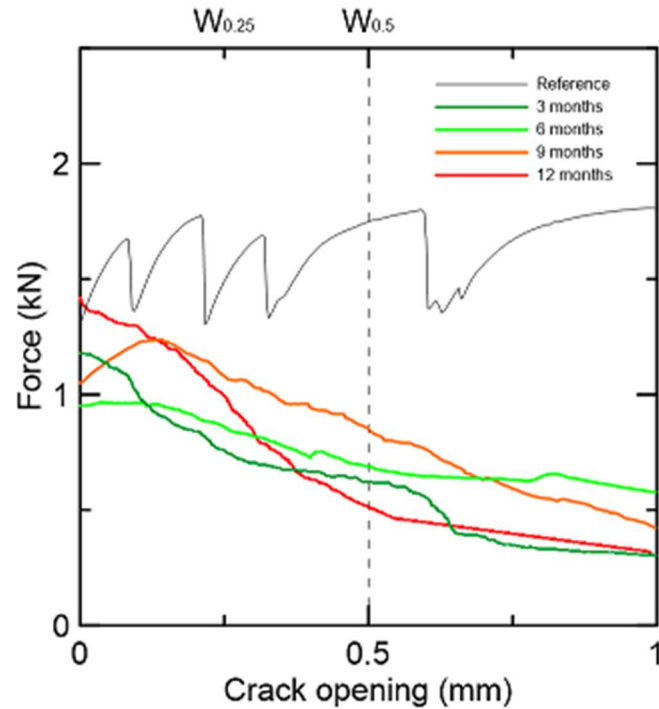
Figure 6-6 Force versus crack opening representative curves for specimens exposed to natural weathering compared to the reference specimen tested at age of 28 days.

Figure 6-6 presents the force versus crack opening representative curves for specimens exposed to natural weathering periods with comparison to the reference tested at the age of 28 days. The data collected in Table 6-2 presents the average values of indicators of fiber pull-out work and maximum pull-out fiber force. The specimens exposed to natural weathering presented lower work indicators in comparison to reference specimen. The difference is visible in the pull-out work up to 0.25 mm crack width, where 0.41±0.05 Nm for reference is higher to any value representing the natural weathering period (0.23 to 0.30 Nm). This difference continues for the work up to 0.5 mm, where reference specimens presented 0.83±0.05 Nm, higher than any other period.

Table 6-2. Average values of the maximum pull-out force (F_{max}), the pull-out work up to crack width 0.25 mm ($W_{0.25}$) and 0.5 mm ($W_{0.5}$) with standard deviation in the brackets.

	F_{max} (N)	$W_{0.25}$ (N m)	$W_{0.5}$ (N m)
Reference	1953 (*193*)	0.41 (*0.05*)	0.83 (*0.05*)
3 months	1232 (*134*)	0.28 (*0.05*)	0.50 (*0.08*)
6 months	975 (*129*)	0.23 (*0.03*)	0.38 (*0.06*)
9 months	1219 (*236*)	0.29 (*0.05*)	0.49 (*0.07*)
12 months	1440 (*106*)	0.30 (*0.01*)	0.49 (*0.02*)

Comparison between the periods of natural weathering exposure did not present significant differences. This suggests that once changed the fiber bridging capacity does not deteriorate with periods of exposure so the initial stage of exposure is crucial to fiber bridging durability.

6.2.3 Matrix durability

Figure 6-7 presents results of compact tension test for TDCB specimens. The graphs present the curves of applied force versus crack opening for 3 specimens which presented the most planar crack propagation.
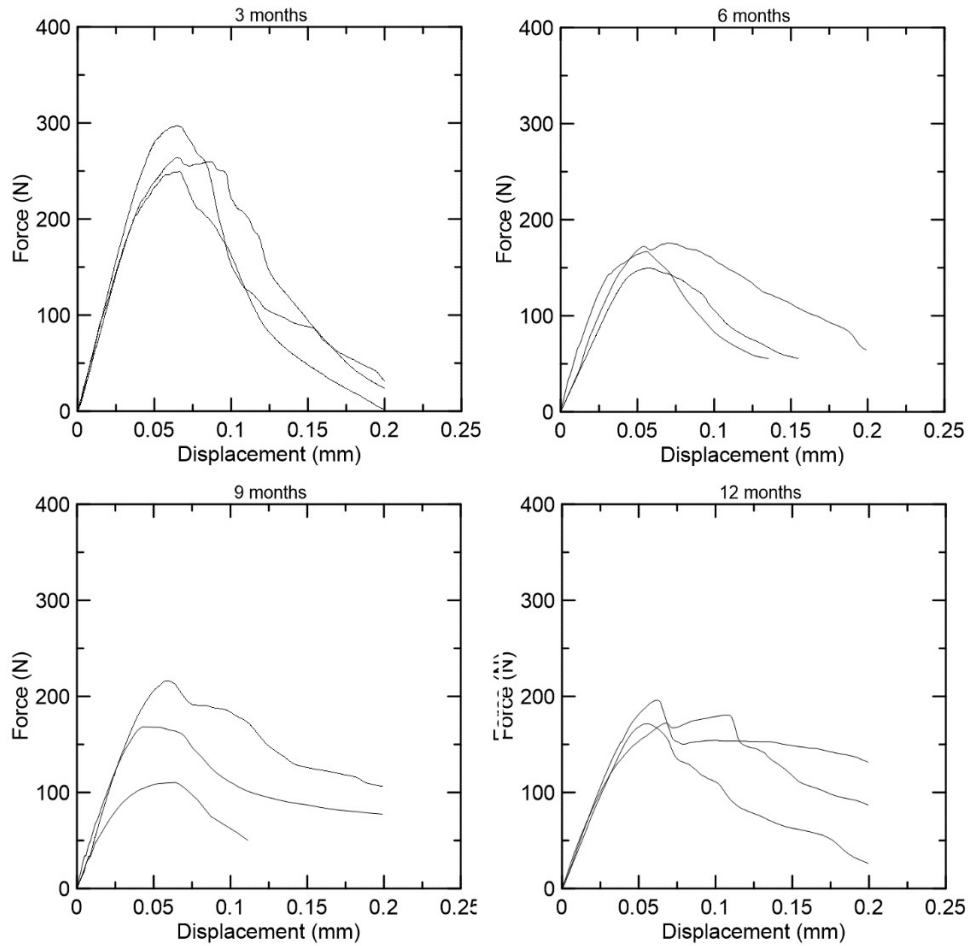
Figure 6-7 Curves of applied force versus crack opening (measured by clip gage) for TDCB specimens exposed to natural weathering period (3, 6, 9 and 12 months).

There is a significant difference between crack propagation between periods. The critical force diminishes from 270 N for 3 months, through 164 N after 6 months to 180 N and 184 for 9 and 12 months respectively. This difference could be correlated with internal changes and matrix embrittlement with time as well as a crack formation at specimens notch which could occur due to temperature and humidity gradient.

Figure 6-8 Crack developed during the exposure to natural weathering conditions.

Figure 6-8 presents the crack developed during the exposure to the natural weathering conditions at the specimen's notch. The cracks developed at the notch were in the range of 3-7 mm.

The fractured surface of TDCB specimens presented the color difference between internal and external regions (Figure 6-9). The internal region presented darker color. The fracture surface was treated with 0.1% of phenolphthalein solution in alcohol (commonly used for carbonation testing techniques). The internal darker region instantly changed color to purple, typical reaction for cement matrix free from the carbonation. The external region maintained its original color and no change was observed. The difference of color between internal and external region indicated the difference of pH values (higher for the internal region).
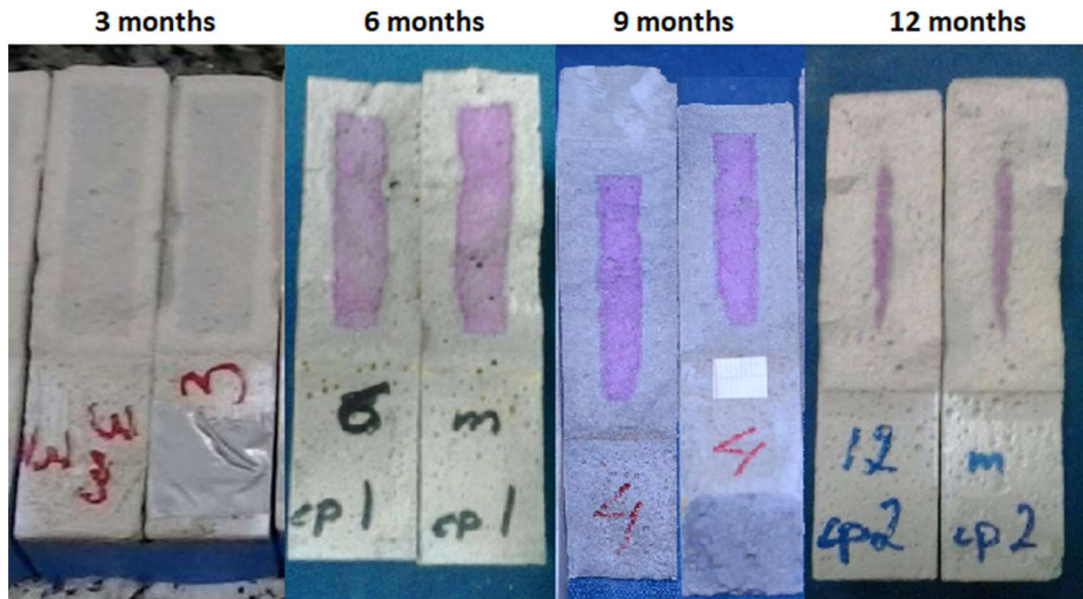
Figure 6-9 Observed color difference between internal and external regions of fracture surface (3 months), purple color due to superficial phenolphthalein treatment (6, 9 and 12 months).

The pH difference was verified on the ground specimens (5 grams) from the internal and external region. The pH test was carried at the temperature of 25° C and results were 10.73 for the colored internal region and 9.21 for external. The change of pH over time as well as the difference of pH along the element cross-section creates an environment where the fiber located close to the center work in higher pH that external region.

For specimens used for carbonation analysis, the color difference after phenolphthalein treatment suggests Calcium hydroxide (CH) presence instead of Carbonate. To increase natural fiber durability in this very cement-based matrix, pozzolanic material (fly ash and metakaolin) was used to react with CH providing matrix free of Calcium hydroxide, preventing the natural fiber from petrification.

Further analysis was necessary to verify compound responsible for pH difference. The additional pulverized specimens were prepared from internal and external regions for 6 and 12 months respectively. The analysis included pH verification, Thermogravimetric analysis and X-Ray Diffraction (Table 6-3).

Table 6-3. pH and thermogravimetric analysis results.

Specimen	pH		TGA			
			Internal		External	
	Internal	External	Water (%)	Carbonate (%)	Water (%)	Carbonate (%)
6 months	10.73	9.21	4.14	3.08 (80.4% am)	2.76	6.39 (48.7% am)
12 months	10.65	9.21	4.96	3.16 (36.5% am)	2.73	6.58 (24.3% am)

The phenolphthalein changes color at 9.6 approximately (OSAWA; GONÇALVES; RAGAZZI, 2006). The internal pH values are higher than 9.6 which justify the color change after phenolphthalein treatment into purple. The identification of oxides of two regions was possible by X-Ray Diffraction analysis. Diffractograms (Figure 6-10) do not show Calcium hydroxide presence nor other type hydroxides, which could be formed by decomposition processes. This result justifies the admixture of pozzolan material for free of Calcium hydroxide matrix.
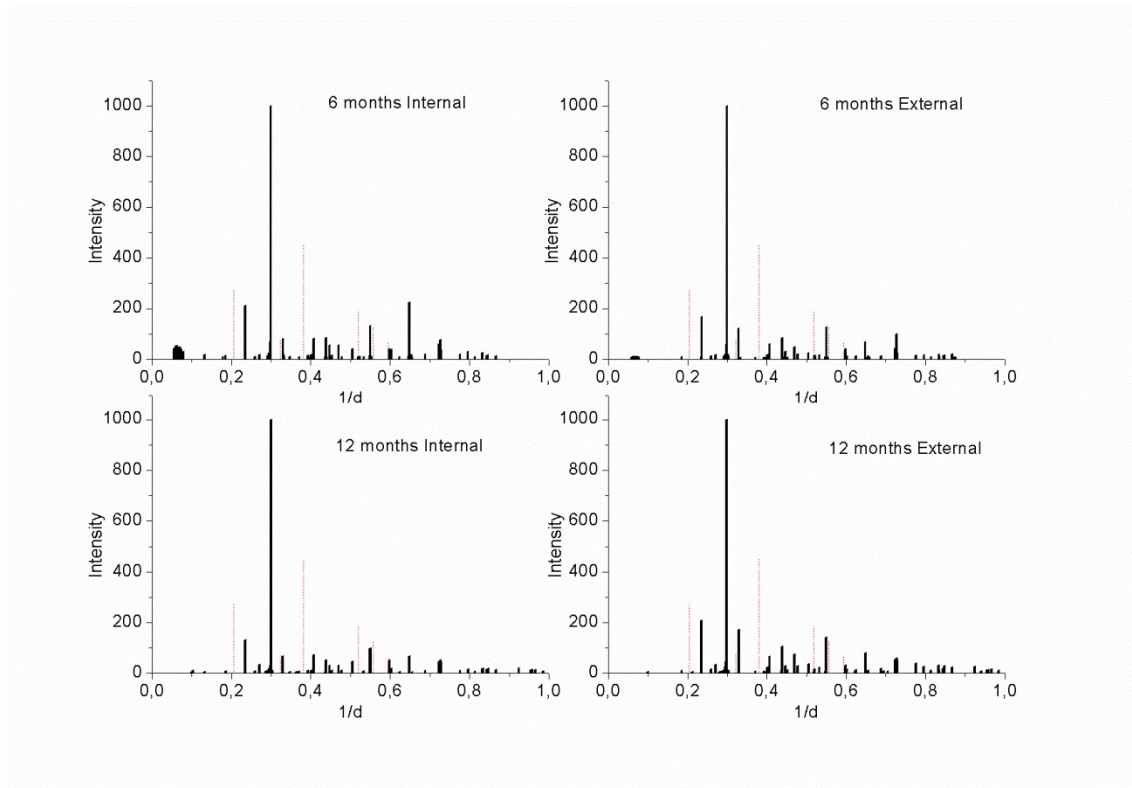
Figure 6-10 XRD diffractograms of internal and external samples at 6 and 12 months. The rows in red are given values of 1/d corresponding to CH (reference 96-100-8781).

Thermogravimetric analysis is extensively used for the quantification of hydroxides and carbonates that are present in cement-based composite pastes. Figure 6-11 presents the dTGA's analysis that indicate their characteristic weight-losses. It is possible to observe that dehydroxylation of CH is not detected. Thermogravimetric analysis shows higher water content of the internal region and lower carbonate content in comparison with the external region.
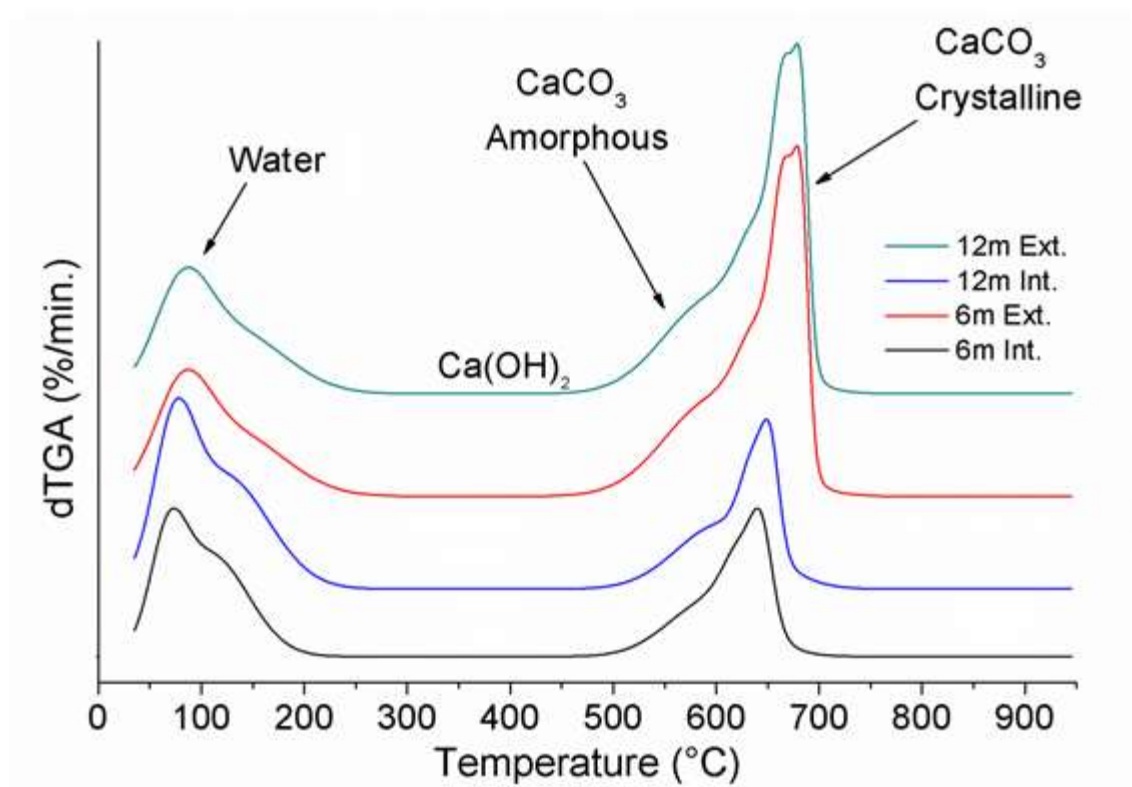
Figure 6-11 Thermograms of external and internal samples of 6 and 12 months.

In thermogravimetric analysis, the amorphous carbonate appears before the decarboxylation of the crystalline carbonate (DWECK et al., 2000), (DWECK et al., 2002). The deconvolution of decarboxylation of the carbonate areas provided the additional data on amorphous fractions of carbonates (WOJDYR, 2010). The carbonates which presented the maximum temperature of calcination lower than 600° C were considered the amorphous carbonates (Figure 6-12). The Thermal Gravimetric Analysis of two specimens presented higher amorphous carbonate concentration for internal region than external.
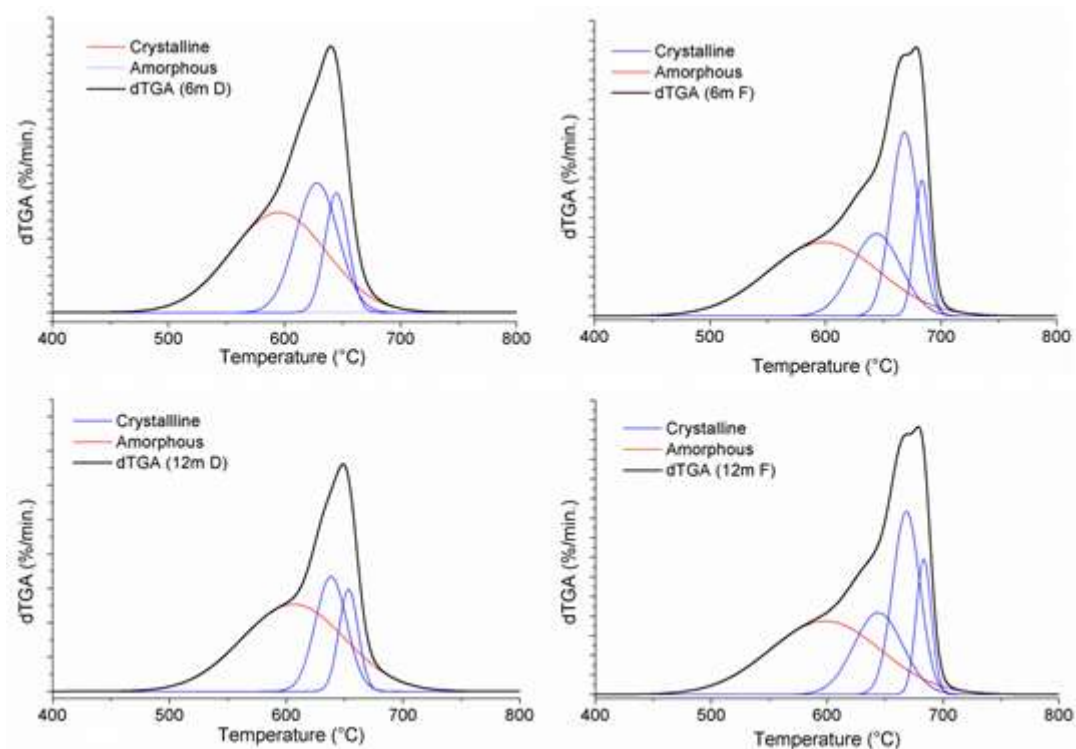
Figure 6-12 Deconvolutions of the thermograms of the internal and external samples of 6 and 12 months for quantification of the amorphous carbonate.

The amorphous carbonate has higher solubility than in crystalline form (BREČEVIĆ; NIELSEN, 1989). The water access to amorphous carbonate can create supersaturated fractions. This supersaturation causes pH to increase and facilitate creation of carbonate crystalline forms already formed by secondary nucleation or by Ostwald ripening (BOTS et al., 2012). This mechanism could justify the internal purple area reduction over time, where the amorphous carbonate due to water access is dissolved and creates the crystalline forms more present in progressing external area (not purple).
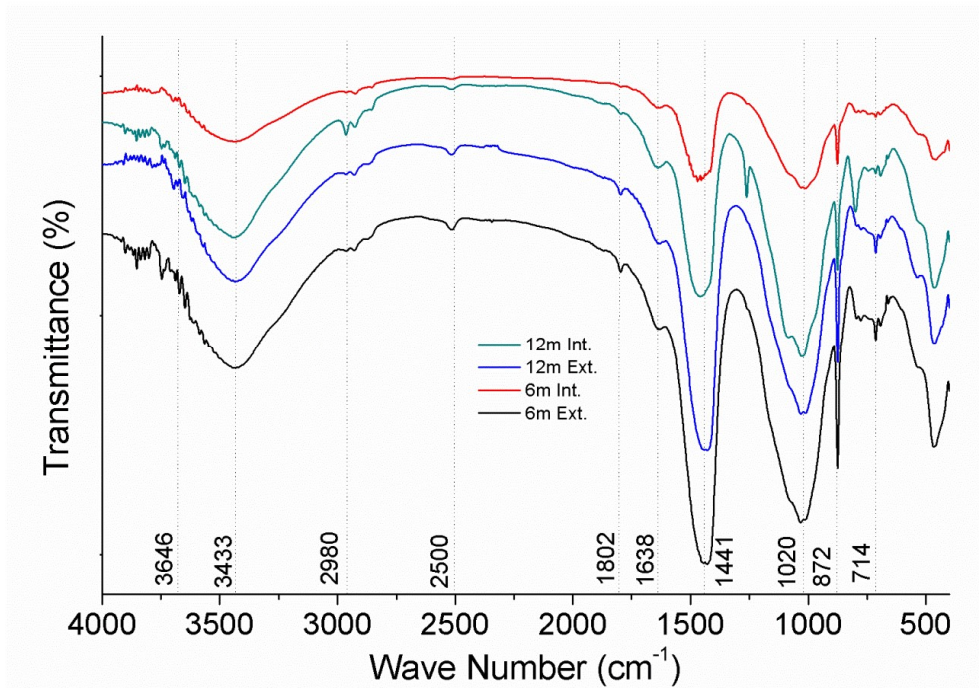
Figure 6-13 FTIR spectra in KBr pellets.

Figure 6-13 shows the infra-red specimens of the internal and external areas at 6 and 12 months. The medium intensity thin band at 3646 cm^{-1}, relative to CH is not observed. Proof of absence of CH as in previous analyzes. In the FTIR spectra, it is possible to observe the following bands: 3433 cm^{-1} (water of hydration of oxides and free water), 2980, 2500 and 1802 cm^{-1} (carbonate overtone bands), 1638 cm^{-1} (Si-O of C2S and C3S), 1441 cm^{-1} (amorphous calcium carbonate), 872 and 714 cm^{-1} (carbonates).

Through the infrared analysis, it was possible to verify the presence of amorphous carbonate in greater quantity in the samples referring to the internal areas. According to (BREČEVIĆ; NIELSEN, 1989) the band at 1441 cm^{-1} corresponds to the amorphous calcium carbonate. The band of higher spectral intensity at 1638 cm^{-1} (corresponding to the Si-O group of C3S and C2S) was correlated with the band referring to the amorphous calcium carbonate. By subtracting the transmittance at 1638 cm^{-1} with the transmittance at 1441 cm^{-1} it is possible to correlate the amount of amorphous carbonate, the lower the value found the higher the concentration. For internal samples of 6 and 12 months, 9.07 and 16.06 were found. In the external samples, the values were 25.94 and 29.61. This indicates that the areas with pink coloration have a higher amount of amorphous calcium carbonate. Due to greater solubility in water, the higher pH values in these areas are justified.

6.2.4 Fiber-matrix bond durability

Figure 6-14 presents the single pull-out test results of specimens which survived natural weathering for 3, 6, 9 and 12 months. The term survived means the specimens were mountable in machine set-up and the pulled out fiber could be held by a grip. For each group of 40 specimens exposed to weathering about half was destroyed (fiber did not survive outside the matrix protection). Especially for the period of 12 months only 11 specimens survived, which 8 presented rupture during the initial test phase so no conclusion for this group is made.
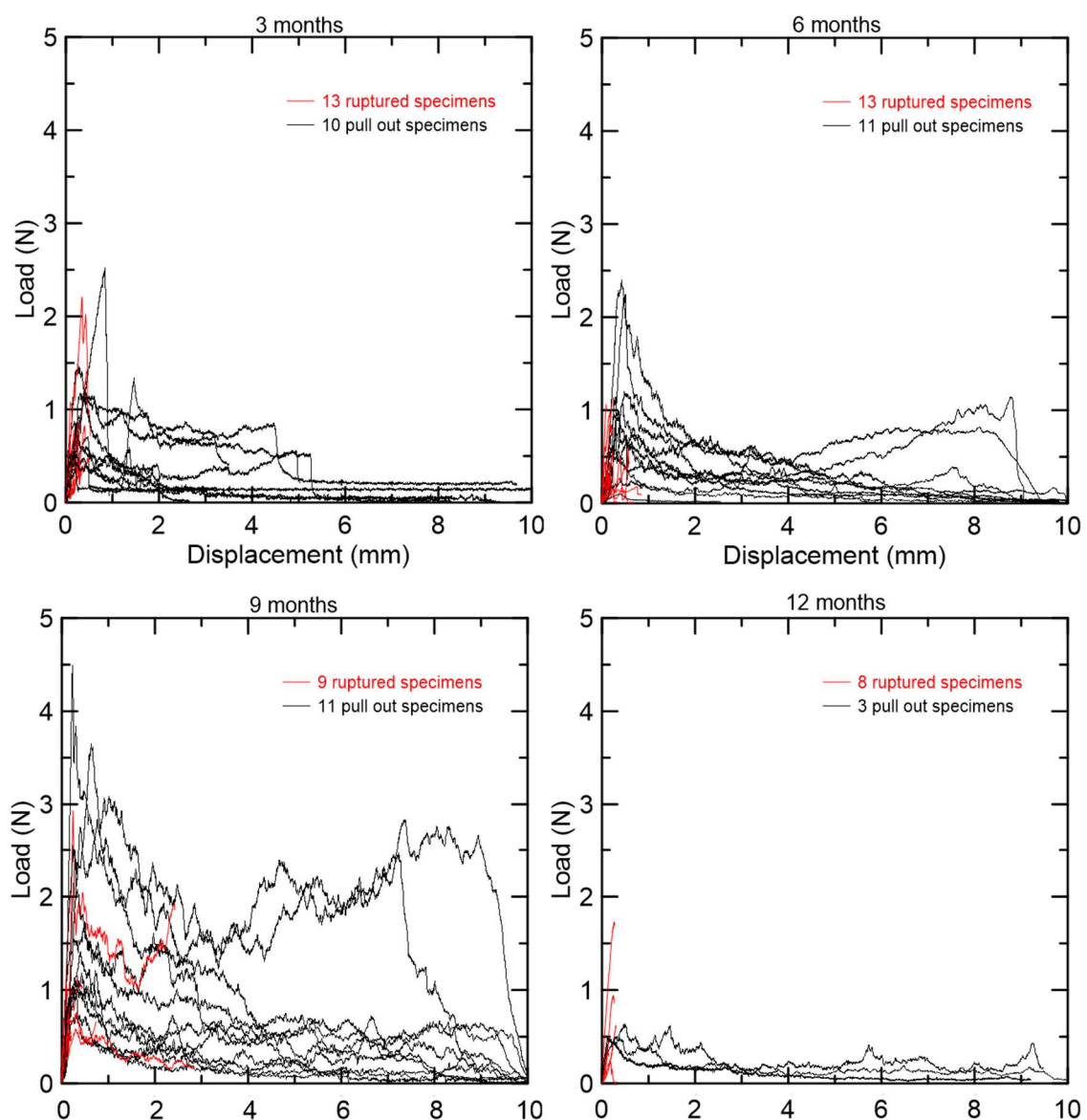

Figure 6-14 Results of single fiber pull-out tests carried on 10 mm embedment length for specimens exposed to 3, 6, 9 and 12 months of natural weathering.

The result of pull-out test proved that the fiber did not petrify in the environment of the designed matrix, which is also proved by the fibers exposed during the tensile test on the dog bone specimens. The pull-out test provided information on still existing fiber-matrix bonding, which is also visible during tensile test of the composite, where the stress-strain curve presented softening behavior instead of rupture.

The values of debonding pull out force for any period of exposure were significantly smaller than for specimens with 28 days only (Table 6-4). The force drop after fiber debonding (P_a - P_b) for 28 days was in a range of 0.34 N, repeated for 9 months specimens. The values of specimens exposed to natural weathering for 3 and 6 months presented force drop of 0.11 N and 0.19 N. This could be an indication of a lower fiber-matrix chemical bond. Due to the loosened connection of fiber to the matrix, the lower force was needed to start a pull-out movement.

Table 6-4. Average values of collected results with their standard deviation in the brackets.

Properties \ Time	28 days	3 months	6 months	9 months	12 months
Tensile Strength (MPa)	2.01 *(0.33)*	1.10 *(0.31)*	1.75 *(0.43)*	2.06 *(0.14)*	2.03 *(0.30)*
Strain-Hardening	Yes	No	No	No	No
Critical Force for TDCB (N)	246.06 *(0.97)*	270.25 *(24.29)*	164.14 *(13.29)*	180.72 *(31.32)*	182.67 *(12.25)*
Crack Tip Toughness (J/m^2)	15	27	24	23	25
10 mm Pull out - P_a (N)	2.22 *(0.90)*	0.74 *(0.67)*	0.96 *(0.79)*	1.59 *(1.24)*	0.45 *(0.04)*
10 mm Pull out - P_b (N)	1.88 *(0.70)*	0.63 *(0.69)*	0.77 *(0.84)*	1.35 *(0.96)*	0.42 *(0.07)*
10 mm Pull out - P_{max} (N)	2.47 *(0.78)*	1.09 *(0.60)*	1.14 *(0.68)*	2.62 *(2.50)*	0.53 *(0.09)*

6.2.5   Visual observations

The visual observation of specimens was carried to verify the hypothesis of lower fiber-matrix connection indicated by pull-out test results. Figure 6-15 presents an example of fiber defibrillation in the matrix. The integrity of fiber is disturbed and singular fibrils are exposed on fracture's surface. The fiber defibrillation could reduce its tensile strength properties. As well as reduce the bond with the matrix, by changing interaction contact from one fiber's surface surrounded by the matrix to many loose fibrils.
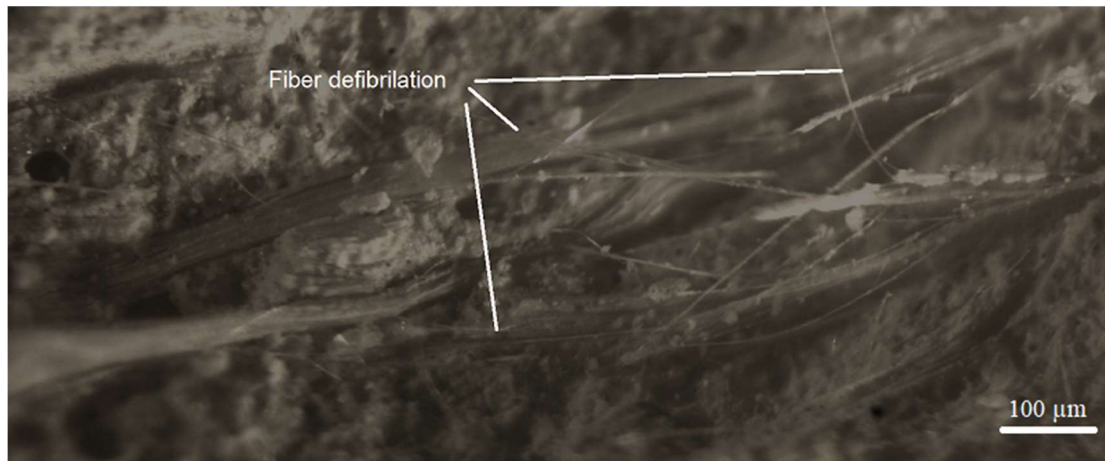
Figure 6-15 Curauá fiber defibrillation in cement matrix.

Figure 6-16 presents a gap between fiber and matrix. The gap (probably caused by fiber swelling and shrinking due to moisture movements) reduced the contact zone between fiber and the matrix. This could justify the lower debonding force during pullout test of specimens exposed to natural weathering in comparison to 28 days specimens which did not suffer any moisture cycles. The gap between fiber and matrix changes the pull-out behavior by providing more frictional relation and reducing the chemical bond.
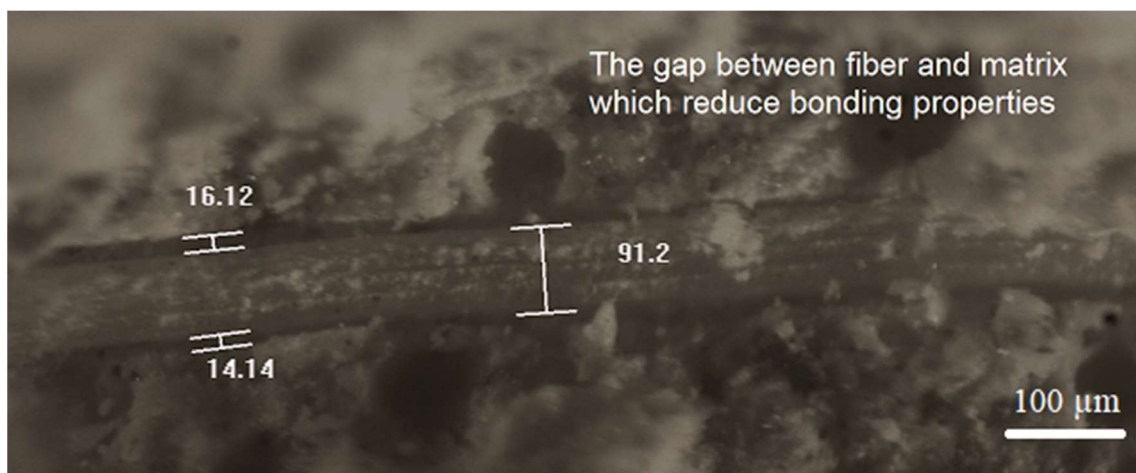
Figure 6-16 Fiber-matrix gap of specimens exposed to natural weathering.

Figure 6-17 presents the matrix products deposited on fiber's surface. This deposition indicates the good interaction between fiber's surface and the matrix, which is favorable for chemical bonding. The matrix products remained on fiber's surface after specimen fracture. This indicates the good interaction between fiber and matrix which is beneficial for bridging properties. However, the visible gap between the fiber and the matrix

indicates that after the exposure to natural weathering periods the connection has been reduced. The deposited matrix products can work beneficially increasing friction during the pull-out phase which could explain the maximum pull-out force (P_{max}) higher in all cases than debonding force (P_a).

Figure 6-17 Matrix products deposited on curauá fiber.

Figure 6-18 presents the imprints of fiber's surface on matrix. The characteristic roving or ribs which are on curauá fiber surface left their imprints on matrix. This indicates that at some point the fiber was closely enveloped by the matrix. It is reasonable to believe that it happened during curing period with stable moisture condition, which would be the reason for higher pull-out results for 28 days cured specimens as well.
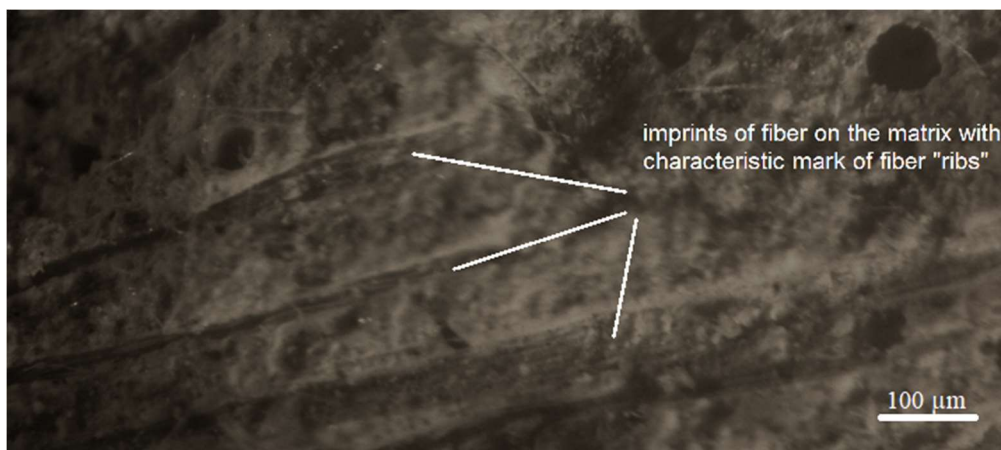
Figure 6-18 Curauá fiber imprints of matrix surface.

93

6.3 CONCLUSIONS

Chapter 6 presented the concept of Strain Hardening Cement-based Composites with natural fiber durability. The carried test presented the data on composite, matrix and fiber-matrix behavior when exposed to natural weathering hazards. To summarize:

- The composites did not present strain hardening behavior after exposure to natural weathering periods of 3, 6, 9 and 12 months, but presented strain softening.
- The loss of strain hardening properties was related to deterioration of fiber-matrix bond. The pull-out tests proved lower values of debonding force and the maximum pull-out force reached for specimens exposed to natural weathering.
- The visual observation of fractured composite indicated the gap between fiber and matrix as main factor responsible for fiber-matrix bond deterioration due to diminished contact area between the fiber and the matrix.
- The fiber imprints on the matrix as well as matrix products on fiber, indicated the good interaction between the two.
- The matrix changes were observed after natural weathering periods. The matrix presented different pH values for internal and external regions which could be an additional stress to fibers.
- No Calcium hydroxide was observed in analyzed specimens, which indicated the matrix free of Calcium hydroxide as intentionally designed.

7 LABORATORY CONTROLLED WETTING AND DRYING CYCLES OF SHCC WITH ALKALI TREATED CURAUÁ FIBER

Chapter 7 presents the degradation of the composites submitted to wetting and drying cycles. The procedure of wetting and drying cycle parameters is defined on dummy specimens. The 3 sets of 10 dog bone specimens were prepared and submitted to the cycles. After 15, 30 and 45 cycles the composites were tested under tensile load in wet (5 specimens) and dry conditions (5 specimens). The composites presented strain-softening behavior. The residual fiber force at rupture and strain was verified on fibers exposed after composite tensile strength test. This procedure was applied to the determination of matrix environment influence on fiber properties. The results were compared to with fibers extracted from composites exposed to 12 months of natural weathering and fibers not enveloped by the matrix.

7.1 INTRODUCTION

The simulation of natural weathering conditions in laboratory scale provides time benefits in comparison to long exposure to environmental hazards. The simulation will never reflect perfectly the environmental stress on composites due to weather variations (annual, monthly, daily variations), but the laboratory-controlled cycles could introduce the similar variations range to the composite. The environmental stress factors which can be easily simulated are temperature gradient and moisture access. The combination of these as Accelerated Aging could provide information on composite deterioration. Depending on the research objective, specimen dimension and material there are various techniques presented in the literature. For example for textile jute cement composites the specimens were exposed to the constant temperature of 40º C at 99% relative humidity for 28, 56, 90, 180 and 365 days for durability verification (FIDELIS et al., 2016).

The different approach was used for the thin cement-based composites reinforced with natural pulp fibers, where the conditions changed cyclically, by immersion in water and drying in elevated temperature (60º C). The composites were submerged to 5 and 25 cycles of wetting and drying and tested in two conditions (saturated and dried). Both conditions presented the deleterious effect of cycles on composite bending strength as well on the specific energy (RODRIGUES et al., 2015).

Wetting and drying cycles applied to cement based composites reinforced with sisal fibers proved to be a form of accelerated aging. The cycles have deleterious effect strength and toughness of the composites. The fiber specimens for "strain-in-cement" submitted to wetting and drying cycles presented accelerating the effect of alkali hydrolysis of fiber's amorphous components and cell wall mineralization, which was indicated by high crystallinity index and low cellulose content. The cyclic changes of humidity at high temperature presented more degradation to composites that static aggressive conditions (WEI; MEYER, 2014).

The "strand-in-cement" test provides data on fiber tensile strength after exposure to a cement matrix. The fiber's ends are resin impregnated and the middle part is enveloped in a cement matrix. After a chosen time period the matrix envelope is removed and fiber is tested for tensile properties (LITHERLAND; OAKLEY; PROCTOR, 1981). Based on the idea of "strand-in-cement" test, the exposed fibers after the composite test were used for the tensile force at rupture determination to verify the influence of wetting and drying cycles on fiber properties when embedded in the matrix.

7.2 METHODOLOGY

7.2.1 Controlled cycles

The wetting and drying cycle parameters (temperature and time exposure) were determined previously on dummy specimens (Figure 7-1). The set of 5 dog bones were weighted after 28 days of curing in a plastic bag with wet paper inner. Then composites were dried at the temperature of 60º C to the point where two consecutive mass measurement presented difference below 1 g. After drying, the specimens were immersed in water for saturation and weighted after 12 hour periods. The mass stabilization was considered as a reference saturation condition. Then the cycle (Table 7-1) was applied to specimens to verify the range of moisture change.

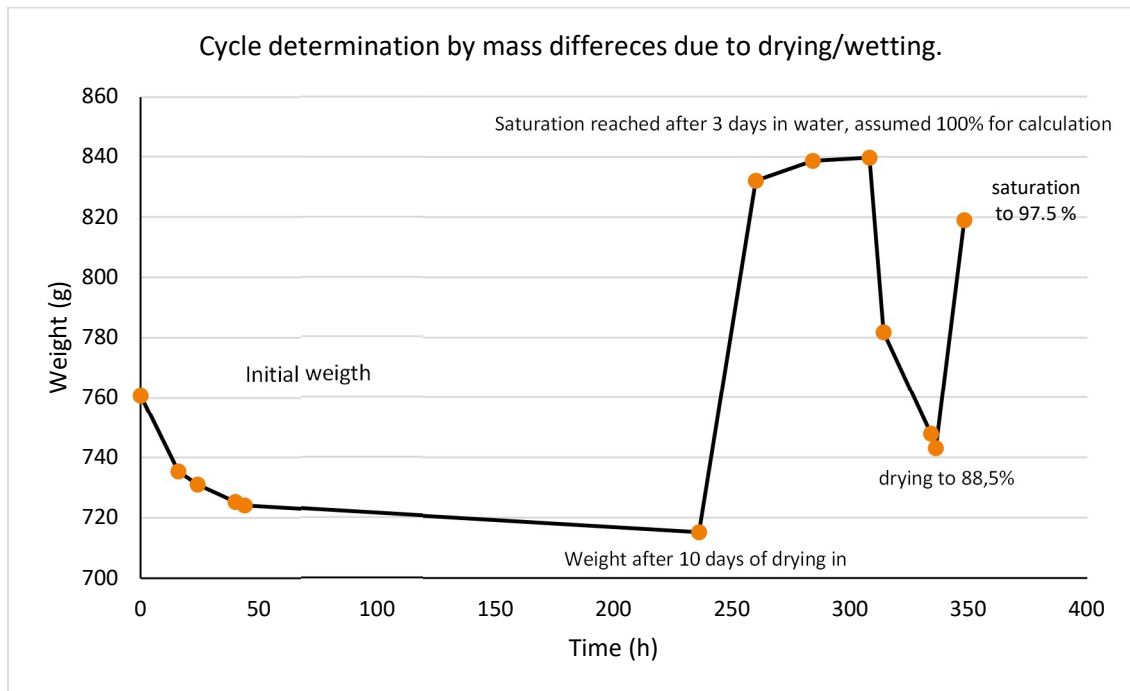*Figure 7-1 Determination of drying and wetting periods on dummy specimens.*

The specimens presented mass variation about 80 g between condition considered dry (740 g) and wet (820 g) state. During the 48 hour cycle, the composites did not reach the full saturation either dried totally, but the moisture movement and temperature gradient were introduced as a simulation of natural weathering exposure.

Table 7-1. Temperature and time periods applied as a cycle to specimens.

Temperature	Time	Rate	Description
25 to 60 ºC	6 hours	0.1 ºC/min	Heating
60 ºC	20 hours	-	Drying
60 to 25 ºC	6 hours	0.1 ºC/min	Cooling
25 ºC	16 hours	-	Water immersion

The first group of specimens was tested after 15 cycles of wetting and drying. The motivation behind 15 cycles lies in the number of days with rainfall which proceeded natural weathering tests (during first three months there were observed 15 days with rainfall over 1 mm). To see the influence of moisture on composite behavior specimens were tested in dry (after drying part of the cycle) and wet (after wetting part of the cycle). The second group of composites was tested after 30 cycles and the last after 45.

7.2.2 Residual fiber tensile strength

After the tensile test of the composite submitted to 45 cycles, the exposed fibers were tested for residual tensile force verification. The remaining fiber was taken from the exposed part after dog bone fracture. The specimens were prepared for 10 mm gage length and results were compared with previous data. Figure 7-2 presents fractured composite with exposed fiber which remained after the tensile strength test.
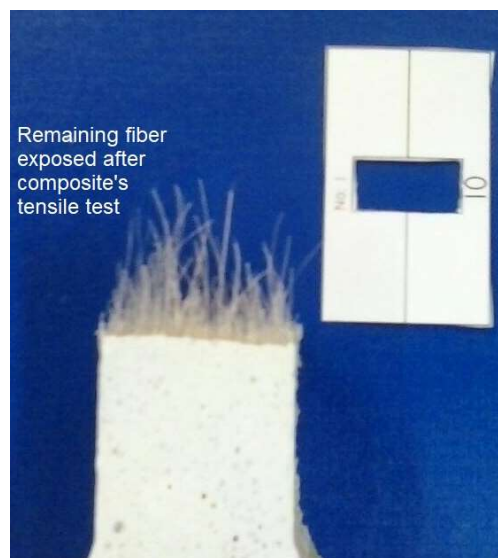

Figure 7-2 Fractured dog bone specimen with exposed fiber and 10 mm gage length mold for the tensile test of remaining fibers.

7.2.3 Visual observation

The rectangular specimens were selected from the tensile region of dog bones and broken into halves to make visual observation of fiber-matrix interaction on the fractured surface. The surface of the specimens was observed under optical microscope and SEM for analysis of fiber-matrix interaction changes after 45 cycles.

7.3 RESULTS AND DISCUSSION

7.3.1 Composite performance

Figure 7-3 presents the result of tensile strength test carried on dog bones in two conditions dry (black) and wet (blue) after 15, 30 and 45 cycles of wetting and drying. After first 15 cycles, the composite presented strain softening behavior instead of strain hardening. Both groups tested presented similar results for tensile strength 2.49±0.31 MPa for dry state and 2.35±0.40 MPa. The difference between the conditions of testing is visible after 30 and 45 cycles where the wet condition presents lower tensile strength (Table 7-2). For 30 cycles, the specimens tested in dry condition presented tensile strength of 3.03±0.51 MPa in comparison to 1.44±0.43 MPa when wet. The results for 45 cycles presented similar difference with 2.36±0.43 MPa for the dry condition and 1.65±0.15 for the wet.
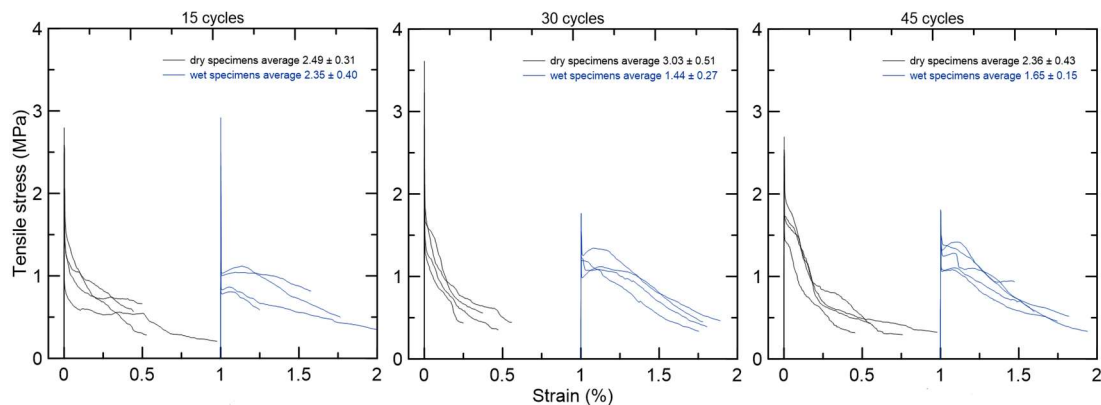

Figure 7-3 Tensile strength of dog bone specimens after 15, 30 and 45 cycles of wetting and drying in dry (black) and wet (blue) condition.

The fiber presented bridging capacity in both conditions which is represented by the post-crack strength. The fiber's bridging was not sufficient to provide strength-hardening

behavior. The difference of post crack stress-strain curve between dry and wet condition is also a clue to understanding the composite behavior. There is a possibility that wet fiber swells and creates more pressure on matrix envelope during pull-out. This will lead to more interaction surface between fiber and matrix and more bridging capacity thus the parabola shape of the post-crack curve for wet specimens and descending slope for dry ones.
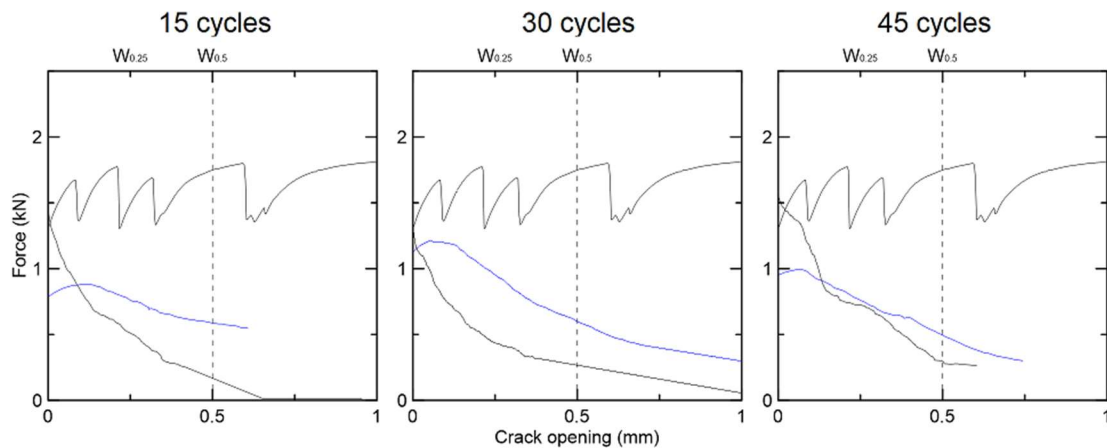
Figure 7-4 Force versus crack opening representative curves for specimens exposed to natural weathering compared to the reference specimen tested at age of 28 days.

The idea of swelled fiber can by supported by the comparison of the work done by the fibers (Figure 7-4). For 15 and 45 cycles both indicators $W_{0.25}$ and $W_{0.5}$ are higher for wet condition in comparison to dry one. Only for 45 cycles the indicators for dry condition are higher.

Table 7-2. Comparison of the tensile results of dog bone specimens submitted to 15, 30 and 45 cycles of wetting and drying as well as fiber pull-out indicators.

	15 cycles		30 cycles		45 cycles	
Condition	dry	wet	dry	wet	dry	wet
Maximum Strength (MPa)	2.49 (0.31)	2.35 (0.40)	3.03 (0.51)	1.44 (0.27)	2.36 (0.43)	1.65 (0.15)
Post Crack Strength (MPa)	1.47 (0.36)	0.98 (0.17)	1.72 (0.21)	1.19 (0.09)	1.96 (0.34)	1.25 (0.13)
F_{max} (N)	1204 (349)	901 (96)	1251 (292)	1127 (104)	1779 (302)	1070 (149)
$W_{0.25}$ (Nm)	0.18 (0.04)	0.21 (0.03)	0.19 (0.03)	0.26 (0.03)	0.27 (0.03)	0.24 (0.03)
$W_{0.5}$ (Nm)	0.28 (0.03)	0.38 (0.06)	0.29 (0.05)	0.46 (0.10)	0.40 (0.05)	0.39 (0.05)

7.3.2 Residual fiber properties

The table 7-3 presents data collected from the tensile test of curauá fiber submitted to the treatment stages and the results obtained on fiber separated from the composites exposed to natural weathering and wetting and drying cycles. The data presents information about gage length used for the test, strain at failure and force at rupture.

Table 7-3. Comparison of 10 mm gage length tensile test results for various groups of curauá fiber

Curauá fiber	Gage length (mm)	Strain (%)	Force at rupture (N)
No treatment *Raw fiber*	10	3.54 (0.50)	4.78 (0.96)
I stage treatment *3 Hot water washing cycles*	10	4.44 (0.34)	6.12 (0.78)
II stage treatment *Immersion in alkali solution*	10	2.75 (0.55)	4.81 (1.62)
12 months of natural weathering *Residual fiber after composite's fracture*	10	2.49 (0.94)	2.91 (1.19)
45 cycles dry fiber *Residual fiber after dry composite's fracture*	10	2.38 (0.56)	2.97 (1.13)
45 cycles wet fiber *Residual fiber after wet composite's fracture*	10	1.80 (1.01)	2.32 (1.40)

The results collected in Table 7-3 present a significant difference between uncovered and covered by matrix fiber's force at rupture. The II stage treated fiber presented force at rupture of 4.81±1.62 N, which is higher than the fiber extracted from the composite (2.91±1.19 N for natural weathering, 2.97±1.13 N for 45 cycles in dry condition and 2.32±1.40 N for wet condition). The lower values of force at rupture suggests that aging processes applied to composites deteriorated the fiber tensile properties. However, there can be an additional damage done on fiber because of extracting procedure. Firstly, the fiber worked in the composite presenting pull-out behavior till being completely exposed and then was extracted and tested for tensile strength. The data suggest that the fibers maintain their integrity inside the matrix. Matrix did not petrified fiber and they still present strain and tensile capacity.

The similar results of force at rupture of fiber extracted from specimens exposed to 12 months of natural weathering and 45 cycles of wetting and drying suggest that the fiber deterioration is similar in these aging conditions and the mechanism responsible is related to the temperature gradient and moisture movement.

The strain of II stage treated fiber (2.75±0.55%) which is the fiber used for casting presented similar value as the fibers extracted from the composites after 12 months of natural weathering (2.49±0.94%) and 45 cycles dry (2.38±0.56%). The wet fibers after 45 cycles presented the lowest strain capacity (1.80±1.01%), which indicates the moisture content as a deteriorating factor.

7.3.3 Visual observations

Figure 7-5 presents the comparison of alkali treated curauá fiber under MEV microscope with fiber's imprint on the composite's fractured surface. The characteristic ribs are visible on fiber's surface as well as Calcium deposited during alkaline treatment. The bottom part presents similar ribs imprinted on the matrix, which suggests the tight envelope of the matrix around the fiber.

Curauá fiber surface after alkaline treatment observed under MEV microscope:
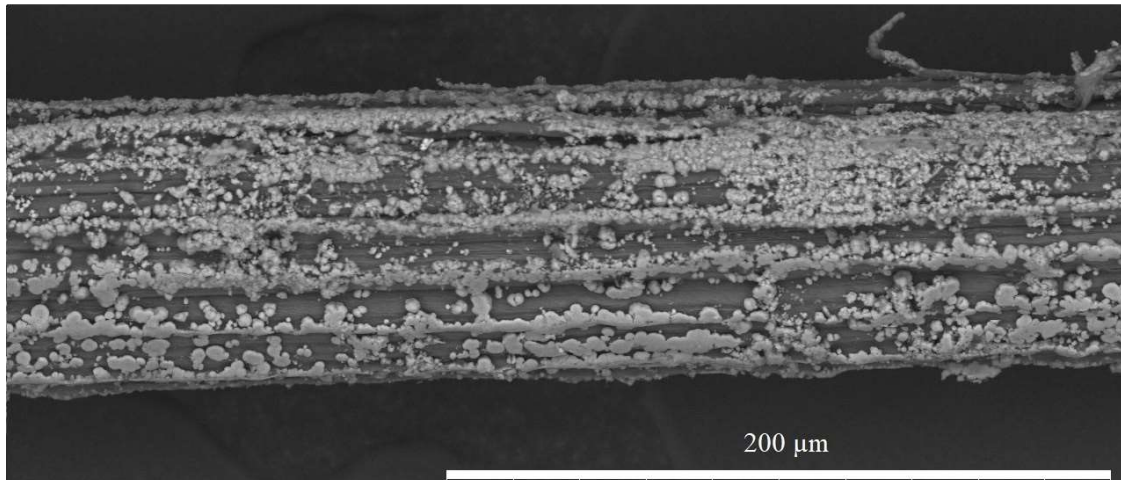
Composite fracture surface obseved under otpical microscope with visible imprint of fiber:
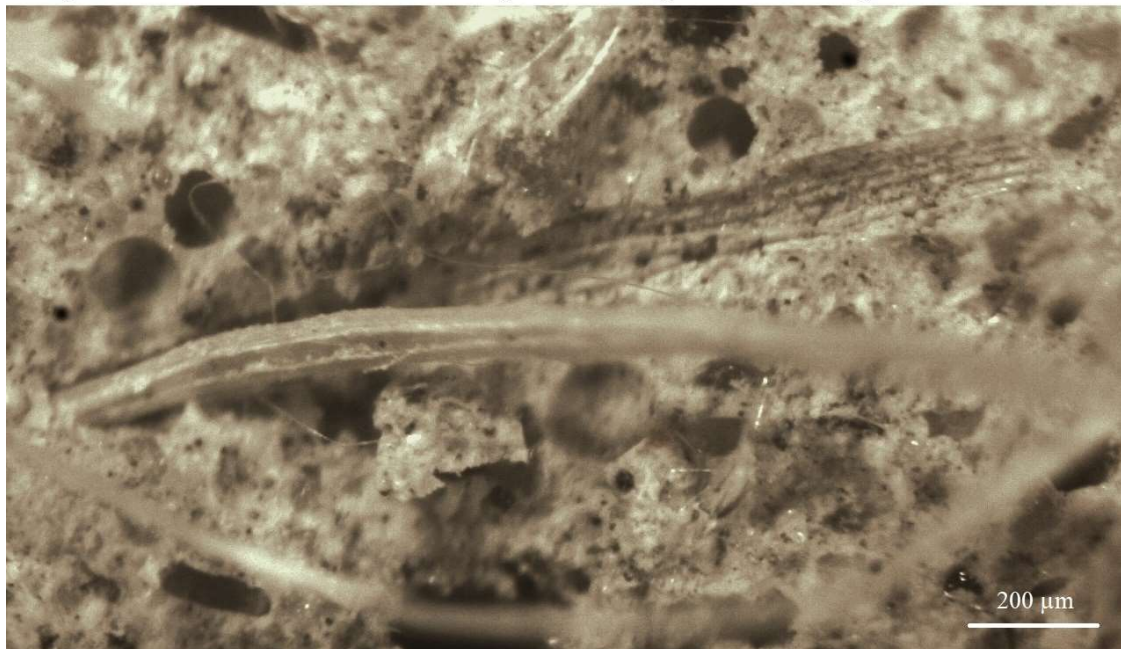
Figure 7-5 Comparison of alkali treated fiber under MEV microscope (top) with the fiber imprint on composite surface observed under optical microscope (bottom).

Figure 7-6 presents the matrix products deposited on fiber's surface as well as fiber-matrix gap and defibrillation. The fiber-matrix gap reduces the contact area between fiber and matrix changing pull-out behavior to more frictional diminishing the influence of chemical bonding.

Specimen after 45 cycles   1 mm

Figure 7-6 Fiber-matrix gap in specimens submitted to 45 cycles of wetting and drying.

Figure 7-7 presents matrix-pore relation in the composite. Fiber is significantly smaller in comparison to pore dimension. The pore's spherical shape has been disturbed by the presence of fiber. The visible gap between fiber and matrix suggest fiber dimensional changes. At some point, the fiber occupied completely the channel next to the pore. This could be the phase of curing when the fiber added to the mix could absorb part of the dosed water. Thus could swell and increase its volume in still soft mix creating a channel for itself which was tightly enveloped by matrix (as fiber's imprints on matrix suggest). The future moisture movements could cause the swelling and shrinking of the fibre reducing its contact with the matrix and creating a gap between. This phenomenon could explain the strain-hardening behavior of composites of 28 days stored in humid condition. The fiber could expand during the curing and occupy the matrix channel as the moisture conditions for the composite were stable. This caused the better fiber-matrix bond and provided sufficient fiber bridging capacity to hold the fracture of the composite till the next crack appeared so the multiple cracking behavior was possible. After moisture

variations (natural weathering, wetting and drying cycles) the fiber reduced their contact area with the matrix and lost bridging capacity that is why strain softening occurred.

Matrix pore with visible fiber   1 mm
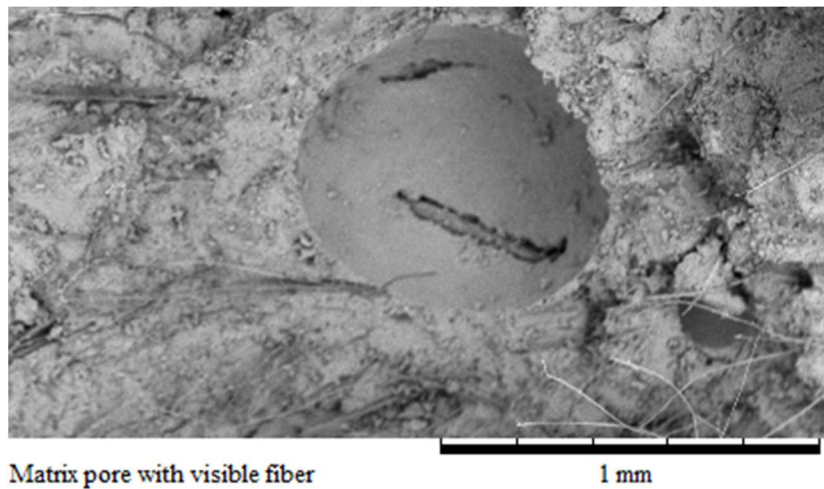
Figure 7-7 Fiber-matrix gap with pore structure in cement composite reinforced with alkali treated curauá fiber.

Figure 7-7 presents the fiber-pore relation in composite. The porosity and pore size of cement-based materials is an important factor influencing the composite's durability when exposed to environmental stress. The lower porosity is generally associated with more durable material (BRANDT, 2009).

7.4 CONCLUSIONS

The moisture movement in cement-based composites reinforced with alkali treated curauá fiber has deleterious influence on fiber-matrix interaction:

- The fiber-matrix contact area is reduced and created gap reduces the fiber-matrix interaction.
- The composites tested in wet (saturated) condition presented lower tensile strength values for 30 and 45 cycles in comparison to the composites tested in dry condition.
- The post-crack behavior represented by the stress-strain curve presented differences.
- The saturated composites the stress-strain after crack presented parabola curve indicating higher bridging capacity in comparison to dry composites (descending slope).

The comparison of fibers extracted from the composites with fibers used for casting presented differences between forces at rupture:

- The lower force at rupture was reported for extracted fibers which suggests the deleterious effect of matrix environment or the procedure of extraction.
- The comparison of strain capacity between the groups presented only the influence of fiber moisture on fiber strain capacity (wet fibers presented lower strain capacity). This could suggest that the extraction process did not affect significantly the fiber properties. The damage done by extracting process should be mechanical (fiber friction during pull-out) so the fiber's integrity would be disturbed thus the strain should be much lower in comparison to not-extracted fiber.

8 SUMMARY

The thesis presented the curauá fiber characterization and the treatments to improve fiber properties (washing and drying cycles) as well as fiber-matrix bond properties (alkaline treatment). The presented research proved that the methodology previously designed for synthetic fibers for tailoring SHCC can be applied to natural fiber as well. The design process of SHCC with short (20 mm) curauá fiber was presented and verified on tensile dog-bone specimens. The influence of fiber length was verified for fibers of 20, 30 and 40 mm. The last length was used for composites exposed to the durability studies. The durability studies presented the challenge of SHCC with curauá fiber. The strain-hardening behavior no longer occurred to specimens exposed to natural weathering, wetting and drying cycles, and freezing and thawing cycles. The fibers survived in the designed matrix during the durability studies, which was proved by the residual tensile strength test of fibers extracted from the composites. The strain-softening instead of strain-hardening behavior of composites submitted to durability studies was justified by the fiber volume changes inside the matrix thus the loss of fiber-matrix bond as observed under the microscope the gaps between fiber and matrix.

To summarize the SHCC-Curauá can be designed and tailored with the micromechanical model support, but the challenge is to maintain the behavior. The possible solution to the durability challenge could be:

• The fiber coating, which could prevent to moisture movement to and from the fiber (reducing volume changes). The coating could be beneficial to fiber-matrix bond, which could reduce the critical volume needed to strain-hardening.

• Hybridization of the fiber reinforcement by an application of synthetic fiber along with natural. A combination of two different type of fiber could link the benefits of synthetic fiber (high resistance, dimension stability, durability) with natural fiber (ecological and economical).

9 REFERENCES

ADRADE, A. C. da S. et al. **Potencialidades e usos do curauá em plantios florestais.** Belem: Universidade Federal Rural da Amazônia, 2011.

ALVAREZ,V. A.; VÁZQUEZ, A. **Thermal degradation of cellulosederivatives/starch blends and sisal fibre biocoposites.** *Polymer Degradation and Stability.*, p. 13–21, 2004.

ALVES FIDELIS, M. E. et al. **The effect of fiber morphology on the tensile strength of natural fibers**. *Journal of Materials Research and Technology*, vol. 2, no. 2, p. 149–157, 2013. ISBN: 22387854.

ARAÚJO, J. R.; WALDMAN, W. R.; PAOLI, M. A. DE. **Thermal propertie of high density polyethylene composites with natural fibres: coupling agent effect.** *Polymer Degradation and Stability*, p. 1770–1775, 2008.

ASTM. **C1557 : Standard Test Method for Tensile Strength and Young ' s Modulus of Fibers**. *Annual Book of ASTM Standards*, vol. 3, no. Reapproved 2013, p. 1–10, 2014.

AZWA, J. R. et al. **A review on the degrability of polymeric composites based on natural fibres**. *Materials & Design*, vol. 47, no. May, p. 424–442, 2013.

BENTUR, A.; MINDESS, S. **Fibre reinforced cementitious composites**. Taylor & Francis, 2007a. 601 p. ISBN: 9780415250481.

BENTUR; MINDESS, S. **Fibre Reinforced Cementitious Composites**. Modern Con ed. New York: Taylor & Francis, 2007b.

BOTS, P. et al. **Mechanistic Insights into the Crystallization of Amorphous Calcium Carbonate (ACC)**. *Crystal Growth & Design*, 2012.

BRAGA, R. da S. et al. **Avaliação do uso de fibra e mucilagem de curauá na produção de papel reciclado para embalagens.** In: *Simpósio de Meio Ambiente*. Viçosa, MG: CBCN, 2010.

BRANDT, A. M. **Cement based composites : materials, mechanical properties, and performance**.Taylor & Francis, 2009. 526 p. ISBN: 9780415409094.

BREČEVIĆ, L.; NIELSEN, A. E. **Solubility of amorphous calcium carbonate**. *Journal of Crystal Growth*, vol. 98, no. 3, p. 504–510, 1989. ISSN: 0022-0248.

BUTLER, M.; MECHTCHERINE, V.; HEMPEL, S. **Experimental investigations on the durability of fibre-matrix interfaces in textile-reinforced concrete**. *Cement and Concrete Composites*, vol. 31, no. 4, p. 221–231, 2009. ISBN: 09589465.

CASTRO COIMBRA CORDEIRO, I. M. et al. **Análise econômica dos sistemas de cultivo com Schizolobium parahyba var. amazonicum (Huber ex Ducke) Barneby (Paricá) E Ananas comosus var. erectifolius (L. B. Smith) Coppus & Leal (Curauá) no município de Aurora do Pará (pa), Brasil**. *Revista de la Facultad de Agronomia*, vol. 26, no. 2, p. 243–265, 2009. ISSN: 03787818.

CHAWLA, N.; KERR, M.; CHAWLA, K. K. **Monotonic and cyclic fatigue behavior of high-performance ceramic fibers**. *Journal of the American Ceramic Society*, vol. 88, no. 1, p. 101–108, 2005. ISBN: 0002-7820.

DITTENBER, D. B.; GANGARAO, H. V. S. **Critical reveiew of recent publications on use of natural composites in infrastructure**. *Composites Part A: Applied Science and Manufacturing*, no. August, p. 1419–1429, 2012.

DWECK, J. et al. **Study by thermogravimetry of the evolution of ettringite phase during type II Portland cement hydration**. *Journal of Thermal Analysis and Calorimetry*, vol. 69, no. 1, p. 179–186, 2002. ISBN: 1388-6150.

DWECK, Jo et al. **Hydration of a Portland cement blended with calcium carbonate**. *Thermochimica Acta*, vol. 346, no. 1–2, p. 105–113, 2000. ISBN: 0040-6031, ISSN: 00406031.

FERREIRA, S. R. et al. **Effect of fiber treatments on the sisal fiber properties and fiber-matrix bond in cement based systems**. *Construction and Building Materials*, vol. 101, p. 730–740, 2015. ISSN: 09500618.

_____. **Effect of hornification on the structure, tensile behavior and fiber matrix bond of sisal, jute and curaua fiber cement based composite systems**. *Construction and Building Materials*, vol. 139, p. 551–561, 2017. ISBN: 9783038356103, ISSN: 09500618.

FIDELIS, M. E. A. et al. **The effect of accelerated aging on the interface of jute textile reinforced concrete**. *Cement and Concrete Composites*, vol. 74, p. 7–15, 2016. ISSN: 09589465.

FUKUYAMA, H. **Application of High Performance Fiber Reinforced Cementitious Composites for Damage Mitigation of Building Structures Case study on Damage Mitigation of RC Buildings with Soft First Story**. *Journal of Advanced Concrete Technology*, vol. 4, no. 1, p. 35–44, 2006. ISSN: 1346-8014.

GRAM, H. E. **Methods for Reducing the Tendency towards Embrittlement in Sisal Fibre Concrete**. *Nordic Concrete Research*, p. 62–71, 1983.

_____. **Durability studies of natural organic fibres in concrete, mortar or cement.** In: *Developments in FIbre Reinforced Cement and Concrete. RILEM Symphosium.* Sheffield: 1986.

GRAM, Hans Erik. **Methods for Reducing the Tendency Towards Embrittlement in Sisal Fibre Concrete.** *Nordic concrete research*, no. 2, p. 62–71, 1983. ISBN: 0419132805, ISSN: 08006377.

HILLEMEIER, B.; HILSDORF, H. K. **Fracture mechanics studies on concrete compounds**. *Cement and Concrete Research*, vol. 7, no. 5, p. 523–535, 1977. ISSN: 00088846.

HOSHIRO, N.; NISHIYAMA, M.; YAMAMOTO, R. **Long-term Durability of Kuralon (PVA fiber) in alkaline Condition**. In: *10th Int. Inorganic-bonded Fiber Composite Conference*, 2006.

JACOBSEN, S. E.; WYMAN, C. E. **Cellulose and Hemicellulose Hydrolysis Models for Application to Current and Novel Pretreatment Processes**. *Applied Biochemistry and Biotechnology*, p. 84–86, 2000.

JAPAN SOCIETY OF CIVIL ENGINEERS. **Recommendations for Design and Construction of High Performance Fiber Reinforced Cement Composites with Multiple Fine Cracks (HPFRCC)**. *Concrete Engineereing Series*, vol. 82, p. Testing Method 6-10, 2008. ISBN: 9784810606409.

JOHN, M. J.; THOMAS, S. **Biofibres and biocomposites**. *Carbohydrate Polymers*, vol. 71, no. 3, p. 343–363, 2008.

KANDA, T. **Design of engineered cementitious composites for ductile seismic resistant elements.** 328 p. - University of Michigan, 1998.

KARIHALOO, B. L.; CARPINTERI, A.; ELICES, M. **Fracture mechanics of cement mortar and plain concrete**. *Advanced Cement Based Materials*, vol. 1, no. 2, p. 92–105, 1993. ISSN: 10657355.

KICIŃSKA-JAKUBOWSKA, A.; BOGACZ, E.; ZIMNIEWSKA, M. **Review of Natural Fibers. Part I—Vegetable Fibers.** *Journal of Natural Fibers.*, no. September 10, p. 150–167, 2012.

KOJIMA, S. et al. **Application of sprayed repair with highly ductile cement composites to upstream concrete of Sanko dam.** *Conrete Journal*, p. 135–139, 2004.

LEE, S. .; WANG, S. **Biodegradable polymers/bamboo fiber ciocomposite with bio-based coupling agent.** *Composites Part A: Applied Science and Manufacturing.*, p. 90–91, 2006.

LI, V. C.; FISHER, G.; LEPECH, M. **Shotcreting with ECC.** *Spritzbeton-Tagung Proceedings of CD*, no. January, 2009.

LI, V. C.; MAALEJ, M. **Toughening in Cement Based Composites. Part I: Cement, Mortar, and Concrete** . *Cement & Concrete Composites*, vol. 18, no. 95, p. 223–237, 1996.

LI, X.; TABIL, L. G.; PANIGRAHI, S. **Chemical Treatments of Natural Fiber for Use in Natural Fiber-Reinforced Composites: a Review**. *Hournal of Polymers and the Environment*, no. February, p. 25–33, 2007.

LITHERLAND, K. L.; OAKLEY, D. R.; PROCTOR, B. A. **The use of accelerated ageing procedures to predict the long term strength of GRC composites**. *Cement and Concrete Research*, vol. 11, no. 3, p. 455–466, 1981. ISSN: 00088846.

LOPES, I. **Emater-Pará**. 2015. retrieved <http://www.emater.pa.gov.br/destaque/202>.

MAGALHÃES, M. **Influence of local raw materials on the mechanical behaviour and fracture process of PVA-SHCC**. *Materials Research*, vol. 17, no. 1, p. 146–156, 2013. ISBN: 1516143920130, ISSN: 15161439.

MAI, Y. W.; HAKEEM, M. I. **Slow crack growth in cellulose fibre cements.** *Journal of Material Science 19*, p. 501–508, 1984.

MANFREDI, L. B. et al. **Thermal degradation and fire resistance of unsaturated polyester, modifies acrylic resins and their composites with natural fibres.** *Polymer Degradation and Stability.*, p. 255–261, 2006.

MARSHALL, D. B.; COX, B. N. **A J-integral method for calculating steady-state matrix cracking stresses in composites**. *Mechanics of Materials*, vol. 7, no. 2, p. 127–133, 1988. ISBN: 0167-6636, ISSN: 01676636.

MELO FILHO, J. A.; SILVA, F. A.; TOLEDO FILHO, R. D. **Degradation kinetics and aging mechanisms on sisal fiber cement composite systems.** *Cement and Concrete Composites*, p. 30–39, 2013.

METHACANON, P. et al. **Properties and potential application af the selected natural fibers as limited life geotextiles.** *Carbohydrate Polymers*, vol. 83, no. 4, p. 1090–1096, 2010.

MITAMURA, H. et al. **Repair construction of steel deck with highly ductile fiber reinforced cement composites – construction of Mihara bridge**. *Bridge Found*, no. 39, p. 88–91, 2005.

NAAMAN, A. E.; REINHARDT, H. W. **High Performance Fiber Reinforced Cement Composites HPFRCC-4: International RILEM Workshop**. *Materials and Structures*, vol. 36, no. 10, p. 710–712, 2003. ISSN: 1359-5997.

NIMER, E. **Um modelo metodológico de classificação de climas.** *Revista Brasileira de Geografia*, no. October/Dezember, p. 59–89, 1979.

OLIVEIRA, E. C. P. DE et al. **Leaf structure of curauá in different intensities of photosynthetically active radiation.** *Pesquisa Agropecuaria Brasileira*, vol. 43, no. 2, p. 163–169, 2008. ISSN: 0100204X.

OSAWA, C. C.; GONÇALVES, L. A. G.; RAGAZZI, S. **Potentiometric titration applied to free fatty acid determination of edible oils and fats**. *Química Nova*, vol. 29, no. 3, p. 593–599, 2006. ISSN: 0100-4042.

RADJY, F.; HANSEN, T. C. **Fracture of hardened cement paste and concrete**. *Cement and Concrete Research*, vol. 3, no. 4, p. 343–361, 1973. ISSN: 00088846.

RAMALHO, E. **Malinche.** *Blog sobre a amazónia*. 2005. retrieved <https://malinche.wordpress.com/2006/10/01/curaua-a-folha-amazonica-que-virou-arte/>.

REIS, I. N. R. de S.; LAMEIRA, O. A.; CORDEIRO, I. M. C. C. **Desenvolvimento do Curauá (Ananas erectifolius L.B. SMITH) a partir de adubação orgânica e de NPK.** *Seminário de Iniciação Científica da Embrapa Amazônia Oriental - VIII*, p. 332–334, 2004.

RODRIGUES, C. de S. et al. **Modification of cellulose-cement Composites by admixture of sugar cane bagasse ash**. *RILEM Proceedings Pro 96. Bagneux: RILEM Publications SARL*, vol. 1, no. 1, p. 569–576, 2015.

SAHIN, Y.; KOKSAL, F. **The influences od matrix and Steel Fibre Tensile Strengths on the Fracture energy of High-Strength Concrete.**, p. 1801–1806, 2011.

SILVA, F. A. et al. **Physical and mechanical properties of durable sisal fiber-cement composites.** *Construction and Building Materials*, p. 777–785, 2010.

SILVA, F. de A.; CHAWLA, N.; TOLEDO FILHO, R. D. De. **Tensile behavior of high performance natural (sisal) fibers**. *Composites Science and Technology*, vol. 68, no. 15–16, p. 3438–3443, 2008. ISBN: 0266-3538, ISSN: 02663538.

SILVA, T. A. L. et al. **Extraction and preliminary characterization of bromelain from curauá (ananas erectifoliu L.B. Smith) puprle and white.** *Chemical Engineering Transactions.*, p. 769–774, 2014.

SNOECK, D.; SMETRYNS, P. A.; BELIE, N. DE. **Improved multiple cracking and autogenous healing in cementitious materials by means of chemically-treated natural fibres**. *Biosystems Engineering*, vol. 139, no. 1998, p. 87–99, 2015.

SOLTAN, D. G. et al. **Introducing a curauá fiber reinforced cement-based composite with strain-hardening behavior**. *Industrial Crops and Products*, vol. 103, p. 1–12, 2017. ISSN: 09266690.

SUARDANA, N. P. .; KU, M. S.; LIM, J. K. **Effects of diammonium phosphate on the flammability and mechanical properties of bio-composites.** *Materials & Design.*, p. 1990–1999, 2011.

SWAMY, R. N. **Natural Fibre Reinforced Cement and Concrete**. London: Blackie, 1988.

TOLEDO FILHO, R. D. et al. **Durability if alkali-sensitive sisal and coconut fibres in cement mortar composites.** *Cement and Concrete Composites*, vol. 22, no. 2, p. 127–143, 2000.

_____. **Development of vegetable fibre-mortar composites of improved durability.** *Cement & Concrete Composites*, p. 185–196, 2003.

_____. **Durability of compression molded sisal fiber reinforced mortar laminates.** *Construction and Building Materials.*, p. 2409–2420, 2009.

TOMCZAK, F.; SATYANARAYANA, K. G.; SYDENSTRICKER, T. H. D. **Studies on lignocellulosic fibers of Brazil: Part III - Morphology and properties of Brazilian curauá fibers**. *Composites Part A: Applied Science and Manufacturing*, vol. 38, no. 10, p. 2227–2236, 2007. ISBN: 1359-835X.

UZOMAKA, O. J. **Characteristics of akwara as a reinforcing fibre.** *Magazine of Concrete Research 28.*, no. September, p. 162–167, 1976.

VASUDEVAN, A. V.; GRABOIS, T. M.; CORDEIRO, GUILHERME CHAGAS, R. D. T. F. and L. P. **A new fracture test methodology for the accurate characterization of brittle fracture properties.**, p. 1–12, 2017.

WANG, B.; CAI, Z.; YU, J. **Study on the Chemical Modification Process of Jute Fiber**. *Journal of engineered Fibers and Fabrics*, p. 1–11, 2008.

WEGST, U. G. K. et al. **Bioinspired structural materials.** *Nature Materials*, no. January, p. 23–36, 2015.

WEI, J.; MEYER, C. **Degradation rate of natural fiber in cement composites exposed to various accelerated aging environment conditions**. *Corrosion Science*, vol. 88, p. 118–132, 2014. ISSN: 0010938X.

WITTMANN, F. H. F. H. et al. **Durability of Strain-Hardening Fibre-Reinforced Cement-Based Composites (SHCC)**. *Durability of Strain-Hardening Fibre-Reinforced Cement-Based Composites*: 2011. 152 p. ISBN: 978-94-007-0337-7, ISSN: 1359-5997.

WOJDYR, M. **Fityk: A general-purpose peak fitting program**. *Journal of Applied Crystallography*, vol. 43, no. 5 PART 1, p. 1126–1128, 2010. ISBN: 0021889810030, ISSN: 00218898.

WONG, K. J.; YOUSIF, B. F.; LOW, K. O. **The effects of alkali tratment on the interfacial adhesion of bamboo fibres**. *Proceedings of the Institution of Machanical Engineers Part L: Journal of Materials:Design and Apllocations*, vol. 224, no. 3, p. 139–148, 2010.

YAMAMOTO, T. et al. **Tunnel repair technology using highly ductile cement composites – An application to a tunnel damaged during Chuetsu Earthquake**. *Proceedings of the 60th Annual Meeting (JSCE). Materials, Concrete Structures and Pavements*, vol. 3, p. 483–484, 2005.

YANG, E. H.; LI, V. C. **A Micromechanical Model for Fiber Cement Optimizaiton and Component Tailoring.**, no. 1992, p. 1–13, 2006.

YANG, E. H.; LI, V. C. **Strain-hardening fiber cement optimization and component tailoring by means of a micromechanical model**. *Construction and Building Materials*, vol. 24, no. 2, p. 130–139, 2010. ISBN: 0950-0618, ISSN: 09500618.

YOUNG, J. F. et al. **The science and technology of civil engineering materials**. Saddle River, NJ: Prentice Hall, 1998.

ZHOU, J. et al. **Improved fiber distribution and mechanical properties of engineered cementitious composites by adjusting the mixing sequence**. *Cement and Concrete Composites*, vol. 34, no. 3, p. 342–348, 2012. ISSN: 09589465.

ZIJL, G. P. A. G. VAN; BOSHOFF, W. P. **Mechanisms of creep in fibre-reinforced Strain-Hardening Cement Composites (SHCC)**. *Creep, Shrinkage and Durability Mechanics of Concrete and Concrete Structures - Proceedings of the 8th Int. Conference on Creep, Shrinkage and Durability Mechanics of Concrete and Concrete Structures*, vol. 1, p. 753–759, 2009. ISBN: 9780415485081.